The effect of wind on multiple, short, natural-draft dry cooling towers

Mehrdad Khamooshi

A thesis submitted to

Auckland University of Technology

in fulfilment of the requirements for the degree of

Doctor of Philosophy (PhD)

2019

School of Engineering, Computer and Mathematical Science

ABSTRACT

The deployment of concentrating solar thermal (CST) power plants in arid areas necessitates the use of dry cooling systems to reject heat from the condenser. Previous research has shown that the capacity of short natural draft dry cooling towers (NDDCTs), used as condensers for CST plants, can be significantly influenced by the prevailing wind condition. From the literature, it is apparent that there is a lack of work relating to how the interactions between multiple cooling towers during windy and no-wind conditions impact the cooling capacity of multiple cooling towers on a common site, and short NDDCTs in particular. This is a particular problem because as the capacity of CSP power plants is increased, additional cooling is required which necessitates the addition of more NDDCTs. When adding these cooling towers, there is a need to be able to position them correctly so that their performance as a group is maximised. To do this, an understanding of the effect they have on one another is needed. Hence, this work aims to characterise the interaction between multiple short NDDCTs on the cooling capacity of the multi-tower system on a common site over a range of typical operating conditions including wind speed, tower spacing, wind incidence angle, and the number of cooling towers.

This study first investigated the effect of different tower spacings on the cooling performance of multiple short NDDCTs using computational fluid dynamics (CFD) under a no-wind condition. The simulated tower in all multi-tower simulations is identical and is representative of an actual steel-membrane cooling tower in a campus of the University of Queensland. The geometry of the used cooling tower in this study is a cylindrical shape with a horizontally arranged air-cooled heat exchanger and is 20 m high with a diameter of 12.525 m. This study has shown that, at a tower spacing of less than two tower diameters (2D) where D is the diameter of the tower, a reduction in the scavenging area

between the towers limits the air supply to the towers and this interaction decreases the cooling performance of the towers.

Secondly, the study investigated the effect of three major parameters: wind speeds (0-8 m/s), wind incidence angles (0°, 45°, and 90°), and tower spacings (1.8D, 2.6D, and 4.2D) on the thermo-flow performance of the cooling towers.

It was shown that the interaction between the towers at a 90° wind incidence resulted in a performance improvement of the towers only at a tower spacing of 1.8D, while for the other tower spacings there was no interaction between the towers. At a wind incidence of 45°, the interference between the towers contributes to a decrease in the performance of the towers at tower spacings of 1.8D and 2.6D. It was found that the thermal performance of the NDDCTs in wind incidence of 0° is superior to other layouts at lower tower spacings. This study found that it helps to add the second tower in line with the prevailing wind direction.

Thirdly, the performance of the three short NDDCTs is also investigated in an inline layout, labelled as windward, middle, and leeward towers. At all tower spacings, the windward tower shields the middle and leeward towers by deflecting the upcoming wind.

Finally, the effect of tower dimensions on the interaction of three NDDCTs with similar sizes was examined and the results revealed that larger towers are less vulnerable to crosswinds due to their higher capacity of the drawing air into the cooling tower compared to smaller cooling towers.

Overall, the most significant outcome of this investigation was to show that when adding additional cooling towers to an existing CSP site, they should be placed along the line of the prevailing wind direction, with a spacing determined by the average wind speed.

CONTENTS

LIST OF FIGURES

LIST OF TABLES

NOMENCLATURE

A	area (m^2)
C_2	inertial resistance factor
C_p	specific heat ($J\ Kg^{-1}\ K^{-1}$)
D	tower diameter (m)
Eu	Euler number
g	gravity ($m\ s^{-2}$)
Fr	Froude number
H	height (m)
h	heat transfer coefficient ($W\ m^{-2}\ K^{-1}$)
k	Turbulent kinetic energy ($m^2\ s^{-2}$)
m	mass flow rate (kg/s)
p	pressure (pa)
q	heat flux ($W\ m^{-2}$)
Q	heat transfer rate (W)
r	Velocity ratio
Re	Reynolds number
S	source term for momentum equations
T	temperature (°C)

ΔT_{lm}	logarithmic mean temperature difference (K)
U	velocity components in x-direction (m s^{-1})
Z	elevation
x,y,z	Cartesian co-ordinates

Greek letters

α	permeability (m^2)
μ	dynamic viscosity (kg $m^{-1}s^{-1}$)
ρ	air density (kg m^{-3})
τ	Tower ratio
ε	Turbulent kinetic energy dissipation rate (m^2s^{-3})
ω	Specific turbulent kinetic energy dissipation rate (m^2s^{-3})

Vectors

v	velocity

Subscripts

a	roughness of the ground
a	airside
cw	crosswind
hx	heat exchanger
i	inside or inlet
l	liquid

t	tower
o	outside or outlet
r	radiator
u	overall
ref	reference value
sum	summation of both towers
i, j, k	Unit vectors of x, y, z direction in Cartesian

Acronyms

ASTRI	Australian Solar Thermal Research Initiative
CST	Concentrating solar thermal
CFD	Computational Fluid Dynamics
NDDCT	Natural draft dry cooling tower
NDDCTH	Natural draft dry cooling tower with horizontally arranged heat exchanger
NDDCTV	Natural draft dry cooling tower with vertically arranged heat exchanger
NDWCT	Natural draft wet cooling tower
RANS	Reynolds-time averaged Navier-Stokes
SIMPLEC	Semi-Implicit Method for Pressure Linked Equations-Consistent
UV	Ultraviolet

LIST OF PUBLICATIONS

Khamooshi, M., Anderson, T. and Nates, R., 2020, A numerical study on interactions between three short natural draft dry cooling towers in an in-line arrangement. International Journal of Thermal Sciences.

Khamooshi, M., Anderson, T. and Nates, R., 2020, Impact of tower spacing on the performance of multiple short natural draft dry cooling towers for calm conditions. Proceedings of the Institution of Mechanical Engineers, Part A: Journal of Power and Energy

Khamooshi, M., Anderson, T. and Nates, R., 2018, "Numerical Investigation of the Effect of Wind on the Performance of the Three Short Natural Draft Dry Cooling Towers in an In-line Arrangement", Proceedings of the Asia-Pacific Solar Research Conference 2018, Sydney, December 2018.

Khamooshi, M., Anderson, T. and Nates, R., 2018, "The effect of wind on the performance of multiple short natural draft dry cooling towers", Proceedings of the 11th Australasian Heat and Mass Transfer Conference, Melbourne, July 2018.

Khamooshi, M., Anderson, T.N. and Nates, R.J., 2017, "A numerical investigation of the influence of wind on multiple short natural draft dry cooling towers", 2017 Asia-Pacific Solar Research Conference, Melbourne, December 2017.

Khamooshi, M., Anderson, T.N. and Nates, R.J., 2017, "Impact of tower spacing on the performance of multiple natural draft dry cooling towers under no wind conditions", Proceedings of the 10th Australian Natural Convection Workshop, Auckland, November 2017.

ATTESTION OF AUTHORSHIP

I hereby declare that this submission is my own work and that, to the best of my knowledge and belief, it contains no material previously published or written by another person (except where explicitly defined in the acknowledgments), nor material which to a substantial extent has been submitted for the award of any other degree or diploma of a university or other institution of higher learning.

Auckland Signature_____

Mehrdad Khamooshi

ACKNOWLEDGMENT

I would like to thank my supervisors Dr. Timothy Anderson and Assoc/Prof. Roy Nates, for the encouragement and advice they have provided throughout my PhD. They have helped me a lot in growing my confidence, improving my critical thinking, developing my problem-solving skills.

A very special gratitude goes out to Dr David White for his support and encouragement throughout my years of study.

I would like to thank my wife Hana Salati for her continuous moral and emotional support and continuous encouragement in completing this task. I am most grateful to my parents, for their love and care to which I will always be in debt. Thank you for encouraging me in all my pursuits and inspiring me to follow my dreams. I am especially grateful to my sister, Somayeh and brothers, Yaser and Ehsan, who supported me emotionally.

I would especially like to thank my research colleagues Hamzah, Delight, and Sulaiman for the valuable discussions and help during this journey. Also, I thank my friends Kiyan Parham, Saeed Mohseni, and Iman Roozbeh for their moral support and best wishes.

Chapter 1: Literature review

1.1. Concentrating solar thermal (CST) power plants

Many power generation processes consume large amounts of fossil fuels. Due to limited long-term availability of these sources, and the consequences of using fossil fuels (global warming and air pollution among other negative impacts), the search for alternative options has increased noticeably. Concentrating solar thermal (CST) power generation systems offer a favourable solution to overcome these energy and sustainability concerns.

CST power generation technologies use mirrors to reflect and concentrate sunlight onto receiver(s) that collect the solar energy and convert it to heat (Figure 1.1). The thermal energy source then can be used to generate electricity using a turbine in a power cycle such as the Rankine or supercritical CO_2 Brayton cycle.

Figure 1.1. CST plants in Nevada.

In saying this, it is worth noting that supercritical power cycles is an effective alternative to steam power cycles (1). Supercritical CO2 cycles have the advantages of compact turbomachinery design, scalable modular, lower operating cost and more efficient than the steam cycle (2).

Irrespective of the cycle type, Figure 1.2 shows a schematic view of a tower/central receiver CST system integrated with a power cycle, and where molten-salt technology is used to store solar thermal energy. The cold tank supplies the cold working fluid to the solar tower, where it is heated to approximately 600-800 °C. The thermal energy from the heated fluid is stored in the hot storage tank where part of the hot salt is pumped for night-time application or when there is insufficient solar energy. The power block of the CST system is the same as that used in a conventional thermal power cycle, where the high pressure and high temperature working fluid generated by the boiler drives the turbine. The exhaust of the turbine gets condensed in the condenser which may include a cooling tower.

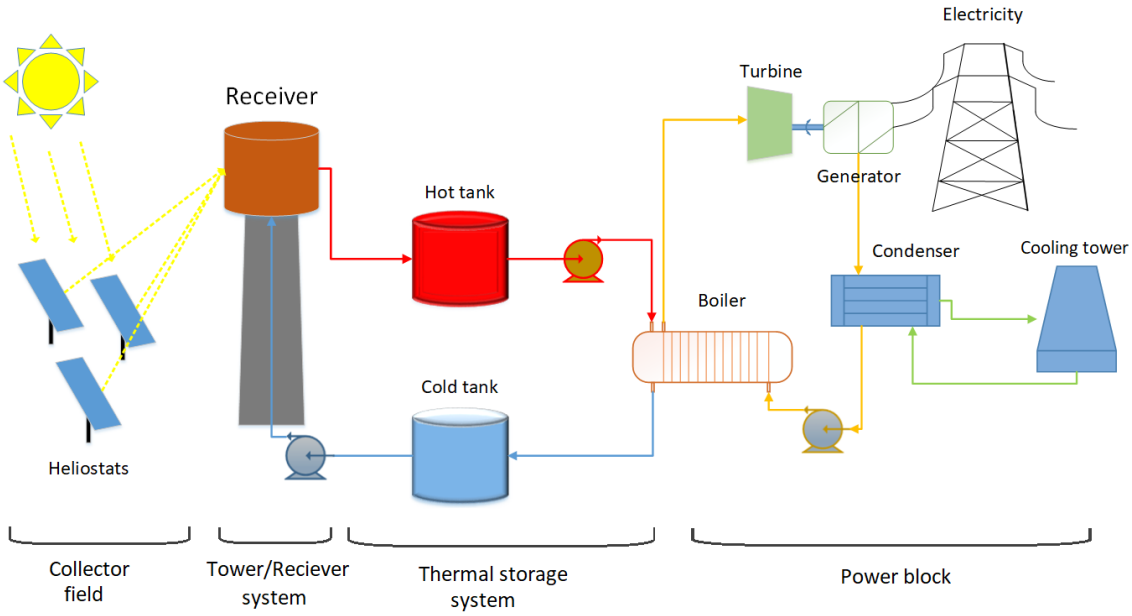

Figure 1.2. Schematic view of a typical CST plant.

The design of the cooling system in a CST power plant can have a significant impact on the cycle efficiency, because the power cycle is sensitive to the heat sink temperature. Typically, the cooling systems used in the power plants could be a once-through system (3), a spray pond system (4), or cooling towers (5).

In a once-through cooling system, a large volume of water extracted from a river, lake or the ocean passes through the plant's condenser a single time to provide cooling before being discharged (6). Figure 1.3 shows the schematic view of a once-through cooling system typically used in power plants with capacities greater than 100 MW (7).

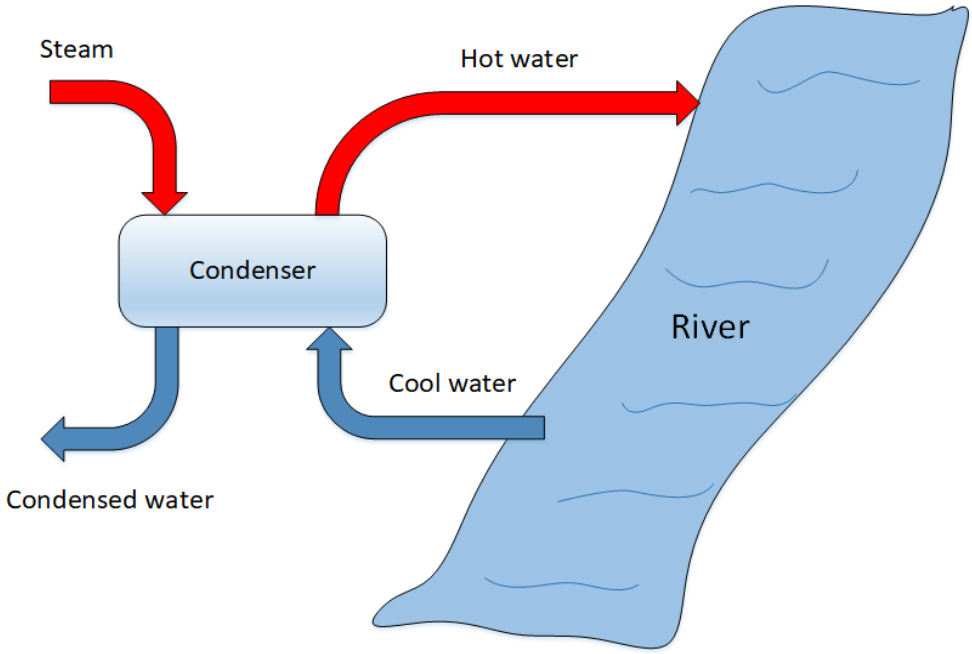

Figure 1.3. Schematic view of once-through cooling system.

In spray pond systems, often used in nuclear power plants, the water from the condenser is sprayed via nozzles into air to evaporate the droplets of water and cool the water (8). Figure 1.4 demonstrates a spray cooling system which was constructed and operated by Ecoclaire Condenser Company (9). The main disadvantages of such systems are, the large area to cool the water (8) and the volume of water lost to the surrounding environment.

Figure 1.4. Spray cooling system (9).

Finally, cooling towers are perhaps the most common heat sink device used in thermal power plants (10). In these systems air is circulated over the condenser tubes with the aid of a fan (mechanical draft), or by the buoyancy effect (natural draft). That said, natural draft cooling towers have been used widely in large thermal power plants and other chemical processes as they have no power consumption, low maintenance costs and no mechanical noise (11-14). These towers are generally divided into natural draft wet cooling towers (NDWCT), hybrid cooling towers and natural draft dry cooling towers (NDDCT).

1.2. Natural draft cooling towers

1.2.1. Natural draft wet cooling tower (NDWCT)

In NDWCTs, the hot water from the condenser is distributed via spray nozzles as shown in Figure 1.5. The hot water sprayed inside the cooling tower and the density of the warm moist air inside the tower is less than the density of the atmosphere outside the tower. Thus, the pressure inside the tower is lower than the external pressure, causing air to flow through the tower. In doing this, the cooled water is collected in the tower's basin and is circulated back to the condenser. The main disadvantage of the wet cooling tower is that some of the water is lost during the cooling process. This can present a serious problem if freshwater resources are limited and expensive, an issue particularly in arid areas where

CST plants may be sited. To this end, hybrid cooling towers have been also proposed as a way to save water in regions where water is scarce and avoid the high cost of full dry-cooling systems. By combining the features of a dry cooling tower and a wet cooling tower, it is possible to create a hybrid cooling tower that offers reduced operating costs for particular conditions (15).

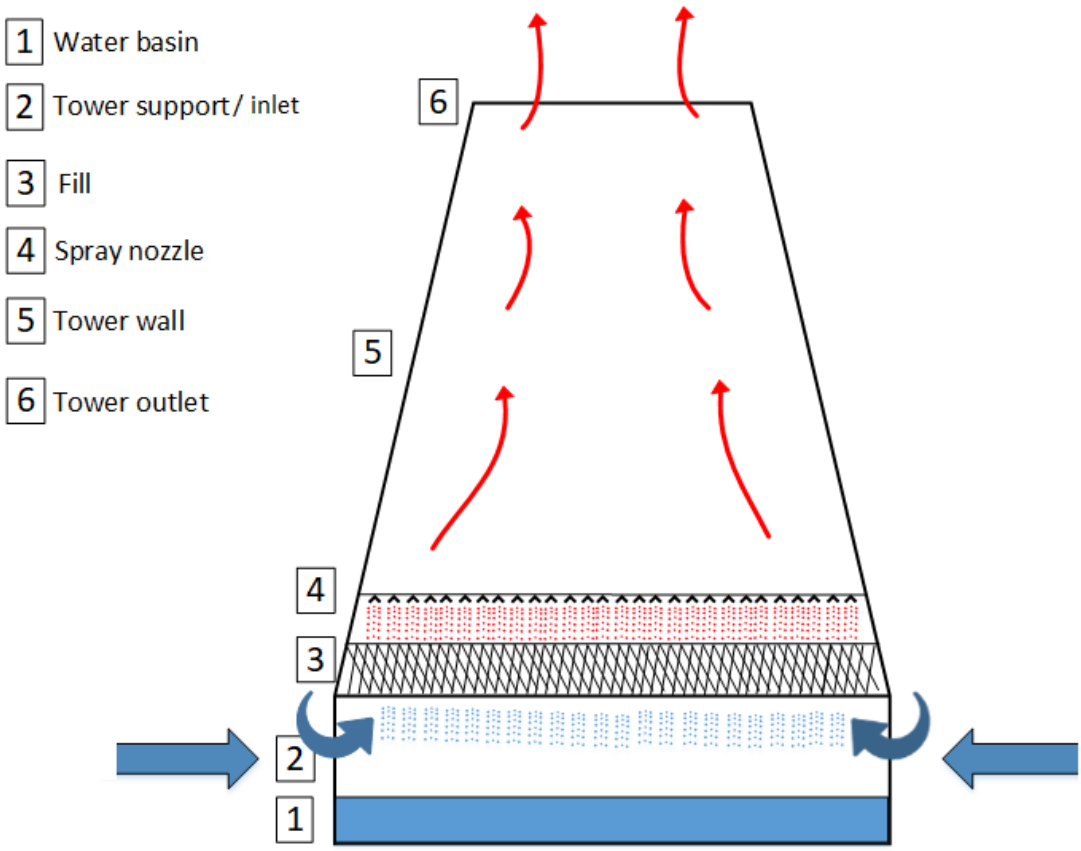

Figure 1.5. Configuration of the NDDWT.

1.2.2. Natural draft dry cooling towers (NDDCT)

In NDDCTs, the density difference due to the temperature difference, between the inside and outside of the tower creates a buoyancy draft, which circulates the inside air toward the top of the cooling tower. The circulating ambient air passes over the radiators, which are installed at the inlet of the towers, and cools the warm water in the radiators (16)

(Figure 1.6). In the cooling process of this system there is no direct contact between the hot water and the ambient meaning there is no water losses.

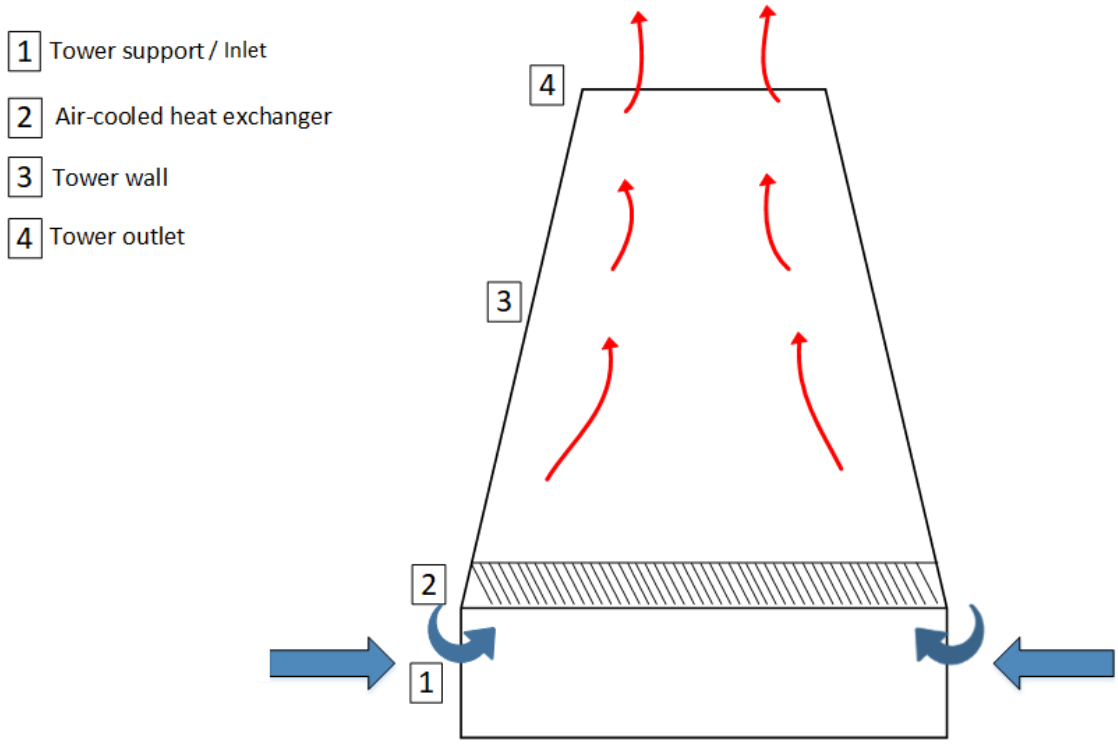

Figure 1.6. Configuration of the NDDCT.

In NDDCTs, the heat exchangers can be arranged horizontally at the inlet cross-section (as seen in Figure 1.6) or vertically around the inlet of the tower. The vertical heat exchanger bundles are usually arranged in form of deltas as shown in Figure 1.7 to maximize the heat exchanger area. In this system, the water distribution is simple due to the bundles are self-supporting which results in lower cost compared to the other layouts.

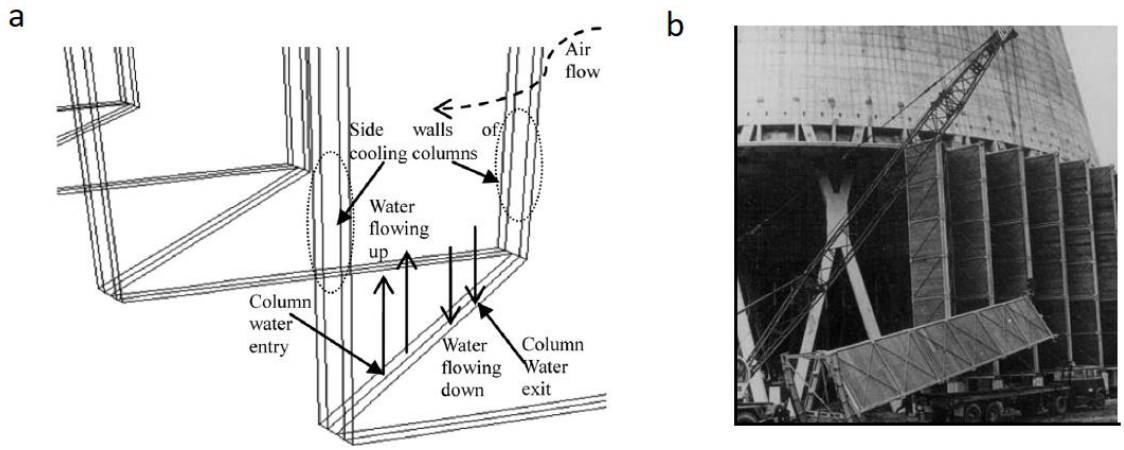

Figure 1.7. a) Sketch of cooling delta and boundaries in one column (17) b) Installing a heat exchanger delta at Gyongyos Hungary (15).

Alternatively, the heat exchangers can be arranged horizontally in the form of an A-configuration (Figure 1.8) in which two heat exchanger bundles are inclined with respect to each other at a specific angle with the delta heat exchanger bundles, the aim of this arrangement is to maximize the heat exchanger area facing toward the buoyant air.

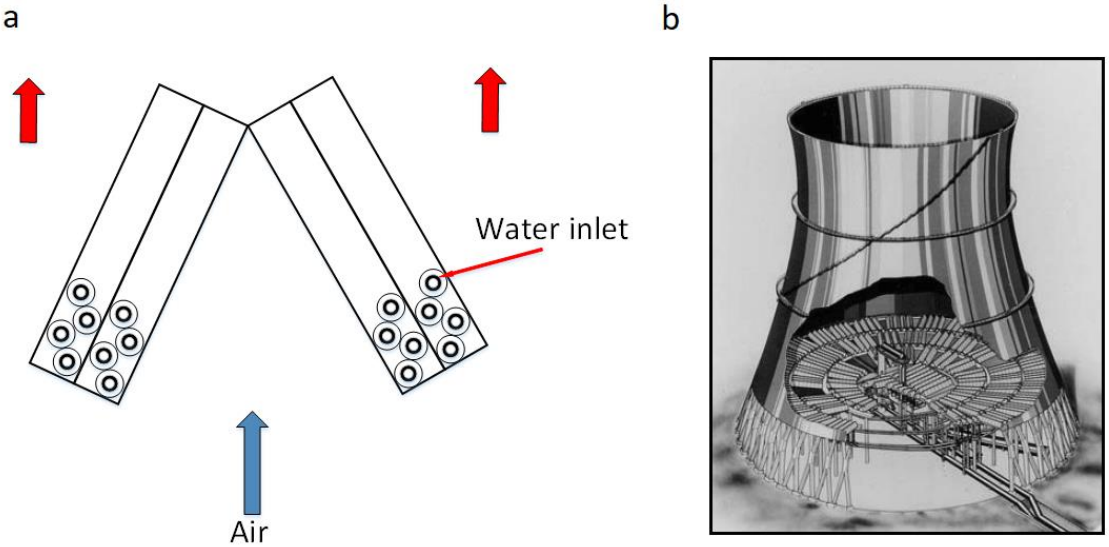

Figure 1.8. a) A single A-frame heat exchanger bundle b) heat exchanger arrangement within Kendal cooling tower in South Africa (15).

1.3. Effect of wind on the natural draft cooling towers

One of the challenges faced by NDDCTs is the effect of the ambient conditions including changes to the ambient temperature, and crosswinds (18-21). Crosswind effects in particular are complicated and difficult to predict, meaning natural draft cooling towers are typically designed on the assumption of calm ambient conditions.

In the absence of the wind, heated air rises undisturbed from the tower's outlet vertical as shown in Figure 1.9a. Wind deflects the plume as it exits the cooling tower causes the effective exit area to become smaller compared with the usual design conditions, as shown in Figure 1.9b. At very high crosswind speeds, the blocked plume leads to a decrease in the air temperature inside the tower to the extent that the density of air inside and outside the tower are nearly identical. This impairs the buoyancy driven flow and decreases the thermal performance of the natural dry cooling tower. In this case, the plume exiting the tower is not visible and results in a phenomena known as cold flow intake, as illustrated in Figure 1.9c (22).

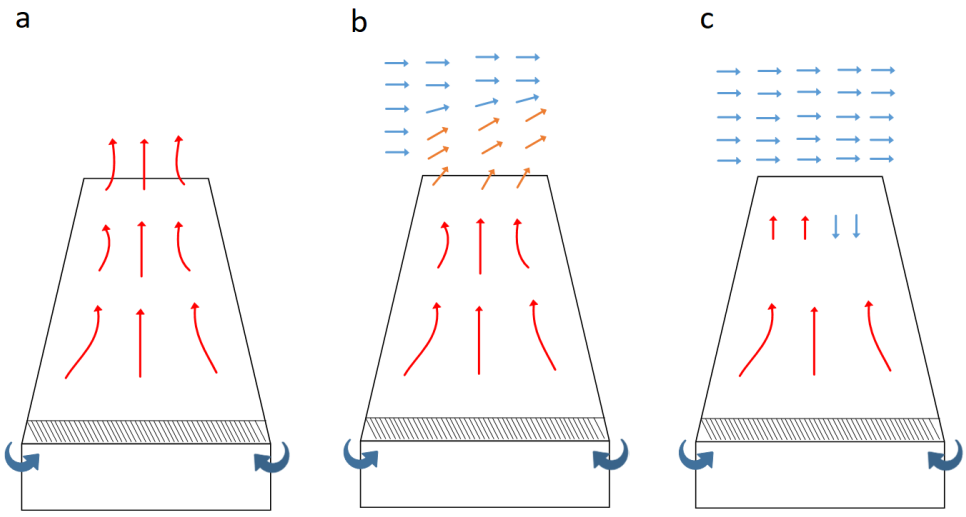

Figure 1.9. Schematic view of velocity vectors at the tower outlet at a) no-wind condition, b) moderate wind speed, and c) dominant wind speed.

For natural draft dry cooling towers with horizontal heat exchanger bundles, the wind passing through the bottom of the tower can cause a low-pressure zone underneath the heat exchanger. This can lead to hot air inside the tower being drawn back through the heat exchanger bundles, thus forming a hot air recirculation that reduces the effective heat transfer area of the bundles as shown in Figure 1.10 (23).

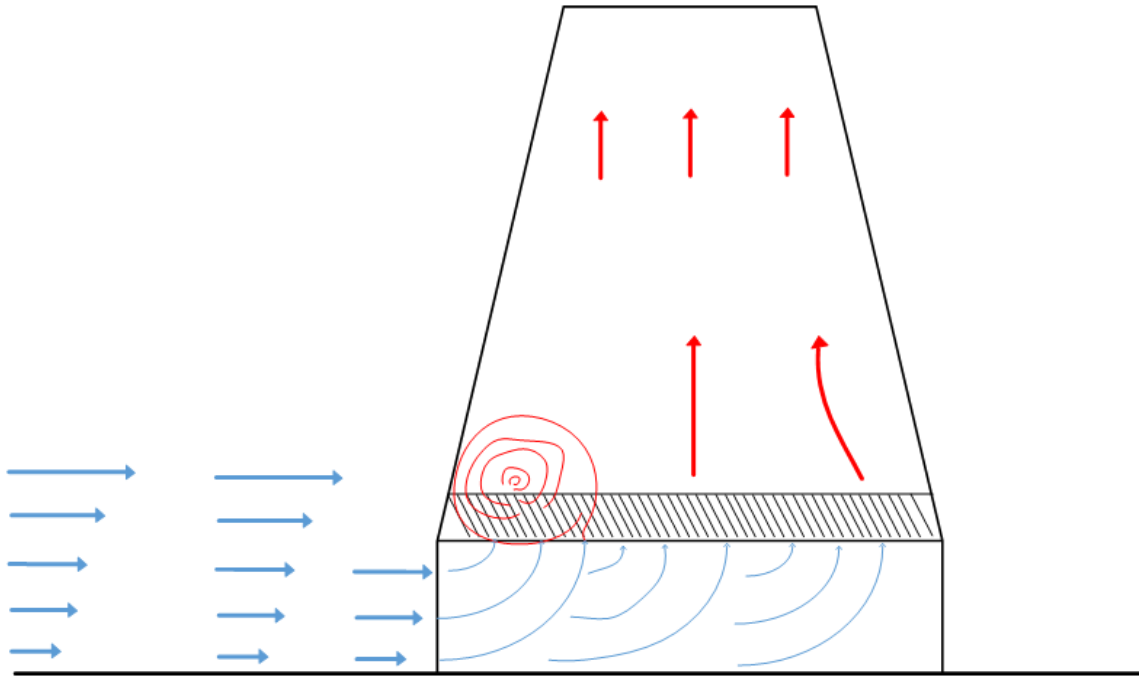

Figure 1.10. Schematic view of flow field at bottom of the tower in presence of crosswinds.

Given these challenges, numerous studies have looked at cooling tower performance using three main methods: full scale/field measurements, wind tunnel (lab-scale) measurements, and numerical and mathematical modelling.

A challenge of full-scale measurements is that they require lots of effort to perform a controlled experiment, and the performance of the system can be affected by the rapid changes in ambient conditions. These rapid changes include the changes in magnitude and direction of the crosswind, air humidity, and weather conditions. Also, installing and maintaining the instrumentation in the real cooling tower is expensive and difficult. Therefore, the findings from the full-scale measurements are often lacking detail and

make it difficult to understand the flow regimes and resultant heat transfer mechanisms (24). That said, Zhang et al. (25) performed a full scale experimental study on the performance of a 150m high NDWCT before and after it underwent structural improvement. The measurements in this study were limited to the crosswind velocity and water outlet temperature.

In another field study, conducted by Wei et al. (26), the temperature field inside a 125m high tower and crosswind speed were measured using temperature sensors and airflow anemometers. However, the only results presented were the mean temperature along the annular radiator and the central axis.

In summary, very few studies have used field tests to systematically investigate the performance of the NDDCTs at different ambient conditions due to the complexity of the instrumentation, and the lack of control over the ambient conditions. Therefore, a number of researchers have used scaled models to investigate the effect of wind on natural draft cooling towers in wind tunnels (26, 27).

Chen et al. (28) used with a scale of 1:100 from a real model of height of 85m. An experimental study on a 1:100 scaled model of a NDWCT was also performed by Alavi and Rahmati (29). According to the theory of dynamic similarity, all relevant force ratio should be identical between model and its prototype. In both (28, 29), the similarity was performed for Froude number which represents the inertial force of crosswind and the driving force of buoyancy and viscous forces were neglected.

Gao et al. (30) conducted an experimental study to determine the temperature profiles inside a NDWCT under crosswind conditions using a scale model 37cm x 68cm x 85cm (top outlet diameter x bottom diameter x height). The results indicated that at a no-wind condition, the heat and mass transfer distributions within the tower were uniform.

However, the height of the scaled model meant that the generated natural draft was much smaller than for a real cooling tower.

Previous studies using dynamic similarity was restricted to considering only the velocity ratio and Froude number. Satisfying both Reynolds number and Froude numbers is not possible in small scale models (24). Therefore, the lab scaled results are mainly considered as qualitative results and are used to provide general understanding of the performance of the real cooling tower. A summary of parameters used for dynamic similarity is listed in Appendix A.

In this regard, previous studies have shown that CFD simulations are reliable and can achieve an acceptable agreement with full scale measurements (31). Perhaps the most frequently used means of examining the heat and mass transfer processes in cooling towers is the use of CFD simulations. If these are accurately and carefully set up, they can provide a useful representation of the processes occurring in real towers. As the thermal and flow terms in the cooling towers subject to crosswinds are highly coupled, CFD simulations can be applied to investigate this complicated phenomenon.

1.3.1. CFD simulation of NDCT with vertical heat exchangers

Chen et al. (32) developed a CFD method to investigate the cooling performance of a 165m high NDWCT. The accuracy of the CFD model was validated by comparing the CFD results with the temperature distribution data obtained from the real cooling tower. CFD simulations have also been used in numerous studies (33-38) to investigate the performance of large NDWCTs for both windy and no-wind conditions, with the CFD simulations validated by comparing the predicted temperature distribution with that inside the tower.

In their study, Ma et al. (39) performed a numerical analysis in an attempt to understand the effect of crosswinds on a NDDCTV, and attempted to introduce windbreak walls around the tower. The results showed that adding a windbreak wall around the tower affected the flow field inside the tower.

An interesting outcome of the CFD simulations in (17, 40) was that flow circulations inside the tower reduce the air mass flow rate passing through the tower that consequently negatively affect the cooling capacity. Similarly, it has been shown that high crosswind speeds lead to a flow separation occuring behind the tower and results in a rotating flow circulation, or vortex. As such, when the swirling velocity of the flow at the leeward section is higher than the draft speed in the tower, the hot air cannot exit via the tower's outlet (41-44). In essence, the crosswind increases the flow resistance at top of the NDDCTV which reduce the outlet flow rate of the cooling tower. As further evidence of this, Wang et al. (43) demonstrated that increasing the crosswind speed increased the extent of vortex at the top of the tower. They also claimed that for crosswinds speed greater than 15 m/s, the crosswind becomes favourable, however, they didn't identify the underlying reason for this behaviour.

To counter the effect of the vortex, and enhance the performance of a NDDCTV, Goodarzi by proposed a novel tower geometry which entails a windbreak at top of the cooling tower (16). The results showed that the proposed configuration could mitigate the negative impact of the crosswinds. In another study Goodarzi and Keimanesh applied radiator-type windbreaks around the NDDCTV (45). They concluded that radiator type windbreakers can significantly improve the cooling efficiency. Also, they proposed using savonius wind turbines as windbreaks for the NDDCTV, however the practicality of the proposed system was not discussed. In these studies, it was observed that changing the geometry of the cooling tower, adding components such as windbreaks, and adjacent

objects could significantly change the flow behaviour around the cooling tower. Appendix A contains the summary of previous studies on NDDCTV.

1.3.2. CFD simulation NDCT with horizontal heat exchangers

The performance of an internal horizontal arrangement (NDDCTH) is less vulnerable to wind compared to an (NDDCTV) arrangement (46). Under equal conditions with the absence of atmospheric disturbances, Du Preez (47) stated that towers where heat exchangers are arranged horizontally inside the tower are less sensitive to crosswinds than NDDCTV. A comparative study was performed by Du Preez and Kröger (48) between NDDCTVs and NDDCTHs. Although the initial costs of a horizontal arrangement are higher than for vertical, the thermal performance of the former in windy conditions was shown to be superior. The weaker performance of the NDDCTV is mainly due to the severely distorted air flow distribution of air passing through the heat exchanger.

Al-Waked and Behnia (19) demonstrated that the performance of the NDDCTH decreasing by increasing the crosswind speed from 0 to 20 m/s. Wu et al (49) investigated the effect of crosswind on the flow and heat transfer characteristics of a NDDCTH. For all wind speeds, the outlet water temperature increased with increasing crosswind speed. Their results demonstrated that during windy condition, the crosswind causes a low-pressure region beneath the heat exchanger bundles located at the windward side of the tower which sucks the hot air back inside the tower, causing flow circulation. The negative effect of the crosswind on NDDCTH occurs in the windward area and during increasing crosswind speed where the affected zone expands.

Different types of cooling tower including natural, mechanical, wet, and dry types were discussed and it was revealed that by using NDWCTs a higher conversion efficiency yield is possible compared to the NDDCT (50). However, the targeted places for CST power plants are often desert areas with high solar intensity and low water availability (51, 52).

Given the scarcity of water in these types of locations, NDDCTs are made to use the atmospheric air temperature alone as the heat sink.

It was discussed that CFD simulations can analyse the performance of NDCTs comprehensively and it was revealed that the airflow behaviour passing through the cooling towers can be affected by the prevailing ambient conditions and objects around or inside the cooling tower.

The height of cooling towers investigated in the previous studies were over 100 m which are of a size suitable for conventional power plants. The overall size CST power plants are likely to be smaller compared to the conventional power plants. A summary of previous studies on NDDCTH can be found in Appendix A.

1.4. Analysis of short NDDCT in CST power plants

In the preceding section it was shown that the prevailing wind speed plays a significant role in the cooling capacity of both wet and dry natural draft cooling towers. However, a common factor of these studies, was that the towers were all over 100m in height (due to the heat load required in conventional power plants). In concentrating solar thermal power plants which are likely to be smaller compared to the conventional thermal power plants, cooling towers are likely to be at a much smaller height. Similarly, CST power plants are likely to be located in arid areas with high solar intensity (51, 52). Given the scarcity of water in these types of locations, it is foreseeable that designers will favour the use of dry cooling approaches, where heat is rejected to the ambient air. With this in mind, research on short NDDCTs has started to gather a degree of attention, particularly from the University of Queensland.

Lu et al. (23) first proposed a small NDDCT for use in renewable power generation, and analysed the concept using computational analysis. This resulted in the suggestion of a cylindrical NDDCT with an internal heat exchanger 15m in height and 12 m diameter.

The rationale for this being that cylindrical towers are more economic to build in remote areas compared to those of hyperbolic shape. CFD simulations of the proposed NDDCT were performed in this study and the results indicated that this short NDDCT was highly vulnerable to crosswinds. In this study, it was shown that increasing crosswind speed resulted in a flow circulation at both the bottom and top of the cooling tower, as shown in Figure 1.11.

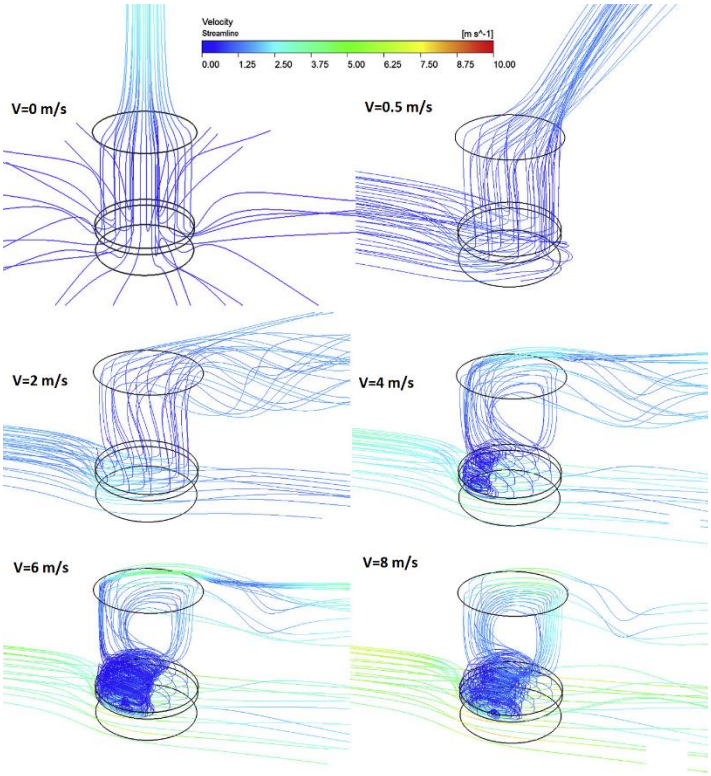

Figure 1.11. Velocity streamlines at different crosswind speeds (23).

The same authors continued their research by introducing an internal tri-blade windbreak system to the proposed NDDCT in another study (53). In this later study, the effect of the wind incidence angle on the performance of the tower was investigated. It was found out that the tower performance could be improved at wind incidence angles of 0° and 60°and that the flow circulations at the bottom of the tower could be characterised using vorticity magnitude. In addition, they suggested that that the tri-blade wind break could be placed at angle of 0° with respect to the most frequent wind direction.

In a subsequent study, the findings of this model were validated using a scaled model (1:12.5) in a wind tunnel test (54), although scaling of the Froude number was not possible. In addition, the study also described the differences in the effect of wind on a short and tall NDDCT. This study showed that the heat transfer rate of the short NDDCT would initially decrease with an increasing crosswind speed, but eventually increases with further augmentation in wind speed. Conversely, they suggested that the heat transfer rate in large NDDCTs continuously decreased with increasing the wind speed.

Having developed an understanding of the performance of short NDDCTs the University of Queensland developed a full-size NDDCT (Figure 1.12) to undertake further research. This cooling tower (Gatton NDDCT) was developed with a view to being used with CST power plants such as those being developed by the Australian Solar Thermal research Initiative (ASTRI). On this basis, Li et al. (55) investigated the performance of the Gatton NDDCT under windy conditions. The results demonstrated that the performance of the tower decreased to a minimum value at a crosswind speed of 6 m/s and then increased at higher crosswind speeds. In exploring the reasons for this, the work focussed extensively on the flow characteristics at the bottom of the tower. At a crosswind speed of 3 m/s, the wind caused a low-pressure region at the windward side of the tower which decreased the upward air flow. This resulted in a reduction in the cooling performance of the heat exchanger in this area.

Figure 1.12. Gatton cooling tower.

In a later study it was suggested that the cooling performance of the Gatton NDDCT could be increased by 18% by optimizing the hot water mass flow rate among the heat exchanger bundles (56) during certain wind speeds. It was proposed that the water mass flow rate in each heat exchanger bundle could be controlled by monitoring the airflow through them.

Li et al. (57) continued their research by performing a full scale experimental study on the Gatton NDDCT. Two constant heat loads of 600 kW and 840 kW with ambient temperatures varying between 20°C and 32°C. The heat transfer coefficient of the heat exchanger bundles was measured and compared with the manufacturer's heat transfer coefficients and were shown to be in close agreement. Another study also examined the effect of crosswind on the Gatton NDDCT using a full-scale experiment (58). The temperature field inside the cooling tower and at the heat exchanger bundles were measured using temperature sensors installed inside the tower. Crosswind speeds recorded in this study were 0.6 m/s, 2.3 m/s, 5.5m/s, and 8.3 m/s. The temperature of the

heat exchanger bundles was compared with CFD simulations and the results were again in close agreement.

As previously mentioned, the cold inflow is an unfavourable air turbulence at the top of the cooling tower and has a significant negative effect on the performance of natural draft cooling towers. The cold flow intake from top of the Gatton NDDCT was performed in a full-scale experiment and the tests demonstrated that cold flow intake can increase the water outlet temperature up to 3°C (59).

Furthermore, experimental and numerical studies have been performed on the transient start-up of the Gatton NDDCT by Dong et al. (60, 61). Start-up time is defined as the time taken from initial running the cooling tower until it reaches a stable operating condition. The results of this study indicated that crosswinds affect the start-up time, and that this parameter is shorter when the flow inside the cooling tower is uniform. As a response to the effect of wind on the Gatton NDDCT, Liu et al. (62) proposed an inlet cover to improve the performance of short NDDCTs. It was shown that an inlet cover did not affect the flow within the tower for the no-wind condition but improved the performance of during windy conditions.

Similarly, in order to improve the performance of the Gatton NDDCT, Lu et al. (63) proposed introducing an air jet into the tower to increase the total air mass flow rate through the heat exchanger bundles. Using a CFD model of the Gatton tower, this group found that the swirling plume enhanced the tower's thermal performance. Previous short NDDCTs are summarized in Appendix A.

1.5. Multi-tower cooling systems

To this point, all the studies mentioned have been devoted to an isolated tower, however the National Renewable Energy Laboratory (64) has shown that there has been a number of CST power plant projects that have been developed over several stages. Despite the

potential for using windbreaks to reduce the effect of wind on the performance of NDDCTs, as the capacity of CST plants is increased, additional cooling is required which necessitates the addition of more NDDCTs. When adding these cooling towers, there is a need to be able to position them relative to prevailing wind conditions correctly so that their performance as a group is maximised. To do this, an understanding of the effect they have on one another is needed, particularly under windy conditions.

Recently companies such as VAST Solar have been working on the development of modular CST power plants in Australia. One of their finished projects is Jemalong with 6MW capacity. As can be seen in Figure 1.13, this CST power plant consists of five modular towers which are connected to a central thermal energy storage unit. In such sites, the power generation can be started after completion of the first module and the cooling could be satisfied by a short NDDCT such as that proposed by University of Queensland. However, to increase the power generation, by adding more modules, there is also a need to increase the condenser area. This can be met by adding more cooling towers to the site.

Figure 1.13. The 6MW Jemalong CST power plant accomplished but Vast Solar.

One challenged posed by this is that most research has been devoted to isolated cooling towers, whereas very few studies have investigated multiple cooling towers under windy conditions. Under these conditions each cooling tower with a group may exhibit different characteristics from an isolated cooling tower. To this end, the performance of two cooling towers under windy conditions was experimentally and numerically investigated by Zhai and Fu (65). Their study discussed the relationship between the cooling efficiency recovery and the size of the wind-break walls. Here, the aim of study was to observe the effect of windbreaks on the flow field and the interactions of the towers during no-wind conditions and windy conditions were not been discussed in detail.

Similarly, Irtaza et al. (66) used turbulence modelling to explore the effect of wind on configurations of three and five cooling towers without modelling the heat exchanger. In this work, the authors did not study the effect of the wind on thermal performance, instead focusing and only a non-dimensional pressure coefficient defined to describe the aerodynamic aspect of multiple cooling towers interacting with each other. In this study the heat exchangers were not modelled and the effect of wind on the tower's shell was addressed.

Wu and Koh (67) developed a mathematical model to predict the behaviour of plumes, including: excess plume temperature, humidity and liquid phase moisture (water droplets), plume trajectory, width, and dilution, at the merging locations from multiple cooling towers. This study also explored the properties of plumes from the top side of four cooling towers but did not explore the cooling towers' thermal performance and the interaction between the towers.

Liao et al. (68) investigated the effect of tower spacing on the performance of two large NDDCTVs. They suggested that during windy conditions, when wind is blowing parallel to the towers, the windward tower could provide protection for the leeward tower.

However, as these results were for large NDDCTs with vertical heat exchanger bundles, it is unclear how this might translate to shorter towers such as the Gatton tower.

The effect of neighbouring buildings on the performance of two large NDDCTVs was examined by Yang et al. (69). In this study, the interaction of the towers during different ambient conditions was discussed and the results showed that at high crosswind speeds, warm air circulation occurs at the side backward surface of the heat exchangers which reduced the cooling performance of the towers.

After the collapse of three natural draft towers at the Ferrybridge Station in the UK (Figure 1.14), found to be due to the tower spacing of the towers, some researchers investigated the interference effects between multiple cooling towers. These included wind pressure, structural response, membrane forces, bending moments, shear forces and displacement (70-75). However, the thermal performance of the towers was not discussed and only the structural behaviour of the towers was systematically investigated. This means the effect of wind on the towers was investigated without considering the thermal source inside or around the cooling tower (heat exchanger). The presence of heat exchangers will impact the flow field and the findings of these studies may change by considering the heat exchangers.

The previous studies investigating the effect of wind on multi-tower systems are summarized in Appendix A.

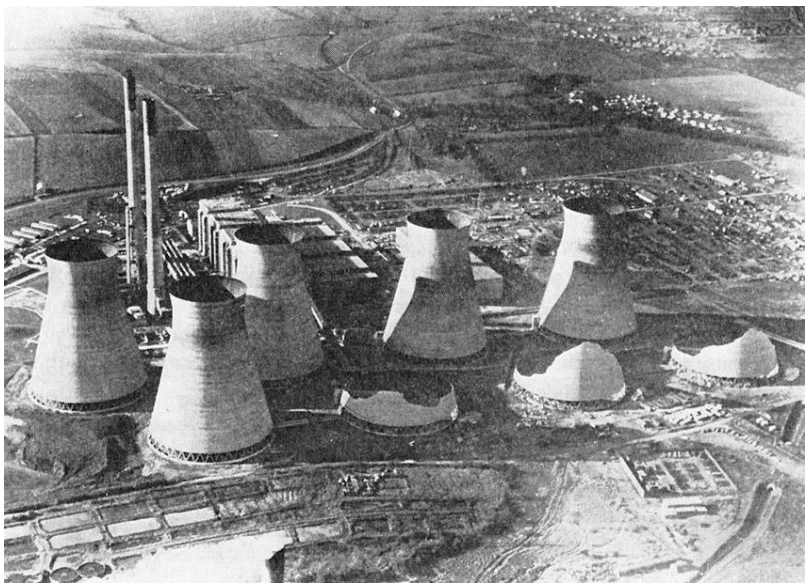

Figure 1.14. Collapses of cooling towers in Ferrybridge 1965 (76).

In summary, in previous multi-tower analysis, the effect of wind velocity has been discussed with regards to the performance of large NDDCTs with vertical heat exchanger bundles. However, the effect of wind velocity on the performance of the multiple short NDDCTs has not been discussed and there is no understanding on how these towers interact with each other at different layout configuration and ambient wind conditions.

1.6. Research question and objective

From the literature, it is apparent that in multi-tower systems interaction may occur between the adjacent towers and that these interactions may change the wind's effect on the towers. The performance of short NDDCTs, which are suitable for CST plants with limited power generation have been shown to be highly vulnerable to environmental conditions, and the initial design of the cooling tower is usually suitable for calm ambient-air conditions. The differences between a small isolated NDDCT and a multi-tower system are not clear, and they merit thorough investigation. The lack of attention paid to the interaction of multiple NDDCTs systems has raised the question of how they can be placed with respect to each other if, for example, a CST plant is expanded and requires additional cooling capacity.

A review of the current literature shows that none of previous studies have investigated the effect of wind speed on the performance of multiple short NDDCTs. Therefore, this investigation will address the current knowledge gaps by addressing the following research question:

How do multiple short NDDCTs interact with each other at different tower spacings and with different tower layouts, and what is the effect on their cooling capacity?

Chapter 2: Performance of NDDCTs for no-wind condition

2.1. Introduction

From the literature review, it was apparent that NDDCTs are affected by wind. However, to appreciate the behaviour of cooling towers under windy conditions, it is important to first understand their performance during no wind conditions. The performance of the NDDCTs at a no-wind condition is unknown and no study has investigated the interaction of the towers at different tower spacings during the no-wind condition. In this chapter, the performance of short NDDCTs subject to the no-wind condition will be examined.

2.2. Performance of a single NDDCT under the no-wind condition

2.2.1. Method

As a benchmark, it was decided to investigate the airflow characteristics around a single NDDCT and compare the results to data available in the literature. Each NDDCT must satisfy the equations 2.1 and 2.2 to achieve aerodynamic and thermodynamic balance:

$$\Delta P \approx (\rho_{ao} - \rho_{ai}) g (H_t - H_{hx}) = (\sum flow\ resistance) \quad (2.1)$$

$$Q = \dot{m}_a C_{pa} (T_{ao} - T_{ai}) = \dot{m}_l C_{pl} (T_{li} - T_{lo}) = h_u A F_T \Delta T_{lm} \quad (2.2)$$

Where ρ_{ao} and ρ_{ai} are the air density at the inlet and outlet of the tower, H_t and H_{hx} are the height of the tower and heat exchangers, $\dot{m}_a$ is the air mass flow rate into the tower, T_{ao} and T_{ai} are the air temperature at the outlet and inlet, and $\dot{m}_l$ is the liquid mass flow rate. Equation 2.1 means the total pressure drop over various components of the tower must be balanced by the buoyancy force. Equation 2.2 states that the heat transferred into the air is equal to the heat extracted from the cooling liquid (water) and that this heat is transferred through the heat exchangers (23).

As the starting point for this no-wind study it was decided to examine the behaviour of a cylindrical tower and horizontally arranged air-cooled heat exchanger. To do this, a cylindrical natural draft dry cooling tower model with 20m height and 12.5m diameter with an inlet height of 5m, as shown in Figure 2.1, was modelled using computational fluid dynamics. This model is an approximation of an actual 20 m-tall steel-membrane hyperbolic cooling tower built in a campus of The University of Queensland (77), discussed in the preceding literature review chapter.

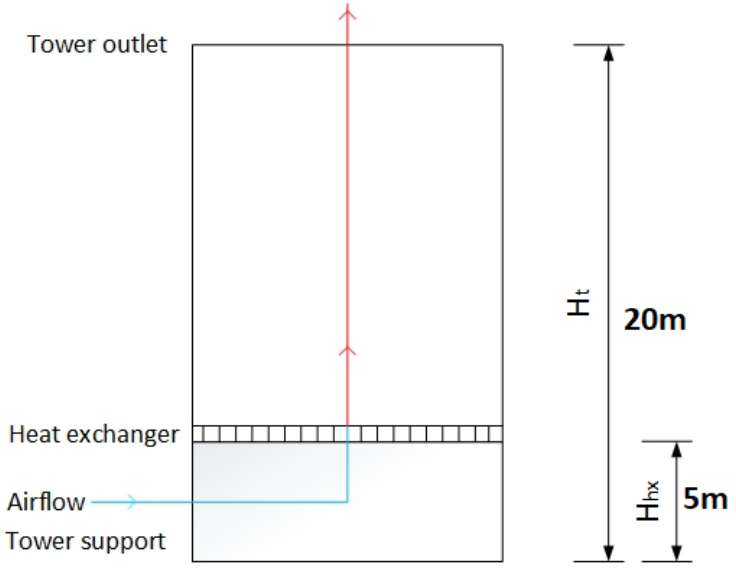

Figure 2.1. Cooling tower configuration.

The airflow resistance in Eq. 2.1 includes the pressure loss coefficient of the tower support, heat exchanger, and tower outlet. In this equation there is no flow resistance related to the wall profile which means that wall profile is not a major factor in determining the airflow resistance within the tower.

In this tower, the heat exchangers are installed horizontally at a height of 5 m off the ground. The heat exchanger parameters taken for the NDDCT were established by the University of Queensland (77) with a tube arrangement as shown in Figure 2.2 and detailed in Table 2.1.

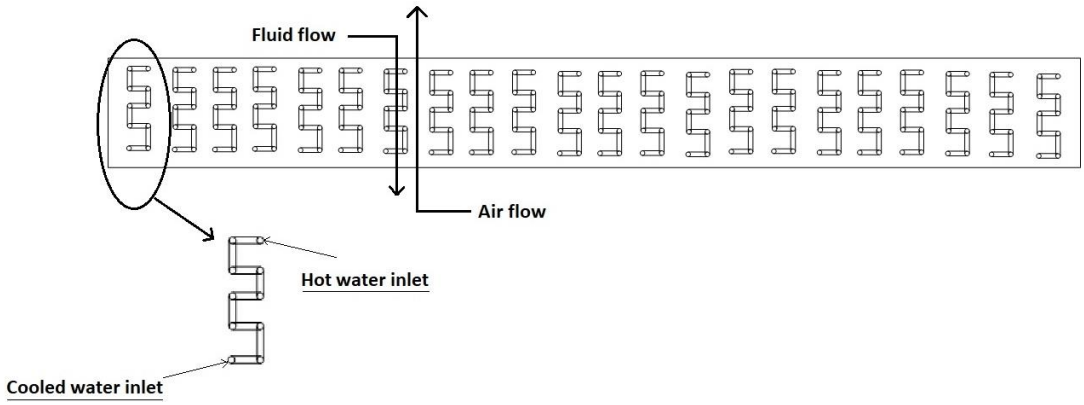

Figure 2.2. Heat exchanger bundle arrangement.

Table 2.1. The detailed data for the heat exchanger and tower dimensions.

Heat exchanger parameter	Value	Unit
Hydraulic diameter of tube	0.009	m
Inside area of tube per unit length	0.0285	m^2
Inside cross-sectional flow area	6.40×10^{-05}	m^2
Length of finned tube	3.84	m
Effective length of tube	3.79	m
Number of tube rows	5	#
Number of tubes per bundle	220	#
Number of water passes	10	#
Fin root diameter	0.0095	m
Fin pitch	0.0021	m
Equivalent circular fin diameter	0.0205	m
Tower height	20	m
Tower diameter	12.525	m
Tower's inlet height	5	m

With this in mind, a single tower was modelled in a cylindrical domain with a height of 90 m, a diameter of 144 m and boundary conditions, as shown in Figure 2.3. This domain was selected since a similar boundary domain had previously been used to investigate the performance of short NDDCTs for the no-wind condition (53, 55). The computational domain and the cooling tower were meshed using structured elements. During no wind condition, the pressure at the boundaries is known which atmospheric pressure is. This enabled, a pressure inlet boundary condition (atmospheric pressure) to be assigned to the side of the domain, and the top of the domain was set to be a pressure outlet (atmospheric pressure) (53).

Grid independence tests resulted in 2,300,000 elements and after mesh sensitivity analysis the deviation of results was found to be less than 1%. The details of the mesh sensitivity analysis for this model is shown in Appendix B.

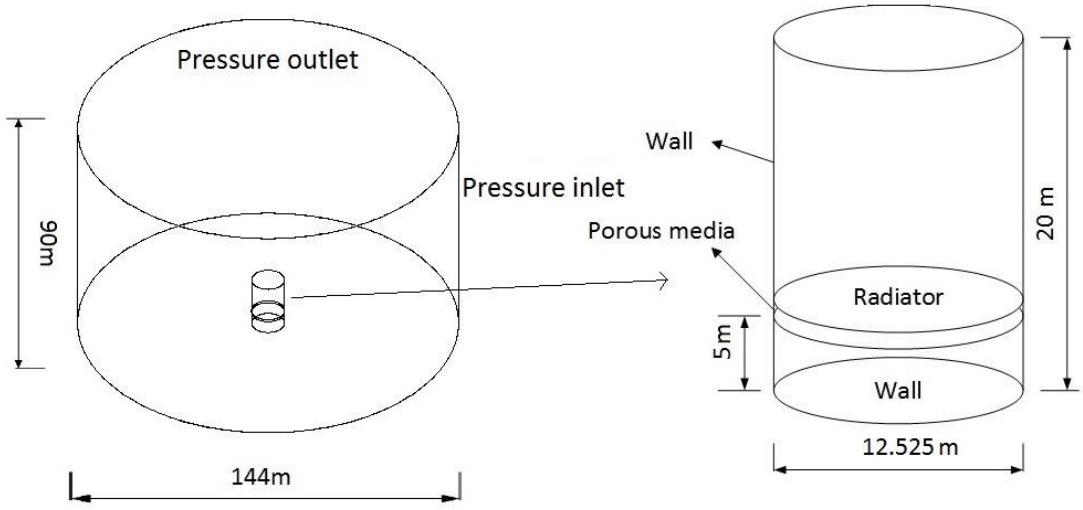

Figure 2.3. Model geometry, computational domain and boundary conditions.

To check the impact of thermal stratification at the boundary domain, a temperature profile was applied to the boundary domain using equation 2.4. During a clear dry day, a temperature-lapse rate of approximately -0.00975 Km^{-1} is often observed in the region of the surface boundary layer. This specifies the ambient air temperature at any elevation (15):

$$T = T_1 - 0.00975z \quad (2.4)$$

where T_1 is the temperature at ground level and z is elevation. However, comparing the simulation results of the domain, initially at constant temperature with that of a stratified temperature, showed that the heat rejection difference is less than 1%. Hence, a constant ambient temperature of T=20 °C was assumed.

Previously, in order to model the heat exchanger in the tower, a combination of a porous media zone and a radiator boundary condition was used, using the data from Table 2.1. The radiator model characterizes the heat transfer, while the porous media is included to capture the pressure loss within the heat exchanger. This effect is realised by adding a momentum sink in the governing momentum equations (55). This approach mirrored that which had been successfully used for heat exchanger modelling in short NDDCTs (23, 53, 55, 57).

Following on from this, the heat rejected to the surrounding air was given by Equation 2.5.

$$\dot{q} = h(T_r - T_{ao}) \quad (2.5)$$

T_{ao} is the temperature of air downstream of the radiator and h is the overall heat transfer coefficient which is estimated by empirical coefficient shown in Equation 2.6 for the tower (58, 63):

$$h = 150v_a^2 + 549v_a + 191 \quad (2.6)$$

For air flow pressure drop, the radiator model can simulate resistance to air flow in the direction normal to radiator face. However, it does not provide resistance in other two directions, i.e. velocity components parallel to radiator face. This will cause overestimation of the possibility of vortices occurring near the radiator, since the real

structure of, as the fin tube heat exchanger bundles can prevent horizontal air flow, allowing air to flow through the heat exchanger only vertically. Therefore, a porous media model is added to represent the pressure loss within the heat exchanger, leaving the radiator model to represent heat transfer only. In the porous media zone, an additional source term S_i representing the pressure loss within the heat exchanger is added to the momentum equation. S_i is expressed by Equation 2.7 (63):

$$S_i = -(\frac{\mu}{\alpha} v_i + C_2 \frac{1}{2} \rho v_i^2) \quad (2.7)$$

Where α (permeability) and C_2 inertial resistance factor are coefficients which were derived from an empirical pressure drop-air speed correlation provided by the manufacturer of the heat exchangers of the Gatton cooling tower (56). For the pressure loss calculation, the viscous resistance factor 1/ α = 331,211 is obtained and the inertial resistance coefficient factor C2 = 6.328 is used (56). The vertical air flow can be guaranteed by setting the resistances in the other two directions to be much larger than that in vertical direction (23).

The flow problem in this study can be stated as a steady state 3-dimensional CFD simulation. In doing this, a commercial RANS finite volume code (ANSYS FLUENT v17.2) was used to carry out these simulations, where the turbulent field was simulated using the realizable k-ε turbulence model. The realizable k-ε model has been extensively validated for a wide range of flows including rotating shear flows, boundary layer flows and separated flows and has been shown to be well suited to modelling both short and large NDDCTs (23, 49).

In CFD, the governing equations can be expressed in the general form shown in Equation 2.8:

$$\nabla.(\rho u\emptyset - \Gamma_\emptyset \nabla_\emptyset) = S_\emptyset \quad (2.8)$$

the expression of the $\emptyset$, $\Gamma_\emptyset, and\ S_\emptyset$ in the above equation are listed in Table 2.2.

Table 2.2. The governing equations of k- ε model.

	$\emptyset$	$S_\emptyset$	$\Gamma_\emptyset$
Continuity	1	0	0
x momentum	U	$-\frac{\partial p}{\partial x}+\frac{\partial}{\partial x}\left(\mu_e\frac{\partial U}{\partial x}\right)+\frac{\partial}{\partial y}\left(\mu_e\frac{\partial V}{\partial x}\right)+\frac{\partial}{\partial z}\left(\mu_e\frac{\partial W}{\partial x}\right)+\frac{\Delta p_x A_c}{V_c}$	μ_e
y momentum	V	$-\frac{\partial p}{\partial y}+\frac{\partial}{\partial x}\left(\mu_e\frac{\partial U}{\partial y}\right)+\frac{\partial}{\partial y}\left(\mu_e\frac{\partial V}{\partial y}\right)+\frac{\partial}{\partial z}\left(\mu_e\frac{\partial W}{\partial y}\right)+\frac{\Delta p_y A_c}{V_c}$	μ_e
z momentum	W	$-\frac{\partial p}{\partial z}+\frac{\partial}{\partial x}\left(\mu_e\frac{\partial U}{\partial z}\right)+\frac{\partial}{\partial y}\left(\mu_e\frac{\partial V}{\partial z}\right)+\frac{\partial}{\partial z}\left(\mu_e\frac{\partial W}{\partial z}\right)+\frac{\Delta p_z A_c}{V_c}$	μ_e
Energy	T	$\frac{1}{C_p}\left(\frac{qA_c}{V_c}\right)$	$\frac{\mu}{Pr}+\frac{\mu_t}{Pr_t}$
Turbulent energy	k	$G_k + G_b - \rho\varepsilon$	$\frac{\mu_e}{\sigma_k}$
Energy dissipation	ε	$C_{1\varepsilon}\frac{\varepsilon}{k}(G_k + C_{3\varepsilon}G_b) - C_{2\varepsilon}\rho\frac{\varepsilon^2}{k}$	$\frac{\mu_e}{\sigma_k}$

Where $\mu_e = \mu + \mu_t; \mu_t = C_\mu \rho \frac{k^2}{\varepsilon};\ C_{1\varepsilon} = 1.44;\ C_{2\varepsilon} = 1.92;\ C_{3\varepsilon} = \tanh\left(\frac{U_{pa}}{U_{pe}}\right);\ G_g = -g\frac{U_t}{\rho Pr}\frac{\partial P}{\partial y};\ C_\mu = 0.09; \sigma_k = 1.0; \sigma_{k\varepsilon} = 1.3; Pr = 0.74; Pr_t = 0.85$

For all simulations (except no-wind validation), the radiator temperature was set at 52 °C while the heat flux was allowed to vary. The pressure-based segregated algorithms: SIMPLEC was applied and the second order of upwind discretization method was applied to discretise the governing equations. The calculation results were obtained with the scaled residuals dropping to the order of 10^{-5}, except energy (10^{-6}), and the monitored variables (average temperature of the tower outlet) were stable.

2.2.2. Validation

To validate the method, and the accuracy of the applied numerical set, the results of the simulation were compared with the experimental results from the real NDDCT at the

University of Queensland (57, 59, 63). In these experimental tests, a constant heat flux was supplied to the NDDCT by an oil-fired heater for different ambient temperatures, and the air temperature leaving the heat exchanger was measured. In the CFD simulation, the same heat flux (845kW) was set as the radiator boundary condition (Figure 2.3), and the effect of changing the ambient temperature on the air exit temperature at heat exchanger was monitored. Figure 2.4 shows the comparison between the CFD results of this study and the experimental data obtained by Li et al. (57, 58), and indicates good agreement between them. These implies that the method is valid, and that the results of the simulation are a good replication of reality.

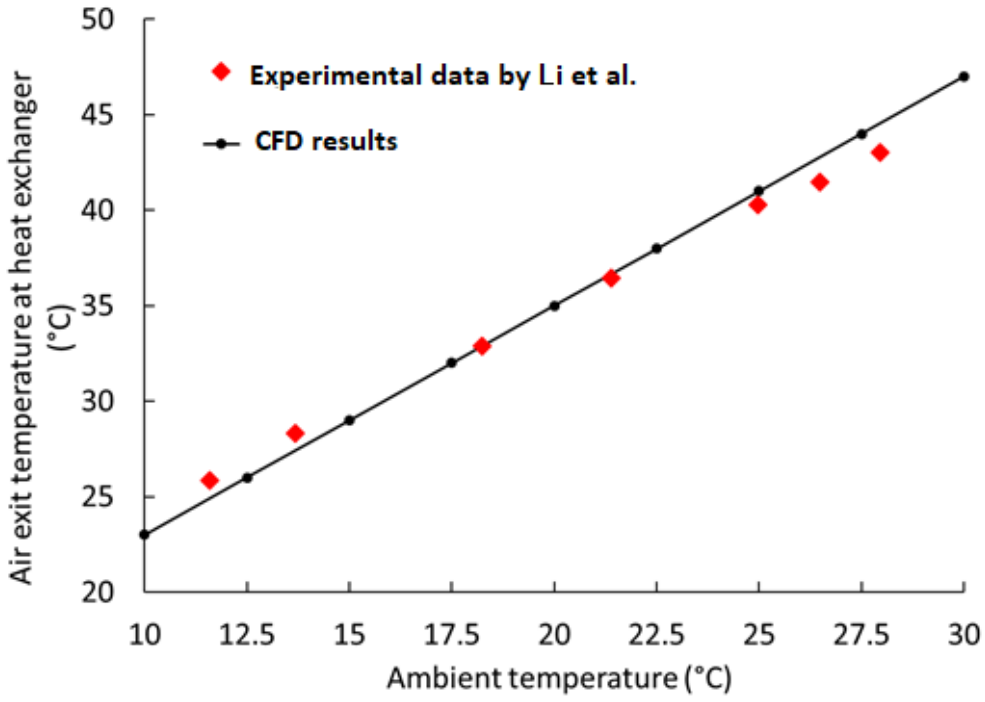

Figure 2.4. Comparison between the CFD results and the experimental data (57, 58, 63).

2.2.3. Results and discussion for a single tower under the no-wind condition

Having demonstrated that the simulation method was valid, in so much that the results obtained were in agreement with those physically measured, it was decided to examine the CFD results in more detail, with a view to understanding the transport phenomena

occurring in the tower. Figure 2.5 shows the temperature, pressure, and velocity distributions in an isolated cooling tower for the no-wind condition. The variable contours indicate an axisymmetric pattern which is likely due to uniform heat transfer throughout the heat-exchanger area, and the ability of the tower to draw air in from around its entire circumference. To demonstrate this, it can be seen that the surrounding ambient air was drawn into the tower through the horizontal heat-exchanger bundles due to the density difference between the inside and outside of the tower (Figure 2.5c). Figure 2.5b shows that the reverse-pressure gradient is noticeably observed inside the tower (low pressure region starts at the heat exchanger bundles and increases towards the outlet), especially around the heat exchangers, to balance the buoyancy force and viscous force.

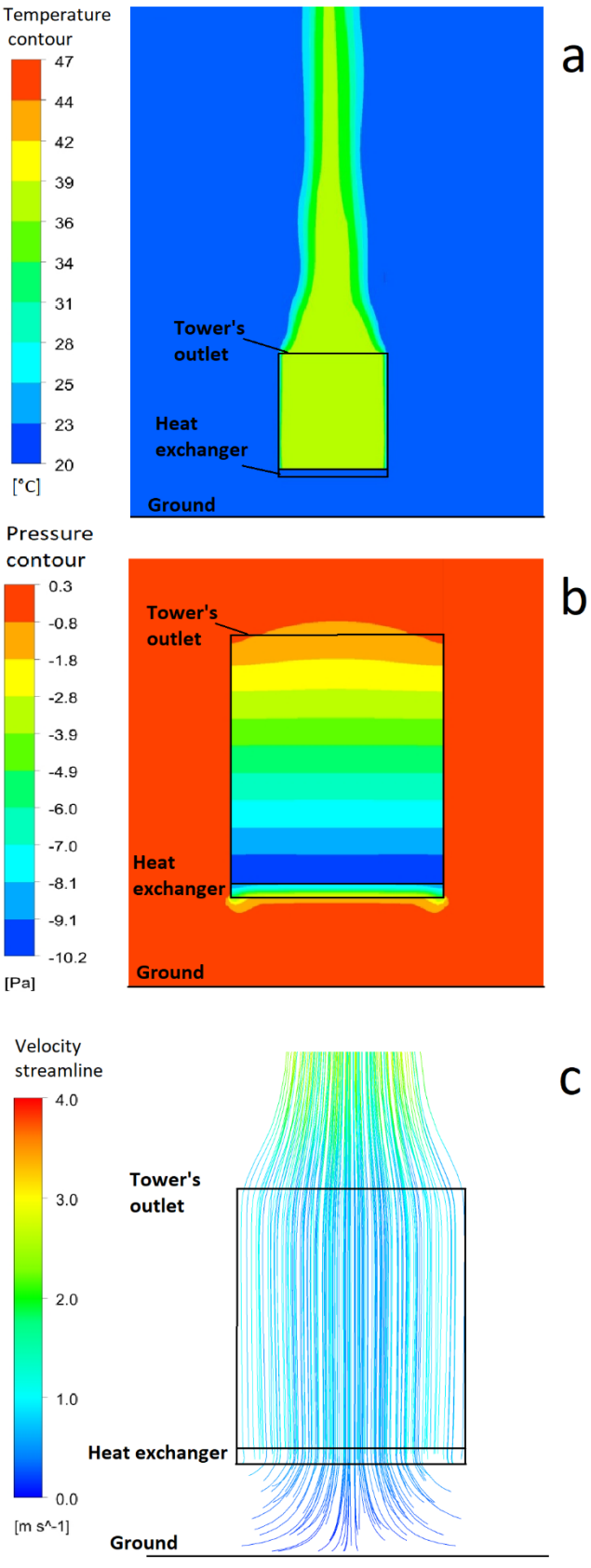

Figure 2.5. a) Temperature contour, b) pressure contour, and c) velocity streamlines at central vertical cross section of single NDDCT.

Furthermore, the velocity streamlines in Figure 2.5c are symmetric suggesting relatively uniform flow through the heat-exchanger. To illustrate this, the air velocity profile at different heights in the tower were examined as shown in Figure 2.6 (where r/R is the normalized radial distance from the centreline). The velocity distribution tends to become more uniform across the tower after passing through the heat exchangers, and the pressure drop caused by the heat exchangers reduces the velocity magnitude within the tower. The slow-moving air from the outlet of the tower is buoyant relative to the surrounding air due to the temperature difference. This temperature gradient causes the stagnant ambient air around the tower's outlet to become warmer and more buoyant which results in an acceleration of the outlet air. This explaining the contraction of the outflow plume seen in Figure 2.6 (line 3). These results are in broad agreement with those previously reported for the Gatton tower (55).

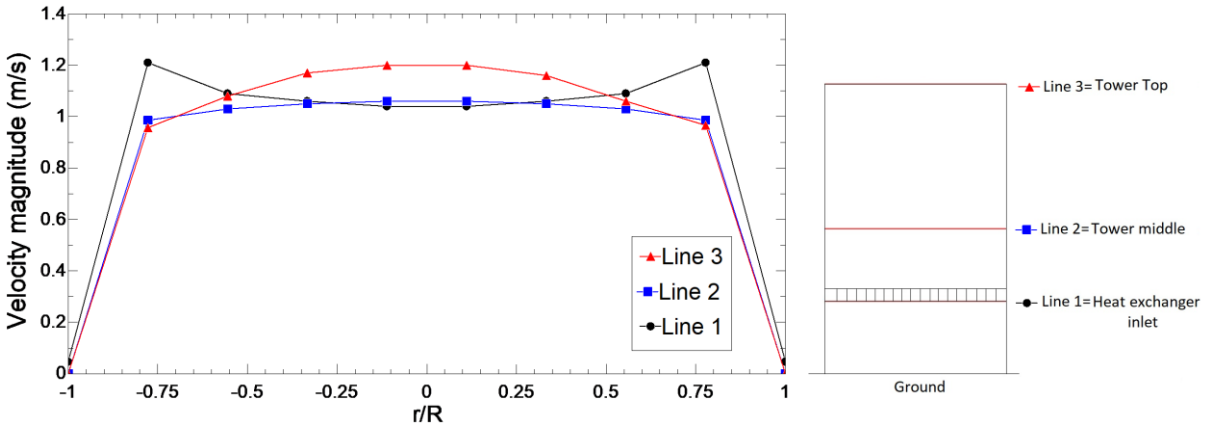

Figure 2.6. Velocity profile at three different tower positions.

2.3. Performance of two NDDCTs under the no-wind condition

2.3.1. Method

Having shown that the modelling method could satisfactorily predict the performance of a single tower during the no-wind condition, this method was then applied to a multi-tower configuration. The two-tower simulations were performed for eight tower pitch spacings, between 5D and 1.1D (where D is the tower diameter of 12.525 m). The

dimensions of the computational domain (Figure 2.7) were selected based on a domain sensitivity analysis which showed that the boundaries did not affect the domain flow field. Similarly a mesh sensitivity analysis was also performed which led to a mesh size of 4.5 million cells being used (Figure 2.8). As simulations were carried out at different tower spacings with the computational domain-size varied according to the tower-spacing size, the smallest computational domain was 280 m x 90 m (diameter x height) while the largest was 380 m x 90 m.

For all multi-tower simulations in this study, the radiator temperature was set at 52 °C while the heat flux was allowed to vary

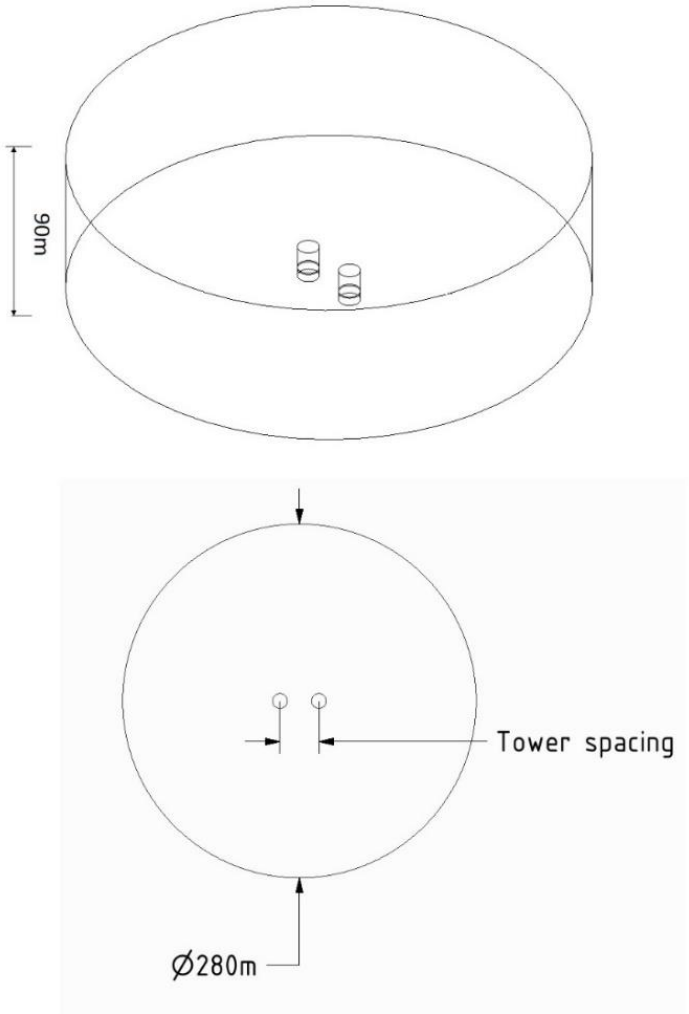

Figure 2.7. Tower layout and computational domain.

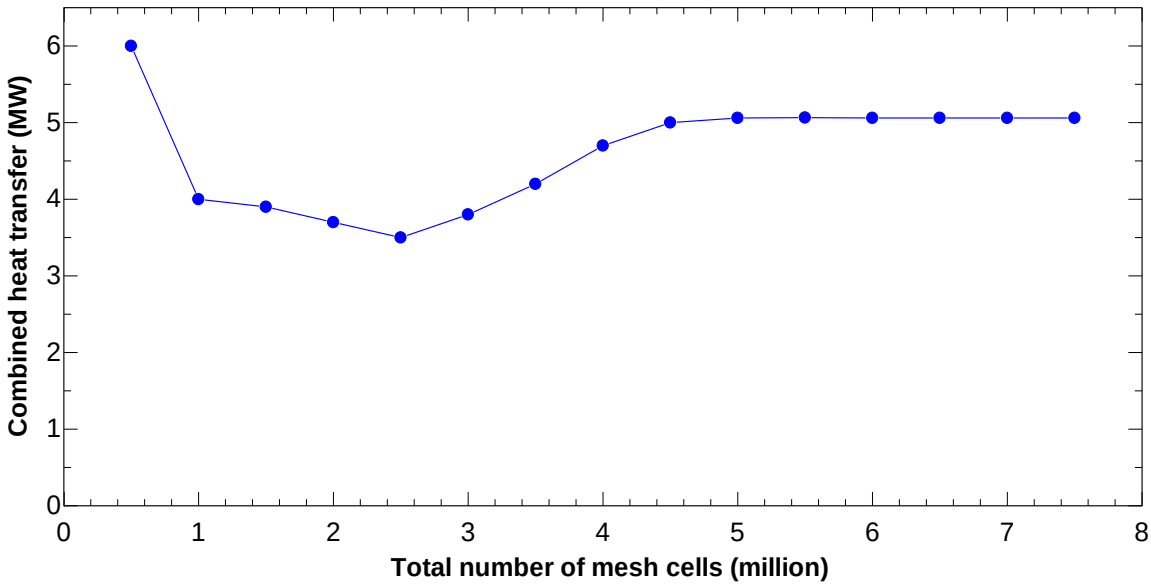

Figure 2.8. Mesh sensitivity analysis based on the combined heat transfer rate of two towers.

2.3.2. Results and discussion for two towers under the no-wind condition

Under calm conditions, heat transfer occurs purely by natural convection so would be very sensitive to small changes in the inlet conditions. In saying this, the rate of air passing through the heat exchangers and moving upward in the tower is a determining parameter of a NDDCT's cooling performance. To explain this further, the overall heat transfer coefficient of the heat exchangers depends on the air mass flow rate across the bundles and an increase in the mass flow rate results in a higher heat transfer rate. The area around the base of the towers acts as an air supply, however, with a small tower-spacing, the heat exchangers are attempting to draw air from a common area between the adjacent towers and hence compete for air supply.

This is demonstrated by the velocity distribution for each tower is no longer symmetrical as the tower spacing decreased. Figure 2.9 shows that there is a weaker air driving force between the towers at low tower spacing, which results in a lower air velocity in the tower. At a tower-spacing of 3D, the velocity vectors are relatively uniform at the inlet of the towers, however at 1.16D, the velocity vectors between adjacent the towers are small compared to the far side.

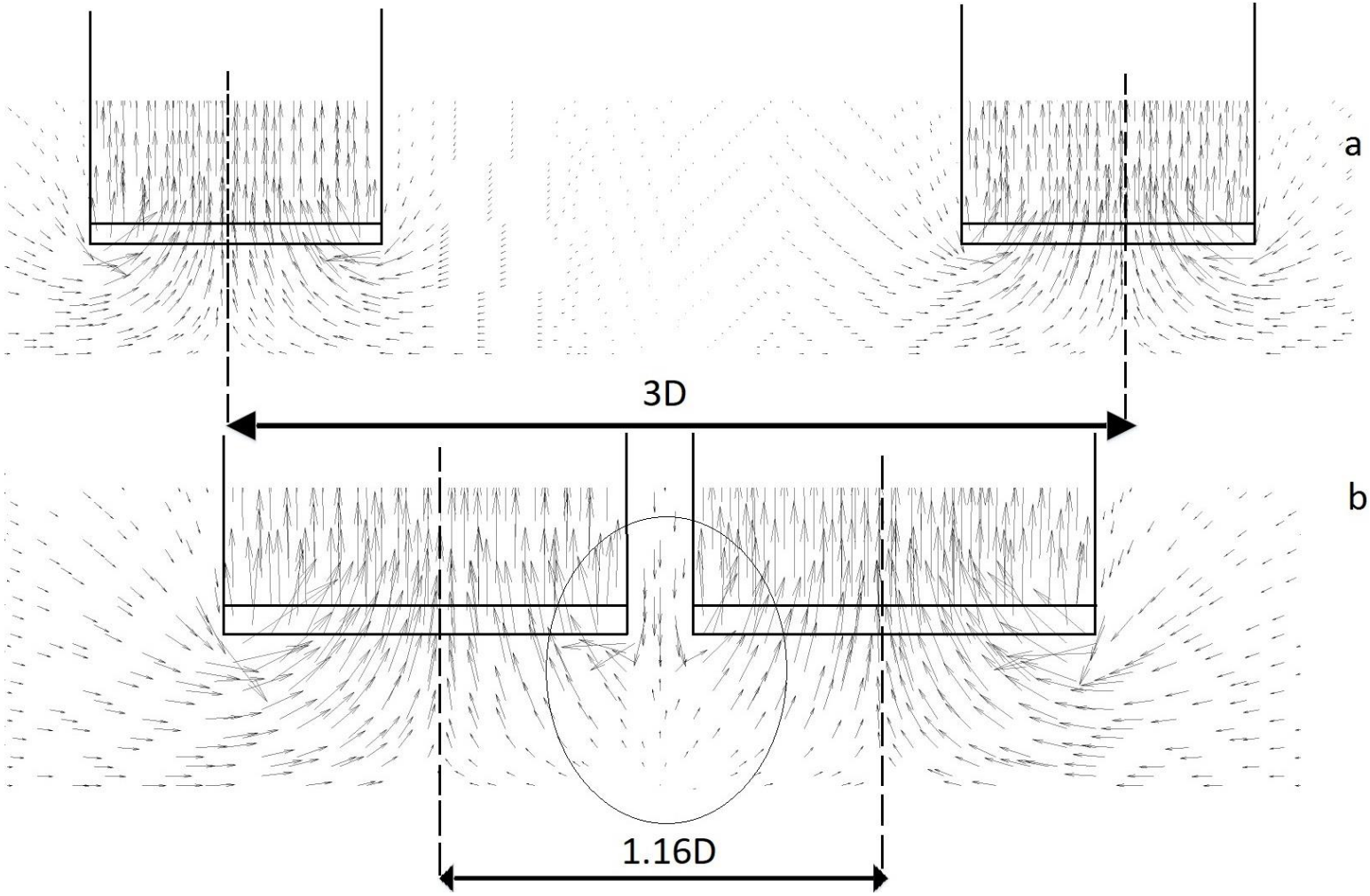

Figure 2.9. Velocity vector at central vertical cross section of two NDDCTs with the tower spacing of a) 3D and b) 1.16D (Zoom view).

This is more clearly illustrated by the velocity profiles at the inlet of the towers shown in Figure 2.10. From these it is apparent that that the velocity profile at a large tower-spacing is like that of an individual cooling tower, whereas with reduced spacing there is a noticeable reduction in the local velocity at the side of the tower adjacent to the second tower. This is due to the fact that when the towers are close together there is a reduction in the scavenge area (i.e. the area around the circumference from which the tower can draw air freely), or more bluntly, the towers compete for air.

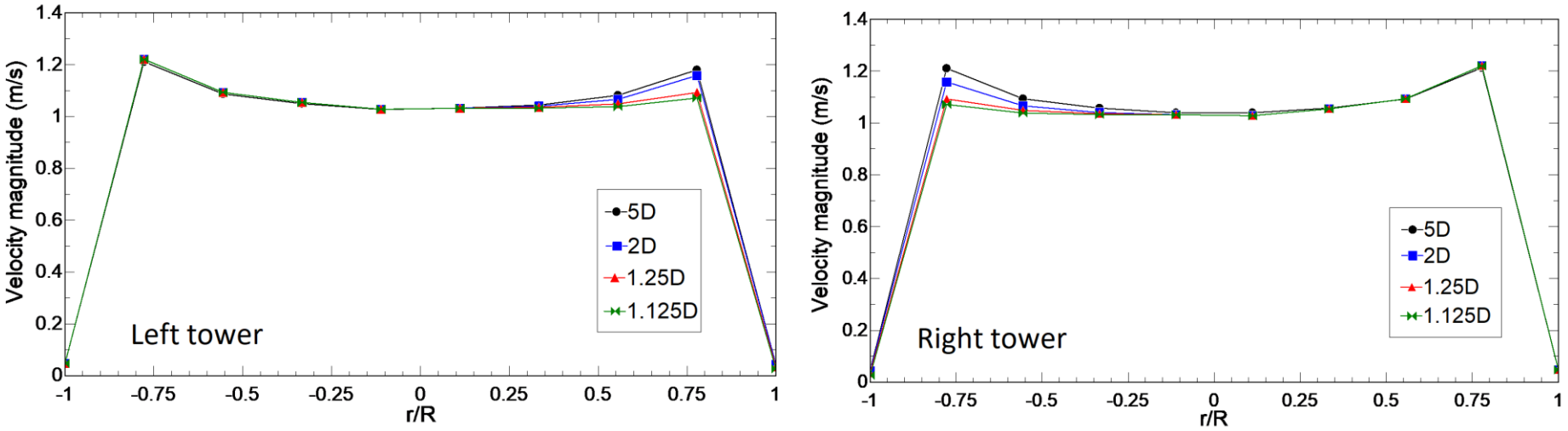

Figure 2.10. Velocity profile at the inlet of the both cooling tower at different tower spacings.

This is further illustrated by the data shown in Figure 2.11 where it can be seen that the heat exchanger temperature at the side adjacent to the neighbouring tower is higher than the opposite side. This means that at a low tower-spacing, the section of the heat exchanger nearest to the adjacent tower was not capable of providing the same level of cooling as the opposite side. Similar behaviour has been observed previously in the thermal performance of two large NDDCTs at low tower spacings. It is also worth noting that the interaction between the large cooling towers disappeared at tower spacings of 2D, the same as findings of this study (68).

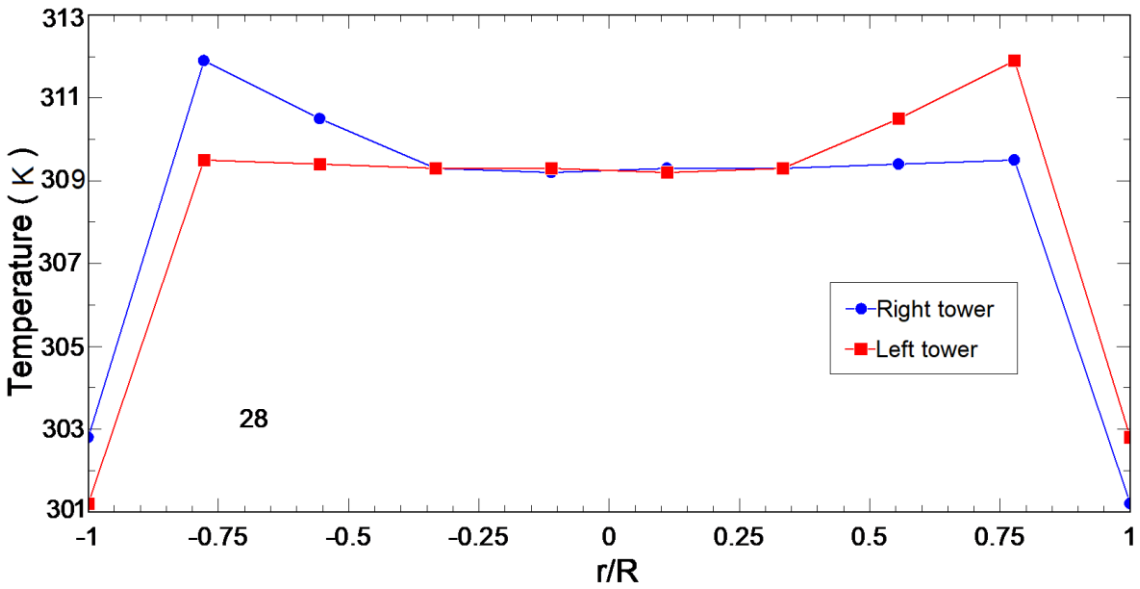

Figure 2.11. Temperature distribution at horizontal centreline at top of the heat exchangers for each tower at tower spacing of 1.16D. Each line is located on top of each heat exchanger inside the towers.

Reflecting on these points, the total heat rejection of the NDDCT at the no-wind condition calculated using equation 2.2, is independently calculated by radiator heat transfer rate of ANSYS FLUENT. Having simulated the cooling performance of two towers in close proximity, Figure 2.12 illustrates the normalized heat rejected relative to the no-wind condition (Q/Q_{ref}), where Q is the summation of the towers' heat rejection and Q_{ref} is twice the heat rejected by an isolated tower under the no-wind condition. From this figure, for a tower spacing larger than 2D the cooling capacity was constant, however, the combined heat rejection from the towers decreased markedly as the tower spacing was decreased

below 2D. This illustrates that the interaction between the towers at low tower-spacing decreases the heat rejection performance of both towers.

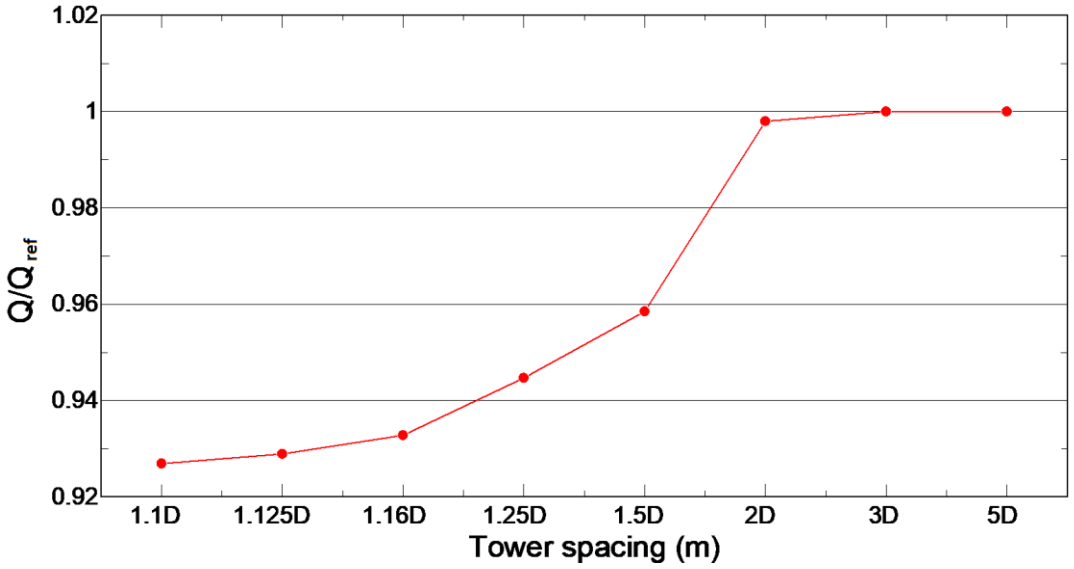

Figure 2.12. Normalized heat rejection of two NDDCTs at different tower spacings.

2.4. Performance of three NDDCTs under the no-wind condition

2.4.1. Method

In understanding the behaviour of three NDDCTs, the same numerical method, boundary conditions, and meshing strategy used in the simulation of two NDDCTs was applied. Similarly tower spacings of 5D - 1.1D were analysed. The boundary domain was extended by adding the third tower and increased by increasing the spacing where the smallest domain size was 300 m x 90 m while the largest was 500 m x 90 m. This led to the cooling towers and computational boundary domain being discretised using 6 million structured elements.

2.4.2. Results and discussion for three towers under the no-wind condition

To understand what occurs when three adjacent towers are placed on a single site, Figure 2.13 shows the velocity vectors at the central vertical cross-section of the towers at spacings of 3D and 1.16D. At a tower spacing of 3D the flow fields around the towers are similar, and the internal airflow appearing to act like isolated towers, as also observed

with two NDDCTs. However, at a tower spacing of 1.16D, the velocity vectors near the inlet of the middle tower are smaller compared with the tower spacing of 3D. The small velocity vectors also can be seen at the sides of the left and right towers adjacent to the middle tower. To further illustrate this, Figure 2.14 shows that the velocity magnitude at the inlet of the middle tower is lower in the middle tower at low tower spacing. At large tower spacings, the velocity profiles at the inlet of all towers are symmetrical and similar across all towers. In summary, the velocity profile at the left side of the left tower and right side of the right tower, does not change with variation of the tower spacing due to there being no interference with the airflow attempting to enter the middle tower.

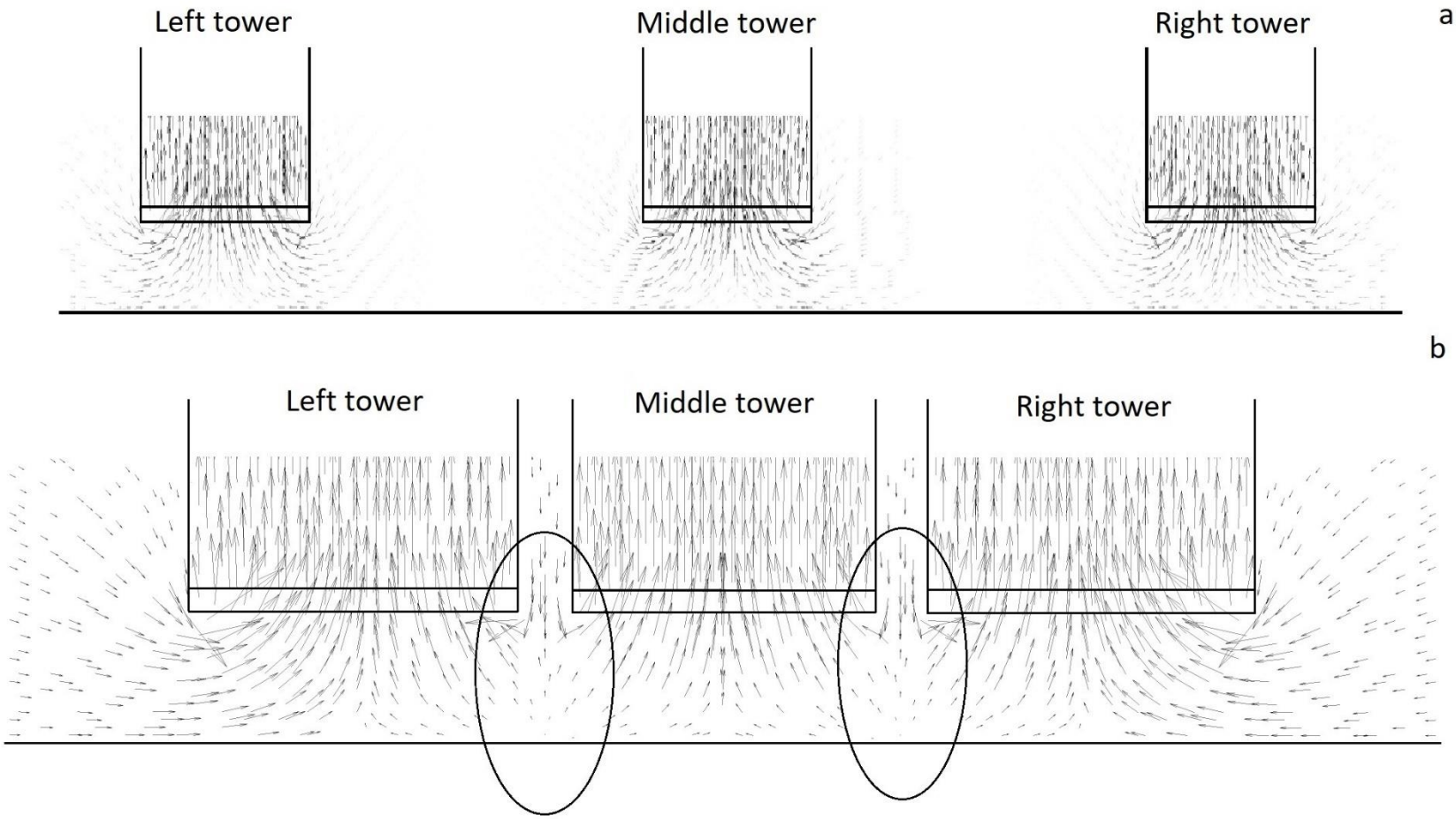

Figure 2.13. Velocity vector at central vertical cross section of three NDDCTs with the tower spacing of a) 3D and b) 1.16D (zoom view).

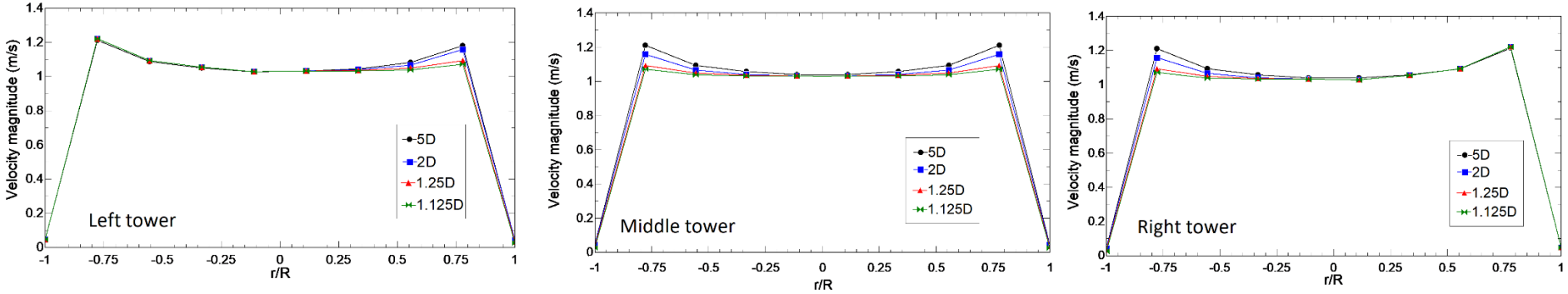

Figure 2.14. Velocity profile at the inlet of the cooling towers at different tower spacings.

The impact of this on the cooling towers' cooling capacity is shown in Figure 2.15, which shows the normalized heat rejection of three NDDCTs at different tower spacing, where Qref is the heat rejection of a single NDDCT. The heat rejection of the left and right tower is identical due to the symmetrical layout. However, the heat rejection of the middle tower is increasingly decreased (up to 15%) when the tower spacing is reduced below 2D. This is because the centre tower is surrounded by two towers on either side which limits the ability of air to reach the inlet of the middle tower. At tower spacings of greater than 2D however the towers act as an isolated tower.

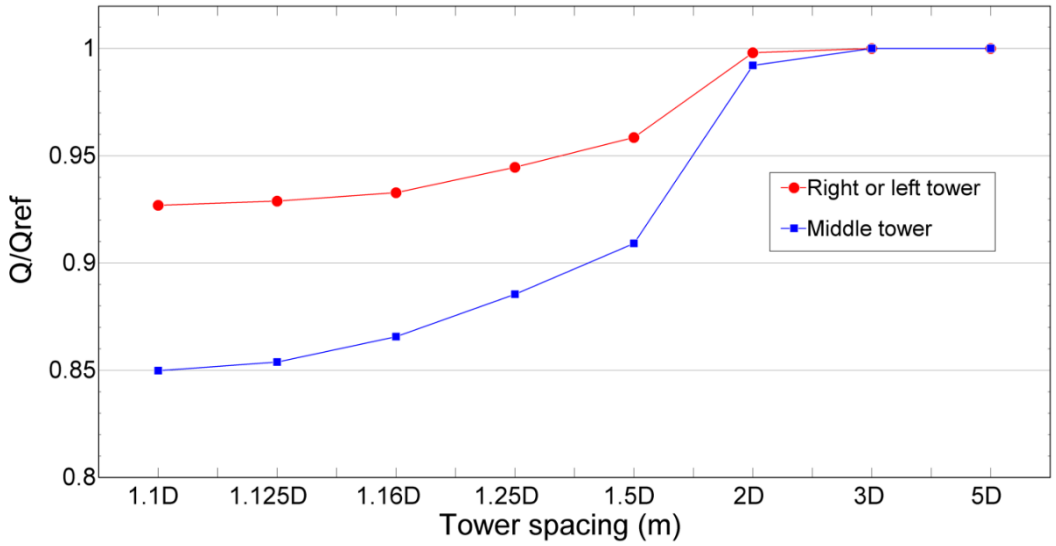

Figure 2.15. Normalized heat rejection of three NDDCTs at different tower spacings.

2.5. Chapter conclusions

In this chapter the thermal performance of the NDDCT in a no-wind condition was corroborated with experimental data obtained by another study for the Gatton cooling tower. Using this validation, it was possible to extend the study to the examination of multiple cooling towers placed on a common CSP power plant site. The results of this study delivered an understanding of how tower spacing can affect the thermo-flow characteristics of the cooling towers. For calm conditions, the heat rejection is very sensitive to small changes at the towers' inlet. It was found out that when two towers were

placed more than 2D apart, both towers act as an isolated NDDCT and the flow characteristics were symmetrical. Smaller tower spacings led to a reduction in the scavenge area between the two towers limiting the air supply for both towers. This results in non-uniform temperature and velocity distributions within them. This interaction between towers at low tower-spacing decreases the performance of both towers. This effect should be considered when adding additional cooling towers to an existing system, particularly at sites prone to calm conditions. Further, the results of three NDDCTs showed that the heat rejection of the middle tower which is surrounded by two towers is highly influenced by the tower spacing and at very low tower spacings, the heat rejection decreases by up to15%. This new finding holds particular design significance if multiple NDDCTs are deployed on CSP sites that experience a high frequency of calm (no-wind) conditions.

Chapter 3: Effect of wind on the performance of two NDDCTs

3.1. Introduction

In the previous chapter, the performance of an isolated NDDCT and multiple adjacent NDDCTs was investigated for no-wind conditions. The effect of tower spacing was discussed and it was shown that the towers' interaction at low tower spacing reduced the thermal performance of the towers. In Chapter 1 literature review, it was also noted that crosswinds and local flow circulations at the bottom and top of the NDDCTs can also decrease the air flow rate and consequently reduce the rate of heat rejection. It was also discussed that short NDDCTs are more vulnerable to the crosswinds compared to the larger towers. Although previous studies have characterised the effect of wind on a single NDDCT, it is not clear how this relates to the performance of additional towers placed in close proximity as CST plants are expanded. Since the performance of a short NDDCT is highly influenced by operating conditions, this chapter aims to investigate thoroughly the interaction between two NDDCTs during windy conditions at different tower spacings, wind speeds, and wind incidence angles.

3.2. Performance of a single NDDCT under windy conditions

3.2.1. Method

The same cooling tower geometry and numerical factors, including boundary conditions and mesh generation method discussed in Chapter 2 were employed to investigate the performance of NDDCTs under windy conditions. A computational domain, as shown in Figure 3.1, was used and the dimensions of the computational domain were selected based on a boundary domain sensitivity analysis that showed that the boundaries did not affect the domain flow field. The NDDCT was placed at the centre of the semi-circular domain,

and the domain was extended in a rectangular shape. This resulted in the simulation domain having a height of 90 m, a breadth of 144 m, and a length of 150 m, consisting of over 3.2 million elements. The mesh sensitivity analysis for a single NDDCT was performed and is presented in Appendix B.

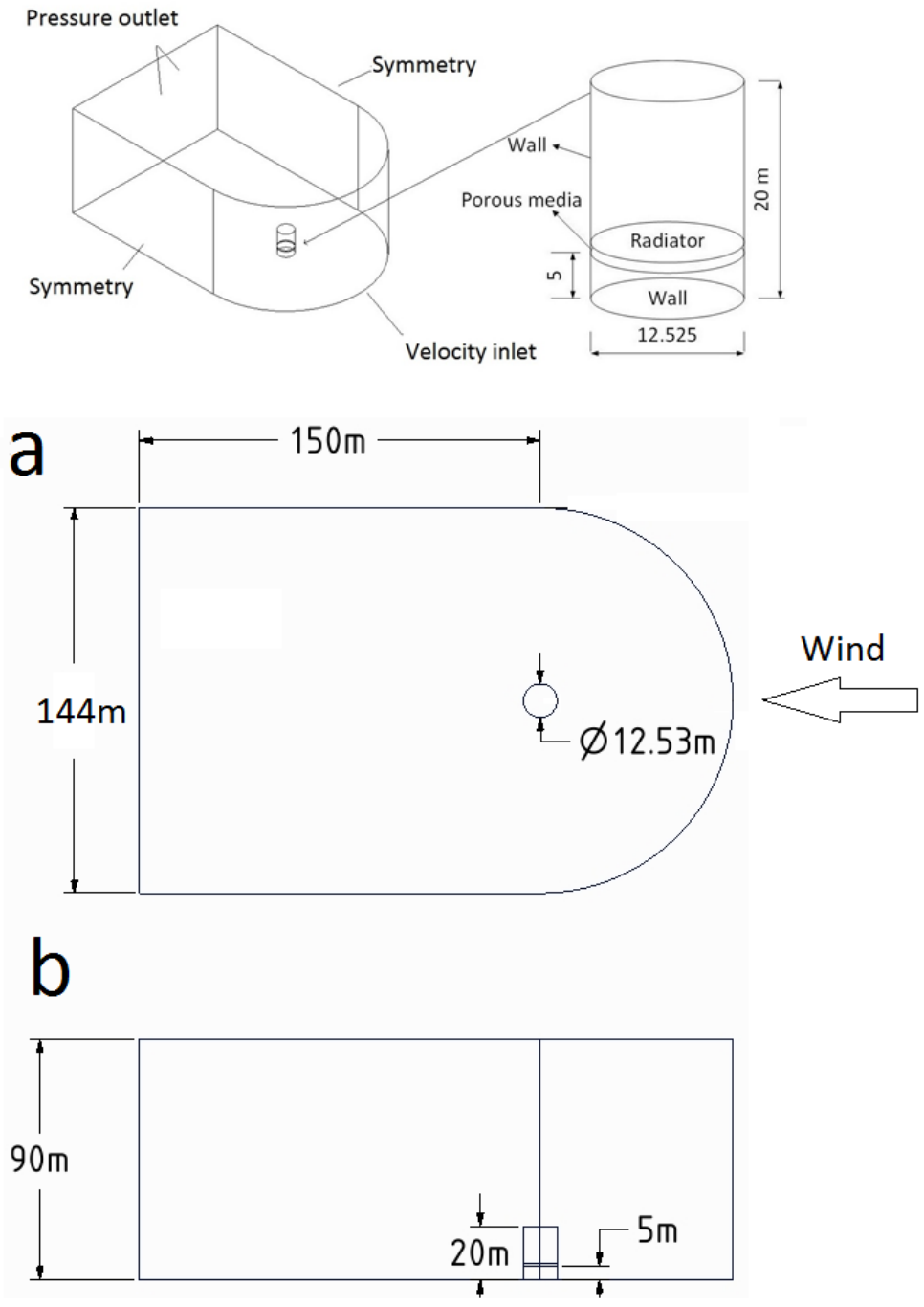

Figure 3.1. Computational domain and boundary conditions at a) plan view b) side elevation, at tower spacing of 1.8D.

To simulate wind, a velocity inlet boundary condition was assigned to the curved surface shown in Figure 3.1. The velocity profile applied was defined by Equation 3.1 as shown in (53, 55):

$$U = v_{cw} = (\frac{y}{y_{ref}})^{a} v_{ref} \quad (3.1)$$

where v_{ref} is a reference velocity at a reference height, y_{ref} =10 m (69) that is generally measured by the local weather office (78). In this study wind speeds (V_{ref}) of 1-8 m/s with intervals of 1 were assigned. Exponent *a* is defined as the roughness of the ground and the stability of the atmosphere, taken to be 0.2 which represents a neutral atmospheric condition [14]. Eq 3.1 represents a fully developed velocity profile at the inlet. Because of the low-turbulence level of advection natural wind, the impact of the turbulence intensity and viscosity ratio was very little at the computation domain boundaries. The value of the turbulence intensity was set at 0.1% and viscosity ratio at 0.1 as suggested by Li et al. [3, 15].

In reporting the heat rejection under windy conditions, it was decided to normalize the value relative to the no-wind condition (Q_{ref}) for an individual tower. Thus Q/Q_{ref} is the fractional change in heat rejected due to the effect of wind, which will be referred to as "normalized heat rejection".

3.2.2. Validation

As with the no-wind condition described previously, Figure 3.2 shows a comparison of the normalized heat rejection (Q/Q_{ref}) of a single cooling tower for windy conditions between this study, those of Li et al. (55), and a theoretical model proposed by Hooman (22). In (55), Li et al. investigated the effect of wind on the heat rejection of a single cooling tower with the same tower dimensions and heat exchanger design used in this study using CFD simulations. Hooman (22) proposed a theoretical method to predict the

effect of crosswind on the performance of natural draft cooling towers. Hooman's model offers the heat transfer prediction of the tower by knowing the draft speed and the heat transfer rate at a no-wind condition.

Hooman's theoretical model predicts the performance of the NDDCT, and both results follow the same trend for wind speeds of lower than 4 m/s. At higher wind speeds, where the forced convection controls the flow regime inside the tower and a significant amount of hot air exits the tower from the circulation occurring at the bottom of the tower, the theoretical model fails to accurately predict the performance of the NDDCT. However, the comparisons indicate that the results of both Li et al.'s study and this study follow the same trend, and the magnitude of the results is broadly similar (less than 5% difference), thus implying a validation of the simulated results from this study.

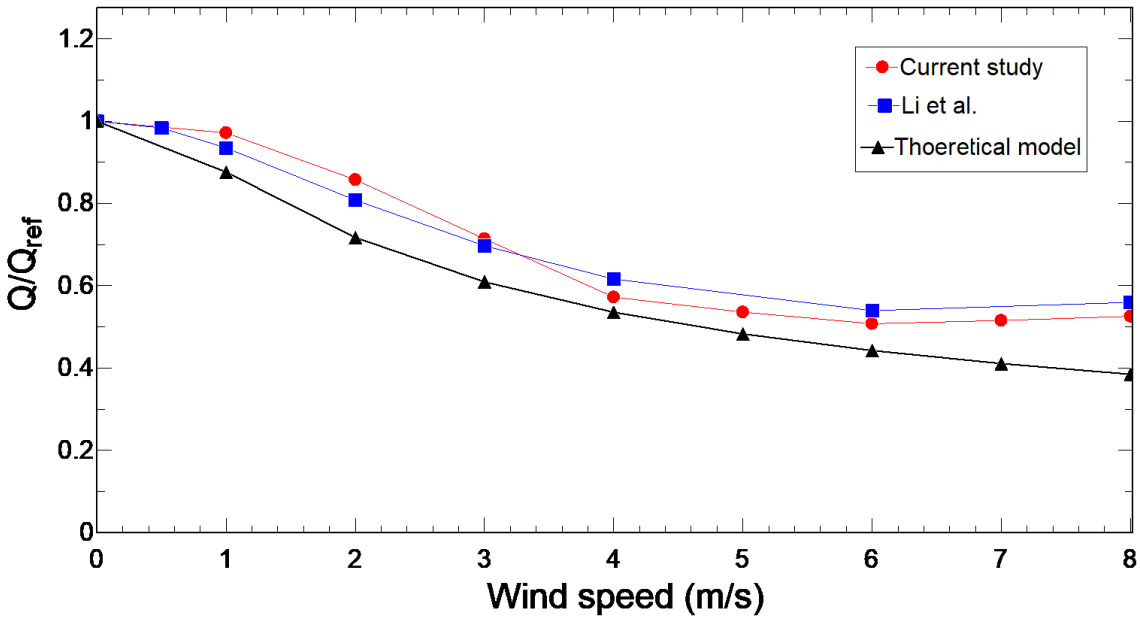

Figure 3.2. Normalized heat rejection of a single NDDCT at various wind speeds, and comparison between the CFD result and previous studies.

3.2.3. Results and discussion for a single tower subject to windy conditions

Having demonstrated that the modelling method could also be applied to NDDCTs subject to windy conditions it was decided to explore, in greater detail, the behaviour of a single tower. Figure 3.3 illustrates the 3D velocity streamlines at different wind speeds. For the no-wind condition (Figure 3.3 A), the ambient air enters the cooling tower from the bottom and moves toward the top of the tower. At a wind speed of 2 m/s (Figure 3.3 B), the air around the cooling tower can easily move through the heat exchanger and exit the outlet of the tower, but in doing so, small vortices (flow circulation) start to appear at the windward side of the tower's inlet and the leeward side of the tower's outlet. This decreases the flow rate through the windward side of the heat exchanger. The vortices (flow circulations) are formed at the bottom and top of the cooling tower once the wind reaches 4 m/s (Figure 3.3 C). In particular, the high velocity beneath the heat exchanger draws down the hot air inside the tower. Further, the wind at the top of the tower acts like a lid, resulting in the deflection of the plume at the exit plane of the tower. The distorted or maldistributed airflow caused by the wind reduces the effective heat transfer area of the condenser in the tower. By increasing the wind speed, the vortices generated at the bottom and top of the cooling tower become dominant, which makes it difficult for air to exit the tower (Figure 3.3 D and E).

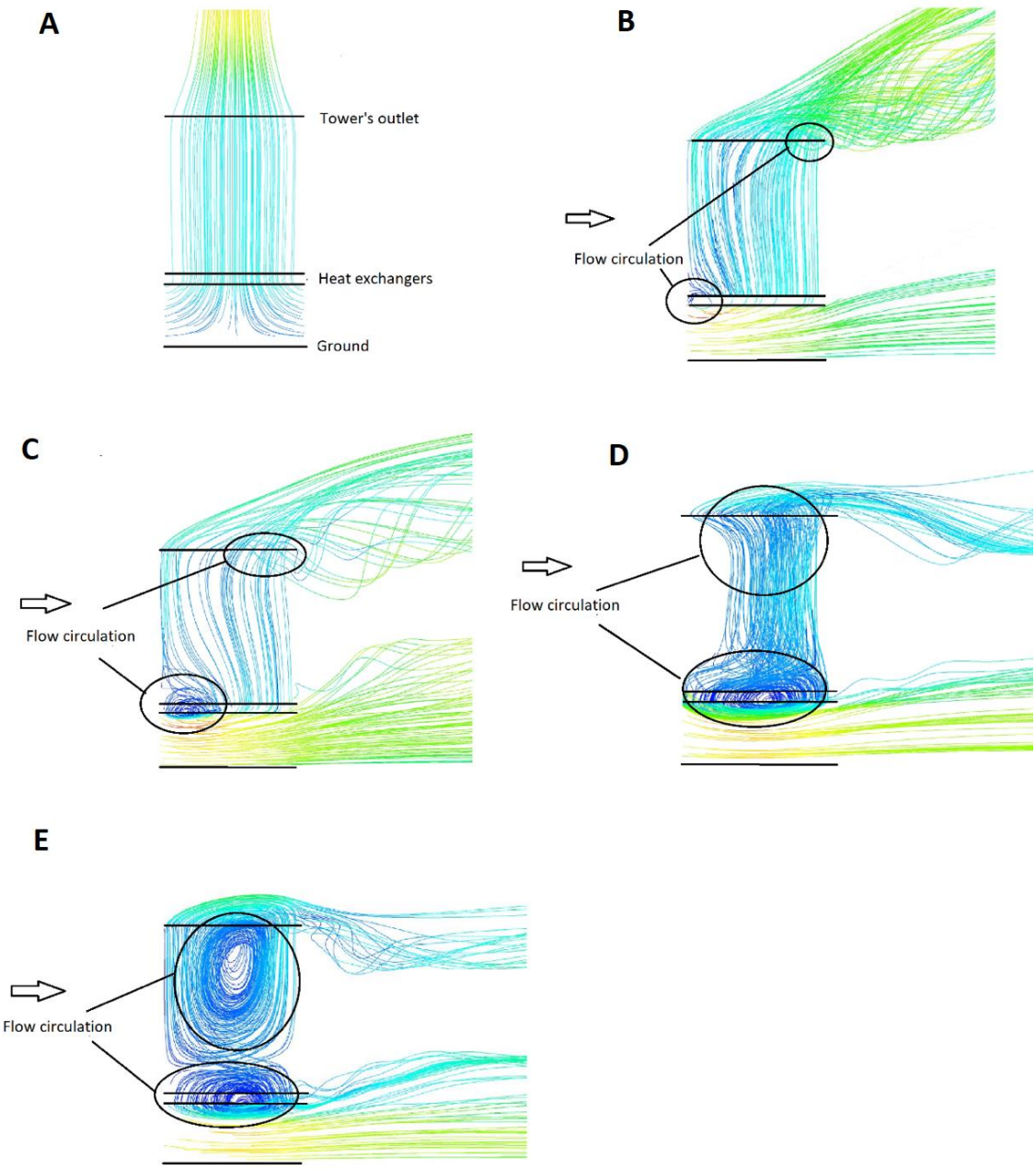

Figure 3.3. 3D streamlines of the cooling tower at various wind speeds, V=0 m/s (A), V=2 m/s (B), V=4 m/s (C), V=6 m/s (D), and V=8 m/s (E).

To have a better understanding of the flow circulations in the NDDCT, the velocity vectors are depicted at the mid-plane in Figure 3.4 and the flow circulations are highlighted. It can be seen that the flow at the bottom of the cooling tower at the windward side of the heat exchanger is circulating within the tower. The velocity vectors at the leeward side of the tower's outlet are also circulating back into the tower.

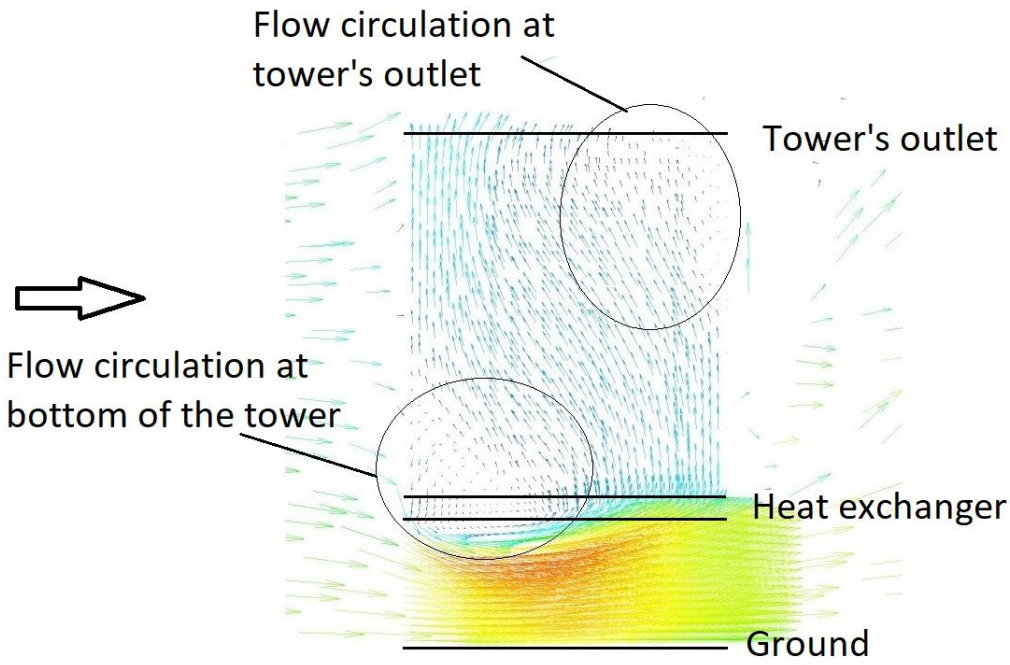

Figure 3.4. Velocity vectors around a single NDDCT at wind speed of 4 m/s.

To investigate the effect of wind on the air flow inside a single NDDCT, the average vorticity (vorticity is a vector field which provides a local measure of the instantaneous rotation of a fluid parcel) at the bottom and top of the cooling tower was plotted at various wind speeds, as shown in Figure 3.5. The vorticity introduced to the local spinning motion of air which can represent the flow instabilities inside a cooling tower, and has previously been used previously to measure flow circulations and disturbances within short NDDCTs (53).

This measure of vorticity is important as flow instabilities inside the cooling tower decrease the heat transfer rate. By increasing the wind speed, the vorticity rises at both the bottom and top of the tower. For wind speed greater than 2 m/s as seen as Figure 3.3 C-E and summarized by Figure 3.5, there is a sudden growth in the vorticity at the bottom of the tower, signalling the vortex's appearance at the windward side of the heat exchanger.

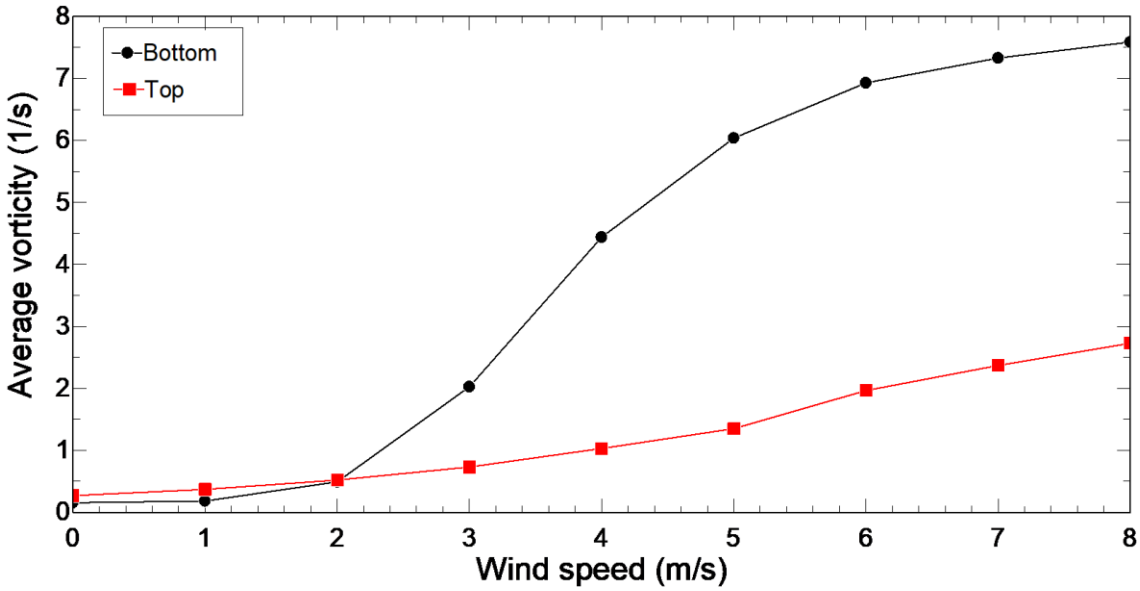

Figure 3.5. Average vorticity at bottom and top of the NDDCT at various wind speeds.

Taking this further, Figure 3.6 presents the pressure distribution at the bottom of the heat exchanger. For the no-wind condition the pressure distribution is uniform, however as the wind speed increases, a low-pressure area is formed at the windward side of the tower. This low-pressure area decreases the air flow at the windward side of the tower and counters the buoyancy-driven flow.

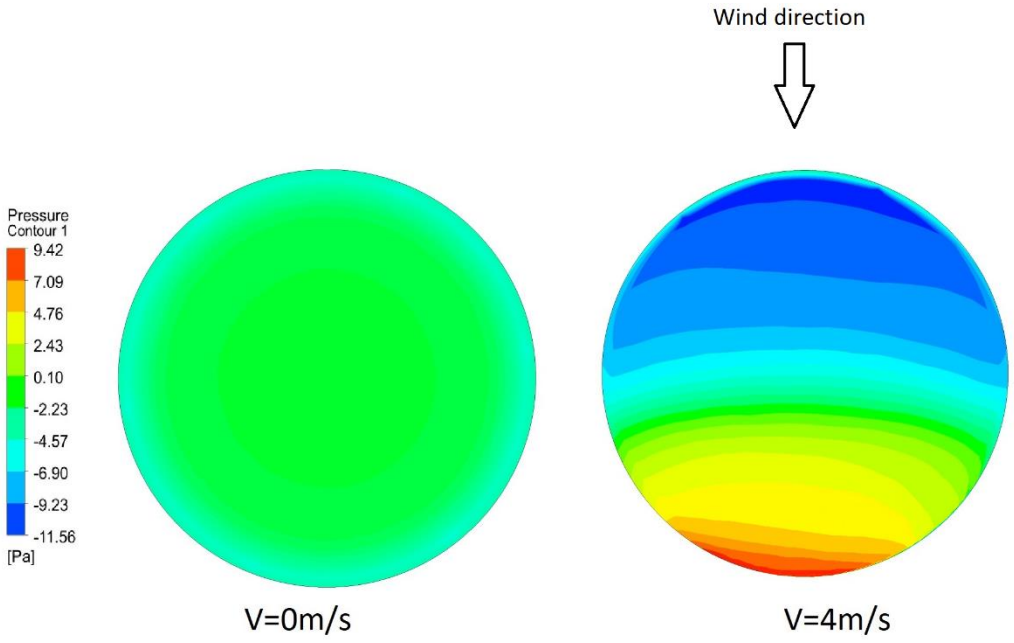

Figure 3.6. Pressure contour at the bottom of the heat exchanger at V= 0 m/s and V= 4 m/s.

Expanding on this, it should be noted that the heat transfer within a NDDCT occurs by two mechanisms: the heat taken away by the air moving toward the top of the tower (by natural convection Q_u), and heat taken away by the air that leaves through the bottom part of the tower after circulating around the heat exchangers driven by a lower vortex (by forced convection Q_d), which will be explained later in this chapter. The sum of these components is equal to the total heat removed from the heat exchangers (radiator), Q, which is independently computed by FLUENT as the radiator heat transfer ($Q=Q_d+Q_u$).

The heat dissipated through the cooling tower outlet, was calculated using equation 2.2, in which the air mass flow rate (m_a) is the net value of the air flowing through the radiator. This can be calculated from the numerical results. The heat exchanger exit-temperature (T_{ao}) was extracted by averaging the numerically calculated air temperature at the tower outlet face, and the air that enters the heat exchanger (T_{ai}), which is the ambient air temperature. The second component Q_d was calculated by subtracting Q from Q_u. For the no wind condition the airflow is unidirectional inside the tower, so Q_d is zero ($Q=Q_u$).

Therefore, the heat transferred by the forced convection increases with increasing wind speed, as shown in Figure 3.7. Increasing the wind speed may increase the heat rejection rate of the cooling tower and compensate for a level of decreased heat rejection in the cooling tower. For wind speeds of less than 6 m/s, the heat rejection rate decreases rapidly as the wind speed increases. For a wind speed of 6 m/s the heat rejection rate of the cooling tower reaches a minimum, and this referred to as the "turnaround" point. Previous studies have shown that the turnaround point occurs at a higher wind speed by increasing the height of the tower (79).

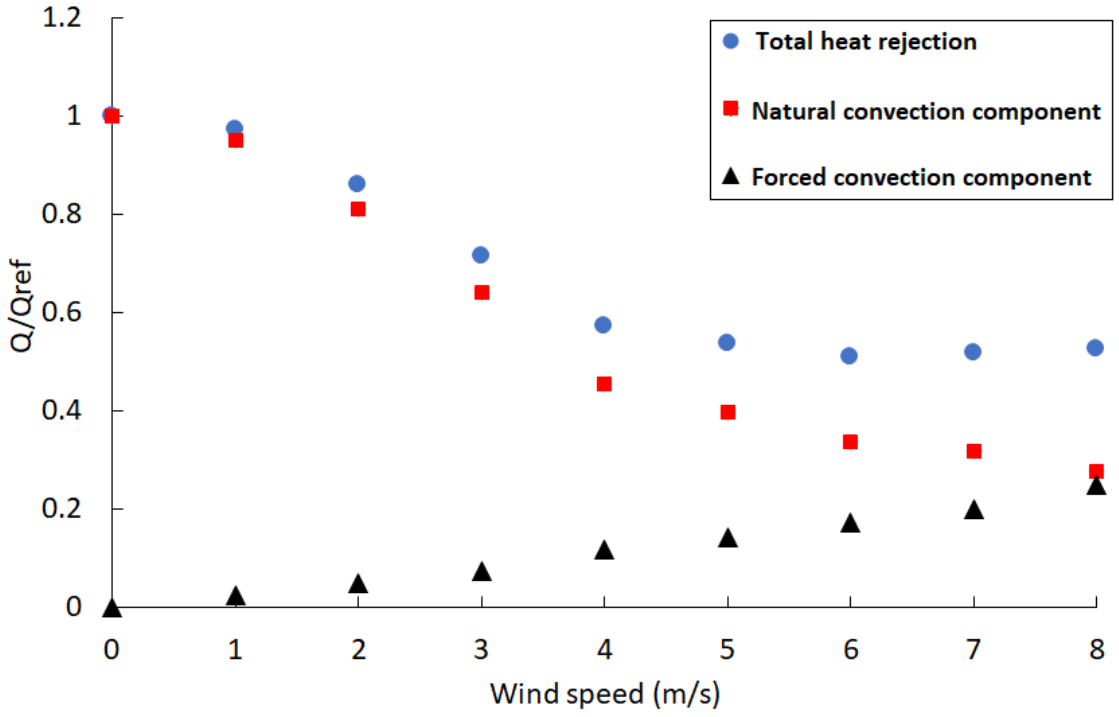

Figure 3.7. The heat rejection component of the simulated NDDCT.

As discussed earlier, at high wind speeds the flow circulation leaving the bottom of the NDDCT takes away the heat from the heat exchanger. Hence, when the effect of wind on multiple NDDCTs is investigated, it may be expected that warm air leaving the bottom of the windward NDDCT will enter the leeward towers and decrease the heat rejection of those downstream towers. To determine if this may be a factor, the air temperature after the single NDDCT was monitored at the inlet height. In Figure 3.8 it can be seen that at

wind speeds of 2 m/s and 4 m/s, the air temperature immediately downstream of the tower is equal to the ambient temperature (293.15 K). At wind speeds of 6 m/s and 8 m/s, the air temperature leaving the tower is higher than at lower wind speeds, showing that heat is taken away from the heat exchanger at the bottom of the tower. However, the results also show that the air rapidly mixes with the ambient air between the towers and reaches the ambient temperature after 0.8D downstream. As such, it is unlikely that any additional towers downstream of an initial tower would experience a change in their inlet temperature as a result of its presence.

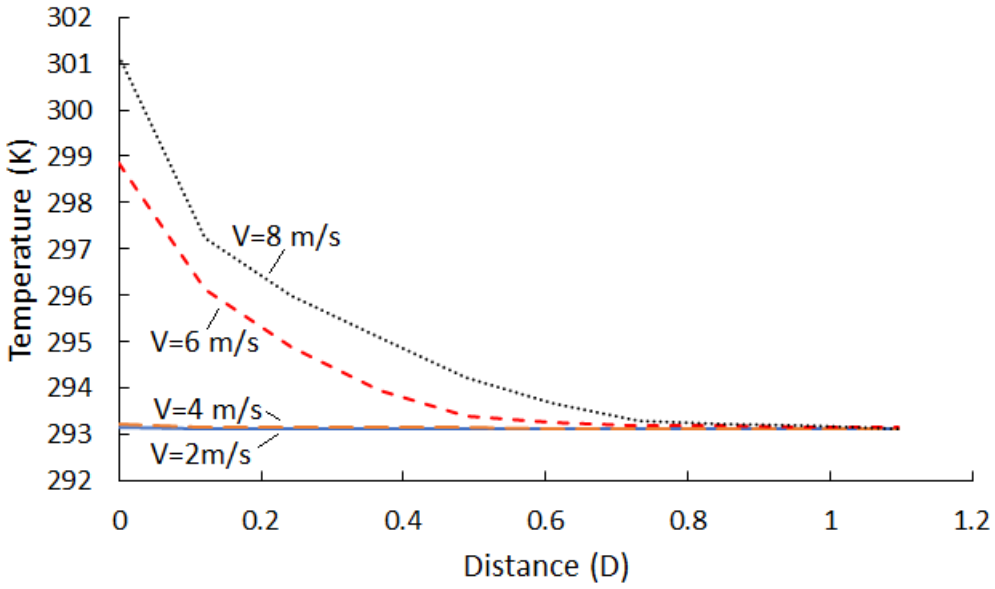

Figure 3.8. The air temperature over a line at the inlet height after the NDDCT.

3.3. Performance of two NDDCTs under windy conditions

3.3.1. Method

Having shown that the model could predict the performance of a single tower, it was applied to a multi-tower configuration. Subsequently, the simulations were performed for two towers, configured with three tower-spacings: 1.8D, 2.6D, and 4.2D (where D is the tower diameter of 12.525 m); three wind incidence angles (θ is the angle between the relative wind direction and the line connecting the tower centres): 0°, 45°, and 90°; and multiple wind speeds (1, 2, 3, 4, 5, 6, 7, and 8 m/s). The minimum tower spacing was

selected based on the findings in Figure 3.8. At different wind conditions, the additional tower spacings were examined to observe whether any opposite trend occurred at a particular distance.

The same computational domain and boundary conditions as used for the single NDDCT were used for two NDDCTs simulation, where the second tower was placed as shown in Figure 3.9. The dimensions of the boundary domain at different tower spacings and wind incidence angles are detailed in Appendix B, and the same meshing method used in the single tower study was used to discretise the multi-tower system. This same computational domain was used in the investigation of a multi-tower system by Zhai and Fu (65).

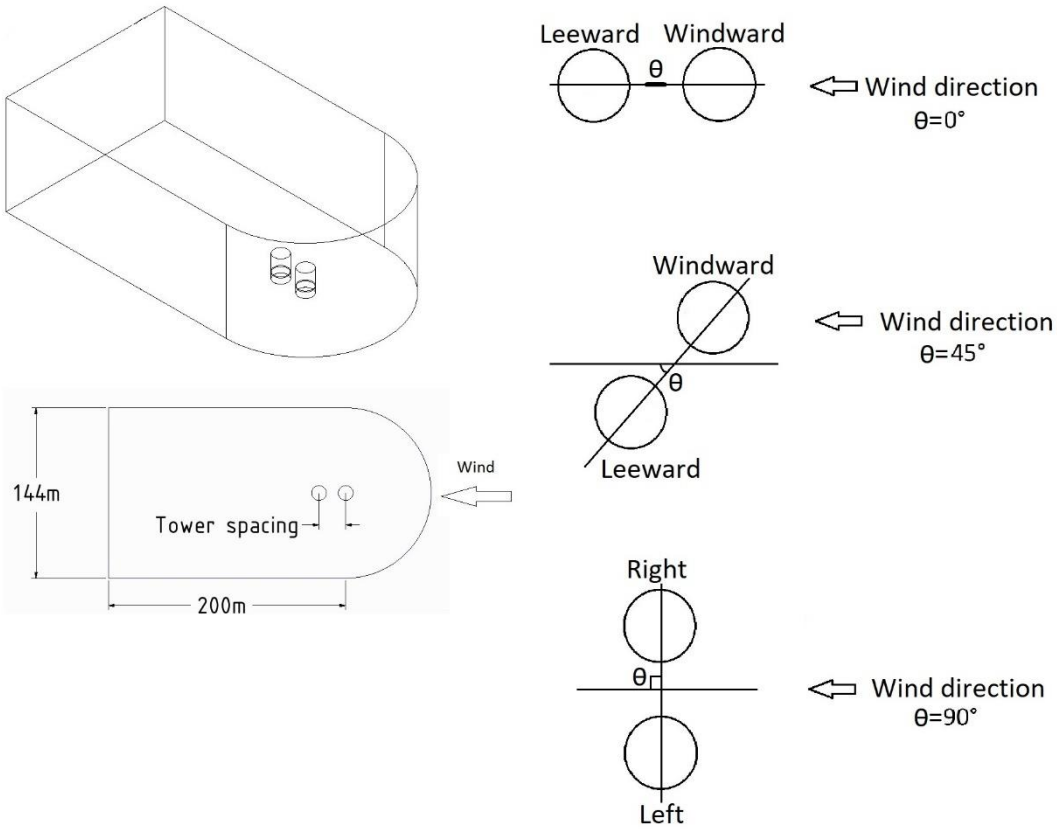

Figure 3.9. Computational domain and towers' layout.

The computational domains used in the simulations were dissimilar at different tower spacings and wind incidence angles. Therefore, at each condition, a separate grid independence test was performed at a wind speed of 4 m/s to find the minimum optimum number of elements at which the simulation's results stabilize. Further mesh refinement is then necessary as this does not change results. The mesh sensitivity analysis for the simulation of two NDDCTs during windy conditions is explained in detail in Appendix B. A good mesh quality was achieved with the maximum skewness of 0.47, minimum orthogonal quality of 0.62, and maximum aspect ratio of 9.7.

3.4. Results and discussion for two towers under windy conditions

3.4.1. Wind incidence of 0°

Figure 3.10 displays the flow field around two NDDCTs at the inlet height, and the heat exchangers' temperature distribution at a tower spacing of 1.8D and a wind incidence angle of 0° for different wind speeds. At a wind speed of 2 m/s, the velocity contours (Figure 3.10.A.i) suggest that, there is low-velocity region between the towers. The velocity streamlines (Figure 3.10.A.ii) show that the air is directed around the windward tower and this protects the leeward tower from the wind (which sits in the wake). This results in a higher temperature at the windward side of the windward tower compared to the leeward tower (Figure 3.10.A.iii). The velocity streamlines also show a low velocity region at the windward side of the windward tower as highlighted in (Figure 3.10.A.ii). This low-velocity region is greater at the windward tower compared to the leeward tower. Viewing this another way, from the velocity streamlines shown by Figure 3.11, for a wind speed of 2 m/s, it can be seen that there is a flow circulation at the windward side of the windward tower compared to the leeward tower. Therefore, the low-velocity region, shown in the velocity streamlines from the top view in Figure 3.10.A.ii, illustrates the flow circulation at the bottom of the tower.

The velocity profile and the location of flow circulation at the bottom of two towers are further discussed in Appendix C. At a wind speed of 4 m/s in Figure 3.10.B, the windward tower protects the leeward tower from the upcoming wind.

The velocity streamlines shown by Figure 3.10.B.*ii*, indicate that the flow is deflected after the windward tower and converges back with respect to the dominant wind direction after the leeward tower. As discussed, at a wind speed of 2 m/s, the low-velocity region shown in the NDDCTs represents the flow circulations at the bottom of the NDDCTs. By comparing the wind speed of 2 m/s and 4 m/s, the larger flow circulations can be noted at a wind speed of 4 m/s, which results in a higher temperature especially at the windward side of the towers (Figure 3.10.B.*iii*).

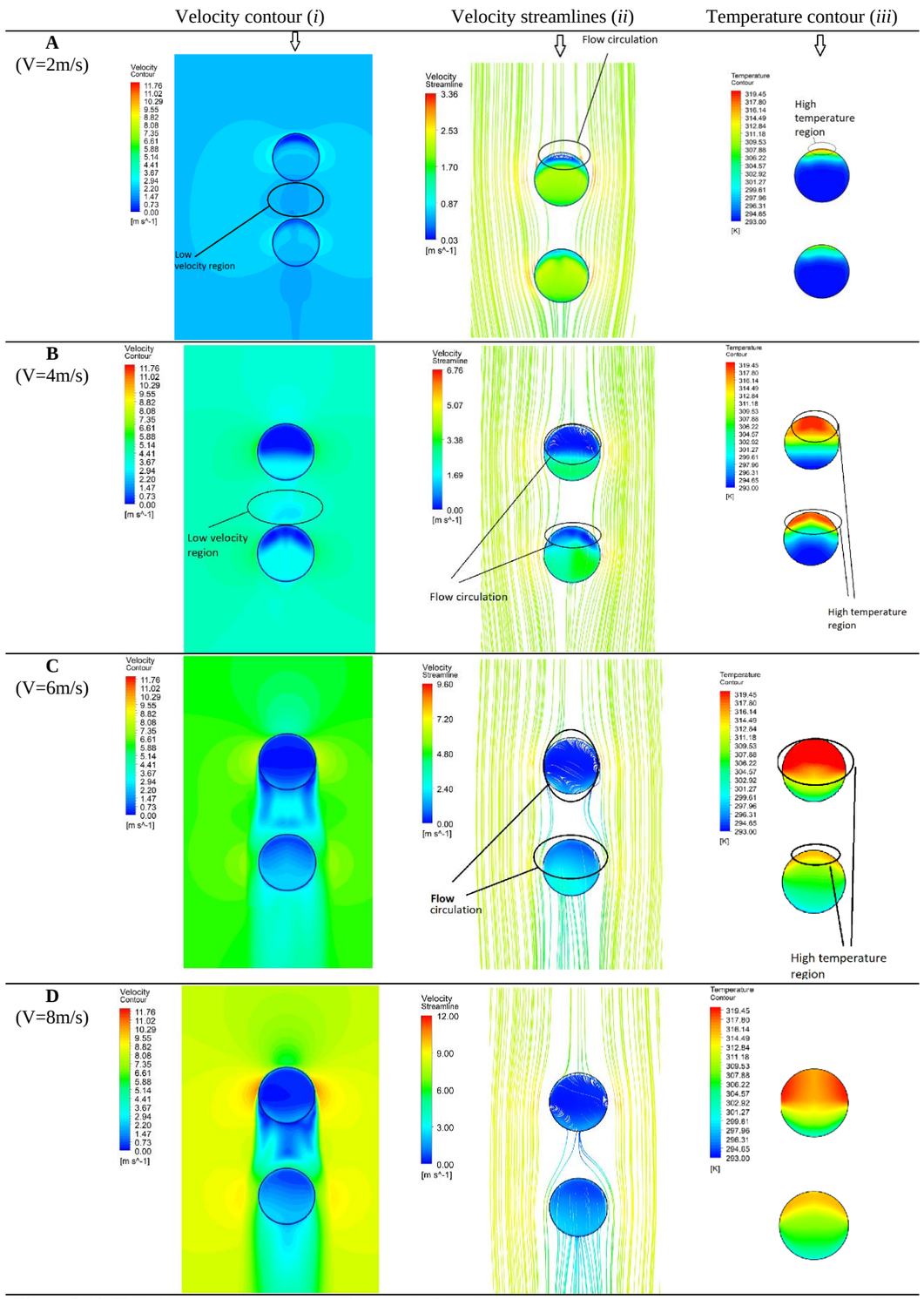

Figure 3.10. Velocity contour and streamlines at the inlet height and heat exchanger temperature contour of both NDDCTs at wind incidence angle of 0°, tower spacing of 1.8D, and wind speeds of 2 m/s (A), 4 m/s (B), 6 m/s (C), and 8 m/s (D).

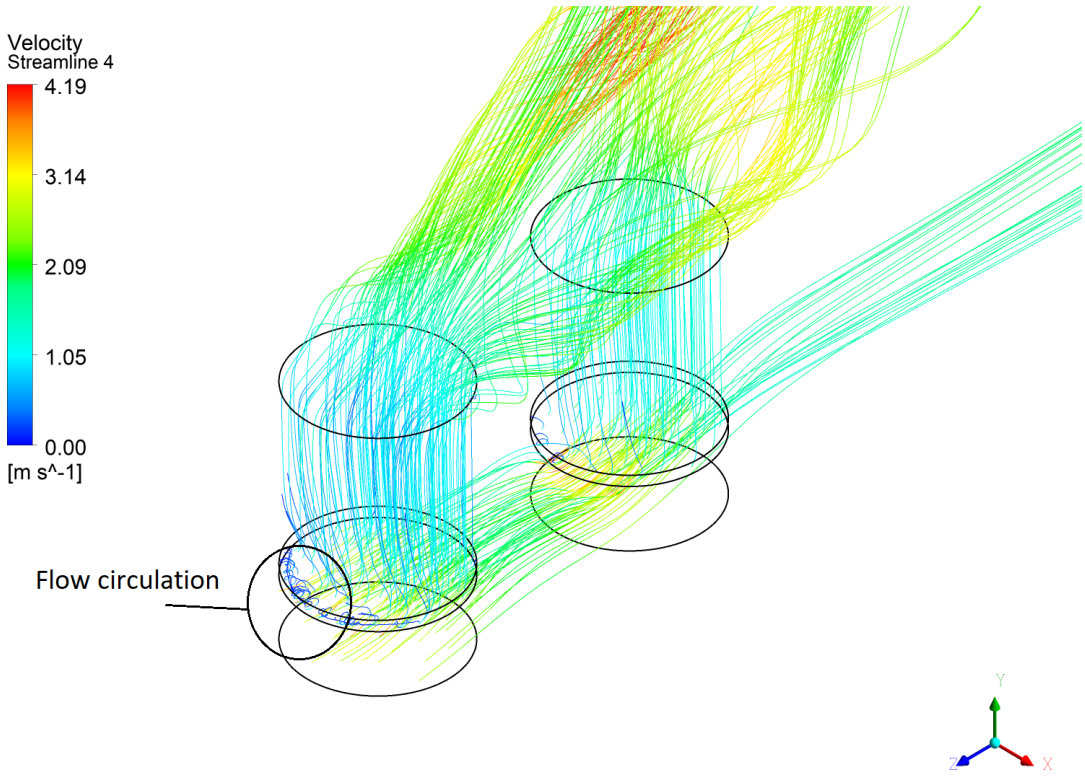

Figure 3.11. Isometric view of velocity streamlines around two NDDCTs at wind speed of 2 m/s, tower spacing of 1.8D, and wind incidence angle of 0°.

The protection of the windward tower results in a smaller flow circulation. Furthermore, the heat exchangers' temperature contours show that the temperature of the windward tower is higher than that of the leeward tower (Figure 3.10.B.*iii*).

Again, with the increased the wind speed to 6 m/s, the heat exchanger temperature of the windward tower increases compared to the wind speed of 4 m/s. The protection provided for the leeward tower from the windward tower is evident, and the difference between the heat exchanger temperature of the windward tower and leeward tower shown by Figure 3.10.C.*iii* is significant. At this wind speed, the velocity streamlines show that the flow circulation at the bottom of the windward tower becomes dominant over the entire heat exchanger surface (Figure 3.10.C.*ii*).

Finally, at 8 m/s, the flow deflected by the windward tower aligns with the wind direction and does not converge in front of the leeward tower (Figure 3.10.D.*i* and *ii*). This results in the leeward tower being protected, even at high wind speeds. The temperature of the windward tower at the wind speed of 6 m/s is higher than the temperature of the windward

tower at the wind speed of 8 m/s (Figure 3.10.D.*iii*) which implies an increase in forced convection from the windward tower.

Previously in the single tower analysis, shown by Figure 3.3, it was noted that the wind deflects the warm air exiting the tower, consequently, the warm air is cooled at the interface of the tower's outlet and reaches the ambient temperature. This causes this cold air to sink back into the tower, which results in a reduction in the effective draft height, an effect known as cold flow intake. To illustrate this behaviour in a tow-tower configuration, Figure 3.12 shows the velocity streamlines around two NDDCTs at a tower spacing of 1.8D and wind incidence angle of 0°. Larger flow circulations at the towers' outlet results in more cold flow intake. To investigate the rise of warm-air vortices in the wake region of windward tower and their interference with the leeward tower's outlet, the streamlines are shown only around the NDDCTs to allow better visualization of flow around the NDDCTs.

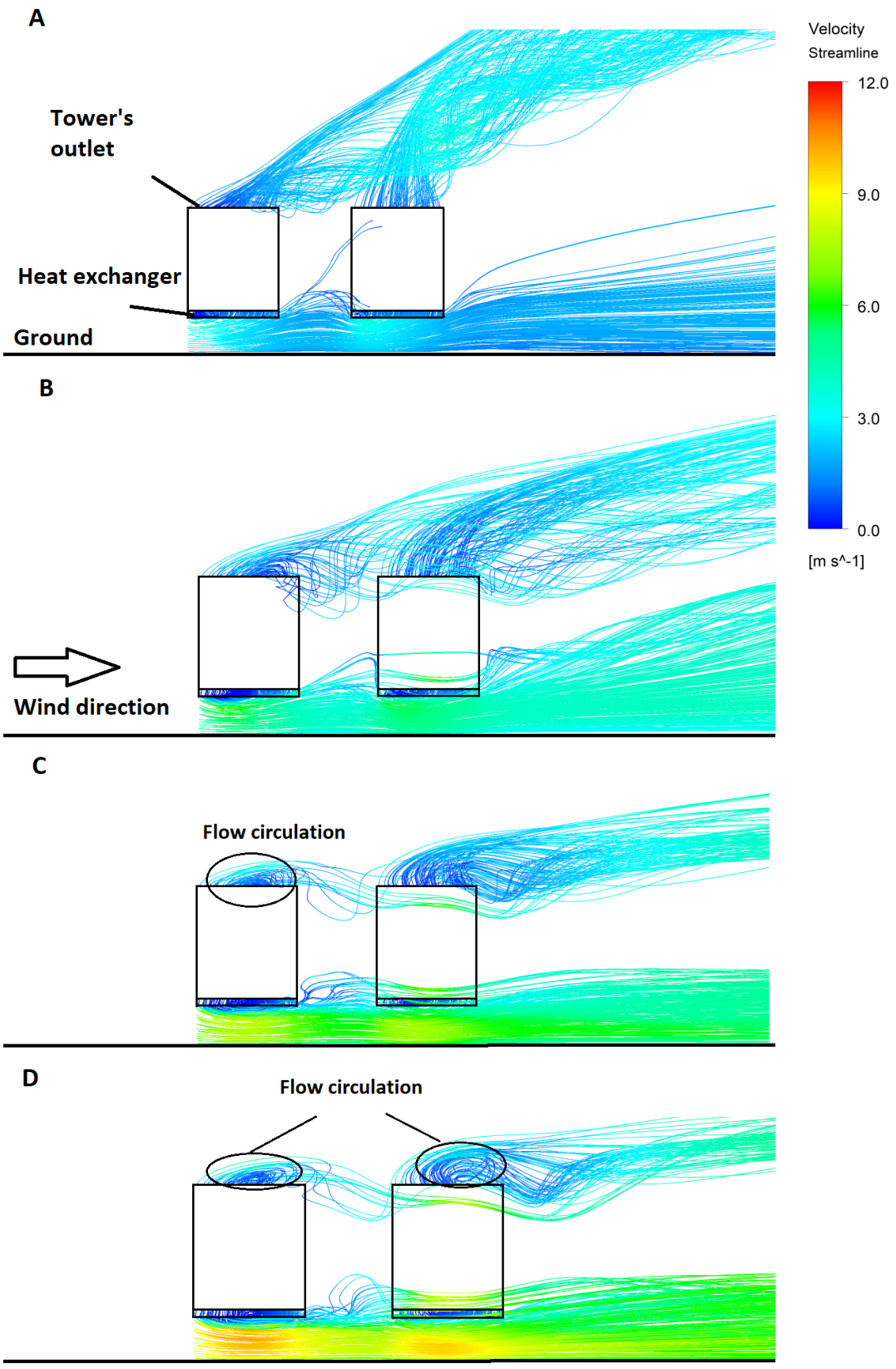

Figure 3.12. Velocity streamlines around two NDDCTs at wind incidence angle of 0° and tower spacing of 1.8D at wind speeds of 2 m/s (A), 4 m/s (B), 6 m/s (C), and 8 m/s (D).

At a wind speed of 2 m/s (Figure 3.12.A), the plume of the windward tower is deflected due to the existence of the crosswind. This deflection is less pronounced in the leeward tower, meaning that the plume of the windward tower protects the leeward tower, though it can be seen that some streamlines rise in the wake region of the windward tower. For all wind speeds, the deflection of the plume of the leeward tower is less than for the windward tower. The flow circulation is evident for the windward tower from a wind speed of 4 m/s (Figure 3.12.B), while this occurs at a wind speed of 6 m/s for the leeward tower (Figure 3.12.C). The reason for the reduced protection of the windward tower compared with the leeward tower at high wind speeds is that at these wind speeds the plume exits almost horizontally instead of moving vertically. When the plume exits the tower's outlet vertically it acts as a barrier and protects the leeward tower outlet from the upcoming wind. At high wind speeds the inertia force exerted on the plume is much higher than the draft speed of the air moving inside the tower, which results in flow deflection.

Having observed that the wake, at an inter-tower spacing of 1.8D, sheltered the leeward tower, it might be expected that increasing the tower spacing will reduce the protection of the leeward tower, as there is enough spacing between the towers for the separated flow of the windward air to reattach. In this regard Figure 3.13 shows the velocity contour and velocity streamlines at the inlet height, and the heat exchangers' temperature distribution at wind incidence angle of 0°, and tower spacing of 2.6D at different wind speeds. At the lowest wind speed shown by Figure 3.13.A.*ii*, the velocity streamlines show that some of the deflected flow from the windward tower is reattached at the front of the leeward tower.

The low-velocity region in front of the leeward tower (Figure 3.13.A.*i*) means there is still flow protection for the leeward tower. The wind causes flow circulations at the windward side of the towers which result in a high temperature at these regions (Figure 3.13.A.*iii*).

At a wind speed of 4 m/s, the wind causes a flow recirculation at the bottom of both towers (Figure 3.13.B.*ii*) while the flow recirculation at the windward tower is much larger than that of the leeward tower. As a result, the temperature contours, show that the heat exchanger temperature of the windward tower is higher than the leeward tower (Figure 3.13.B.*iii*), which means there still protection for the leeward tower is provided by the windward tower. By comparing these results with the tower spacing of 1.8D, the heat exchanger temperature of the leeward tower has been shown to increase by increasing the tower spacing. This demonstrates that increasing the tower spacing reduces protection provided by the windward tower.

Taking this to it's extreme, at a wind speed of 8 m/s the separated flow from the windward tower does not reattach in front of the leeward tower, which results in a low-velocity region between the towers (Figure 3.13.D.*i* and *ii*).

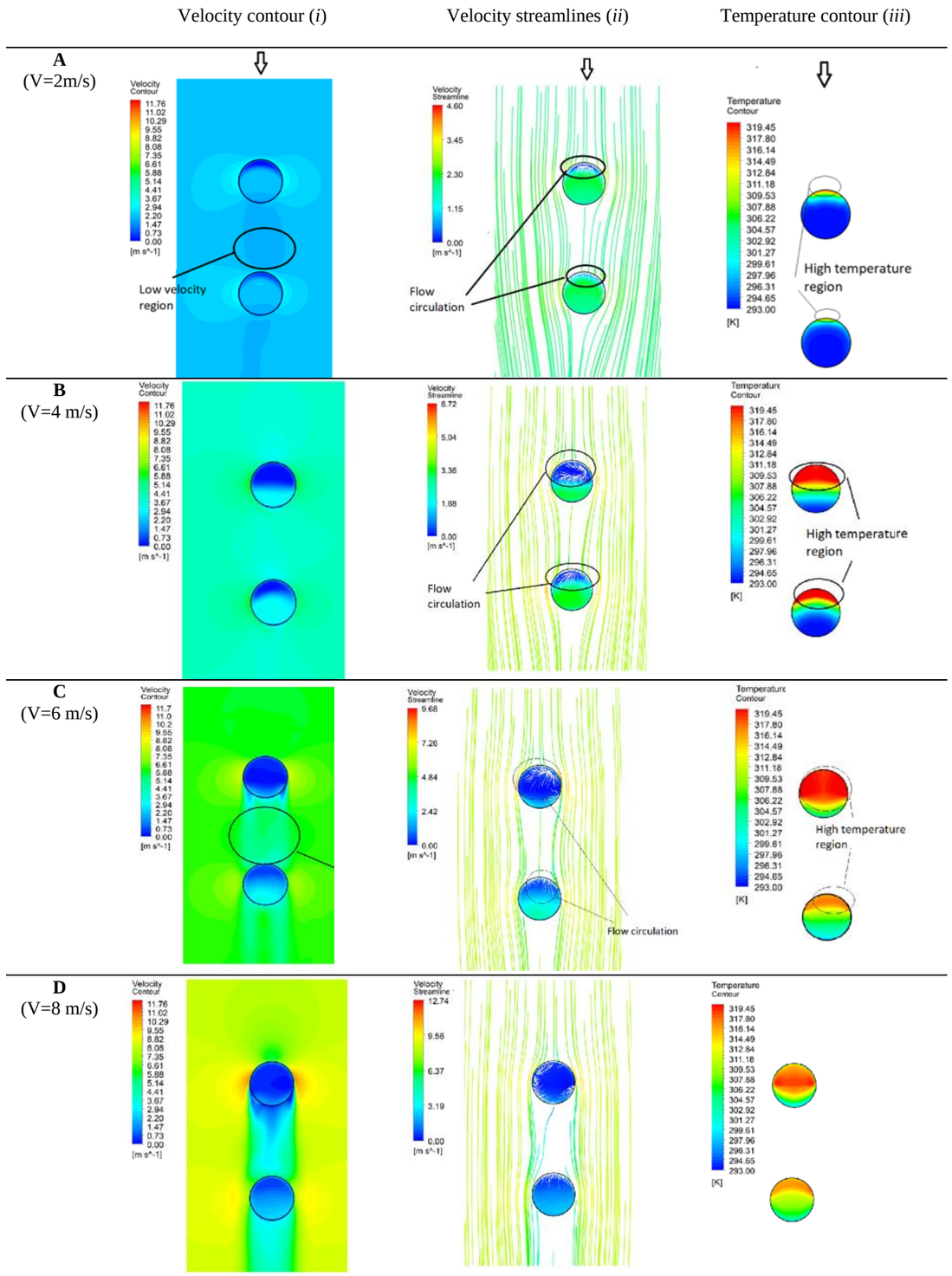

Figure 3.13. Velocity contour and streamlines at the inlet height and heat exchanger temperature contour of both NDDCTs at wind incidence angle of 0°, tower spacing of 2.6D, and wind speeds of 2 m/s (A), 4 m/s (B), 6 m/s (C), and 8 m/s (D).

This increase in wind speed increases the required length for the separated flow over an object to reattach. Hence, the velocity streamlines show that no velocity lines interfere with the windward region of the leeward tower.

Viewing this result in another way, Figure 3.14 shows a side view of the velocity streamlines around two NDDCTs at a wind incidence of 0° and tower spacing of 2.6D. As for the tower spacing of 1.8D, the plume of the windward tower exits the tower's outlet vertically at low wind speeds and horizontally at high wind speeds. The wind deflects the plume, and this deflection increases as the wind speed increases. Previously, it was noted that the deflection of the plume reduces the heat rejection of the tower. The deflection of the leeward tower's plume is less than that of the windward tower's, which means that the windward tower outflow protects the leeward tower's outlet. The plume of the windward tower effectively acts as a windbreak. At a wind speed of 8 m/s (Figure 3.14.D), the plume of the windward tower exits horizontally and does not provide protection for the leeward tower.

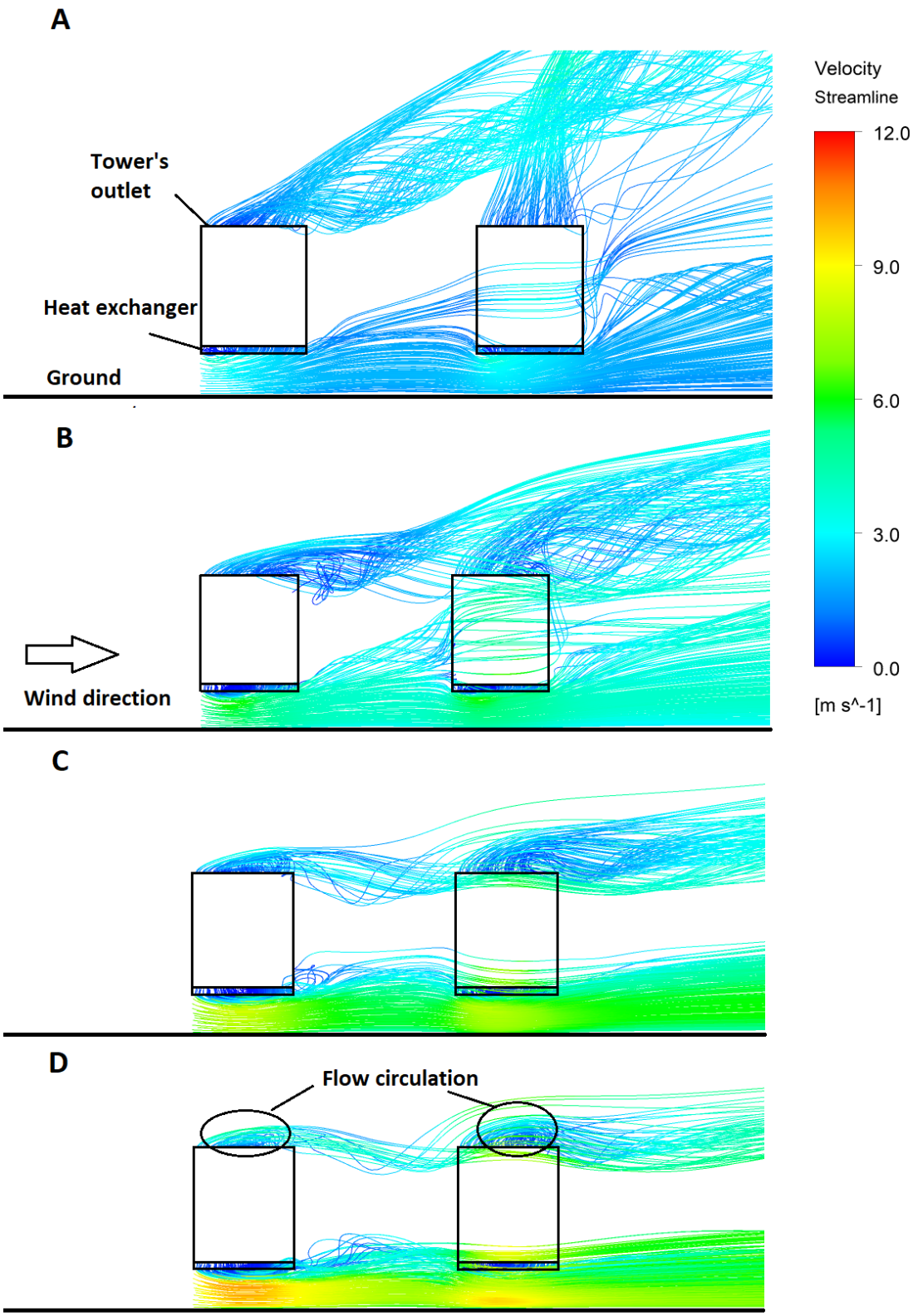

Figure 3.14. Velocity streamlines around two NDDCTs at wind incidence angle of 0° and tower spacing of 2.6D at wind speeds of 2 m/s (A), 4 m/s (B), 6 m/s (C), and 8 m/s (D).

Finally, if the spacing between the towers is increased enough, such that the separated flow from the windward tower reattaches in front of the leeward tower, it would be expected that the windward tower protection of the leeward tower would decrease. Figure 3.15 shows the velocity streamlines and contours at the inlet height, and heat exchanger temperature distribution at wind incidence of 0° and wind speeds, when the tower spacing is increased to 4.2D. The temperature contour shows that there is a difference between the heat exchanger temperature of the windward and leeward towers, which means there is still protection from the windward tower at a wind speed of 2 m/s (Figure 3.15.A).

At a wind speed of 4 m/s, the protection provided by the windward tower is the same as for the tower spacing of 2.6D and 1.8D (Figure 3.15.B.i and ii). The temperature contour shows that there is protection for the leeward tower, however, this protection is not significant as it results in a similar heat exchanger temperature (Figure 3.15.B.iii).

By increasing the wind speed to 6 m/s, the difference between the heat exchanger temperatures of the NDDCTs becomes more noteworthy (Figure 3.15.C.iii).This is because at high wind speeds the distance needed for reattachment of the separated flow (deflected flow) over the windward tower becomes greater (Figure 3.15.C.ii). This means that the local velocity between the towers decreases (Figure 3.15.C.i).

The flow protection for the leeward tower is notable at a wind speed of 8 m/s (Figure 3.15.D.ii). The low-velocity region between the towers is highlighted (Figure 3.15.D.i), which results in different heat exchanger temperatures of the windward and leeward towers (Figure 3.15.D.iii).

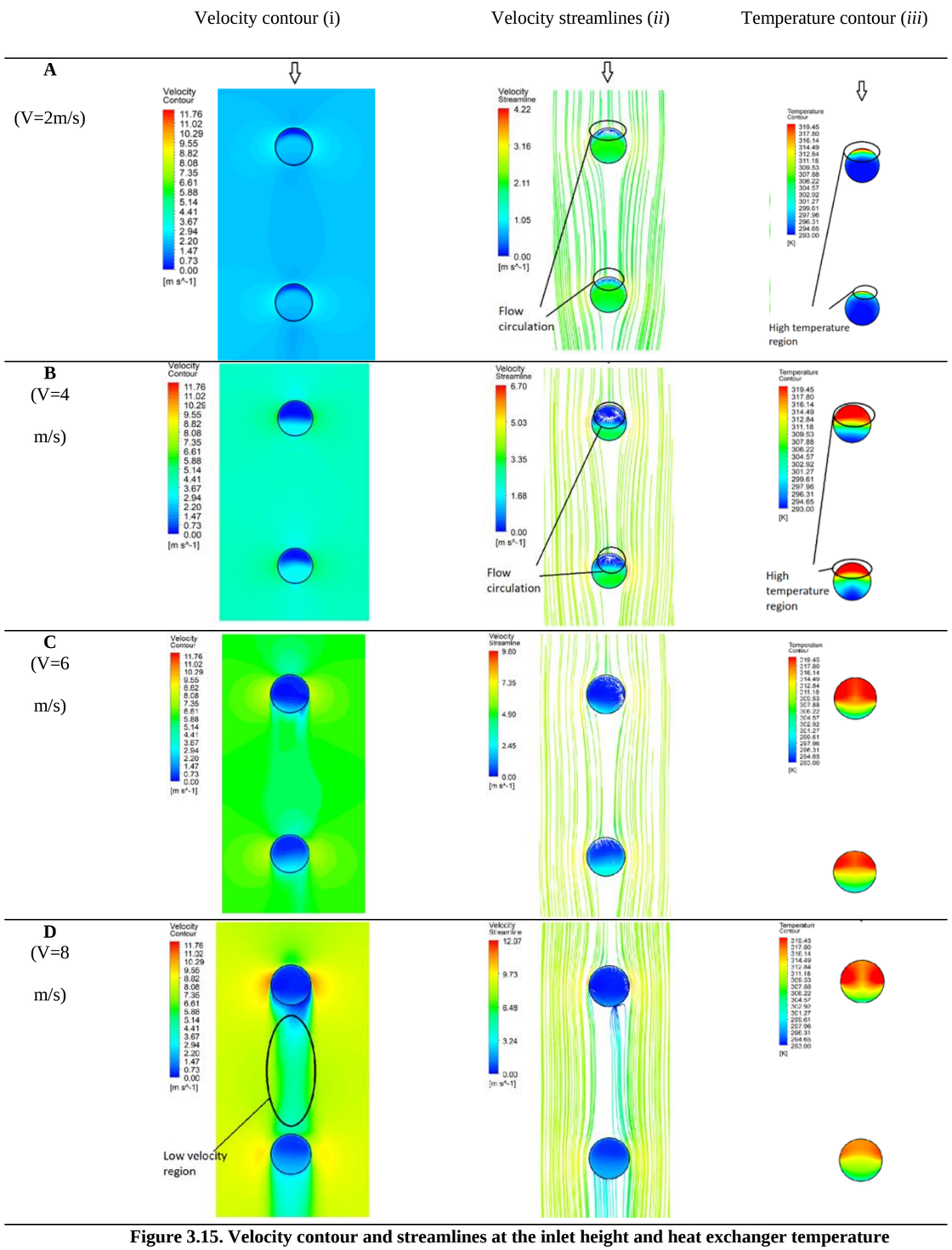

Figure 3.15. Velocity contour and streamlines at the inlet height and heat exchanger temperature contour of both NDDCTs at wind incidence angle of 0°, tower spacing of 4.2D, and wind speeds of 2 m/s (A), 4 m/s (B), 6 m/s (C), and 8 m/s (D).

To investigate the interference of the NDDCTs from the outlet, the velocity streamlines around the NDDCTs at a wind incidence of 0° and tower spacing of 4.2D is illustrated in Figure 3.16. At a wind speed of 2 m/s shown by Figure 3.16.A, the plume deflection of the windward and leeward towers is not substantial. The flow in the wake of the windward tower rises gradually toward the leeward tower's outlet and interferes with it. This also can be seen at the wind speed of 4 m/s (Figure 3.16.B), and the flow circulation at this wind speed can be seen, as highlighted. At wind speeds of 6 m/s and 8 m/s, the flow in the wake region of the windward tower does not rise and move vertically toward the next tower (Figure 3.16.C and D). At high wind speeds, the windward tower cannot protect the leeward tower's outlet since the plume of the windward tower exits horizontally and cannot act as a windbreak.

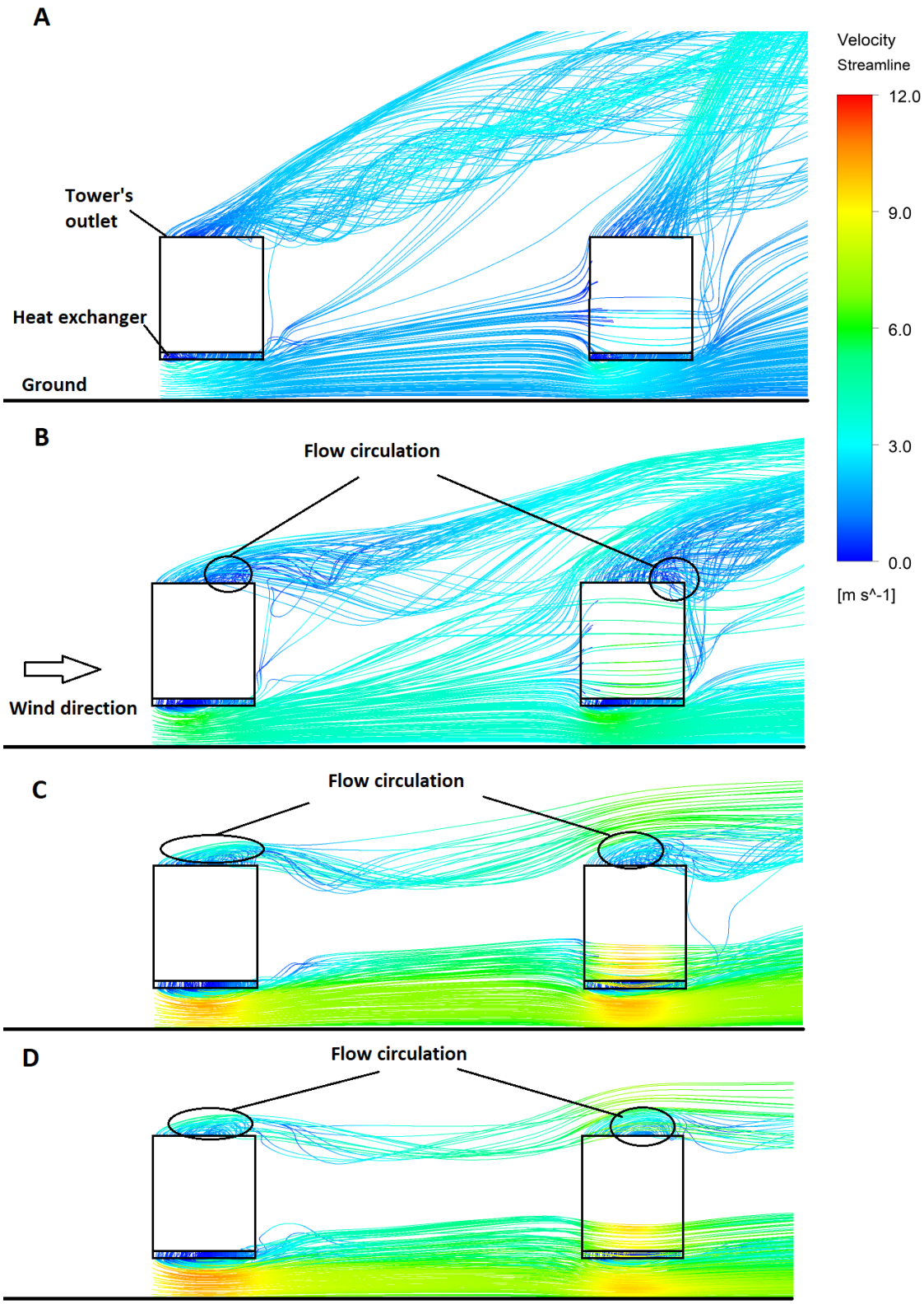

Figure 3.16. Velocity streamlines around two NDDCTs at wind incidence angle of 0° and tower spacing of 4.2D at wind speeds of 2 m/s (A), 4 m/s (B), 6 m/s (C), and 8 m/s (D).

Therefore, at a wind incidence of 0°, the flow and temperature fields demonstrate that the windward tower provides significant protection for the leeward tower at all wind speeds for both the bottom and top of the tower. The flow and temperature fields also suggest that by increasing the tower spacing the protection of the leeward tower will decrease. To illustrate this point Figure 3.17 presents the normalized heat rejection of the two NDDCTs at a wind incidence of 0° and at different tower spacings. The heat rejection from the windward towers is similar to that of an isolated tower. Conversely, the heat rejected by the leeward tower is highest at a tower spacing of 1.8D and lowest at a tower spacing of 4.2D, which means that increasing the tower spacing decreases the protection provided by the windward tower.

At tower spacings of 2.6D and 4.2D, the heat rejection of the leeward tower increases for wind speeds beyond 6 m/s. As the flow field analysis suggested, the reattachment length of the separated flow from the windward tower increases as the wind speed increases. This provides a low-velocity region in front of the leeward tower as shown in flow field analysis.

There is a consistency between the current results and findings of (68) which indicates that at wind incidence of 0°, the closer the two towers are, the thermo-flow performance of the leeward tower is. This has also been indicated in wind tunnel test visualization which is described in Appendix D.

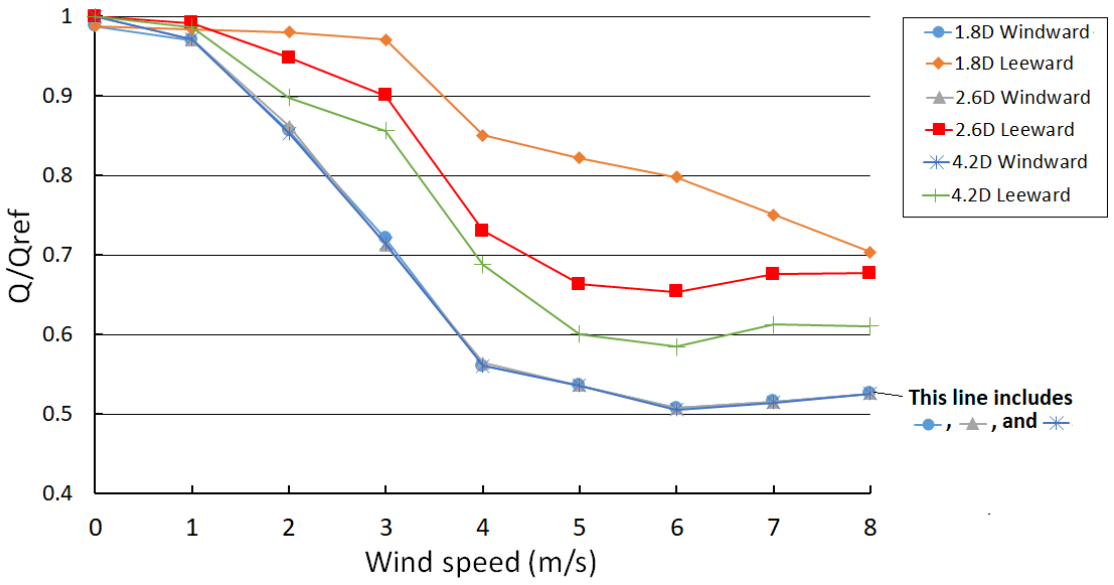

Figure 3.17. The normalized heat rejection of two NDDCTs at wind incidence of 0°.

3.4.2. Wind incidence of 45°

In the previous section it was demonstrated that when the towers lay along the line of the wind direction, the windward tower would act as a passive windbreak. However, this may not be true once the wind direction changes. To examine this effect the leeward tower was orientated at 45° to the windward tower's axis.

Figure 3.18 shows the velocity streamlines and contours, and heat exchanger temperature, of two NDDCTs at a wind incidence angle of 45°, tower spacing of 1.8D, and different wind speeds. At a wind incidence angle of 45°, the windward tower deflects the flow as it did previously, however, the flow deflected from one side of the windward tower moves toward the leeward tower. The NDDCTs' orientation creates a contractive passage which accelerates the flow between the towers. At a wind speed of 2 m/s, this flow acceleration between the towers is not significant (Figure 3.18.A.i and ii). This results in a similar heat exchanger-temperature distribution (Figure 3.18.A.iii). At a wind speed of 4 m/s, a high-velocity region is highlighted (Figure 3.18.B.i). The local high-velocity region in that region may cause flow instabilities, which result in a higher temperature region at the right side of the leeward tower compared with the left side of the tower (Figure 3.18.B.iii).

Again, at wind speed of 6 m/s, the high-velocity region between the towers is highlighted (Figure 3.18.C.i), and the temperature distributions of the heat exchangers show that the leeward tower temperature is higher than that of the windward tower (Figure 3.18.C.iii).

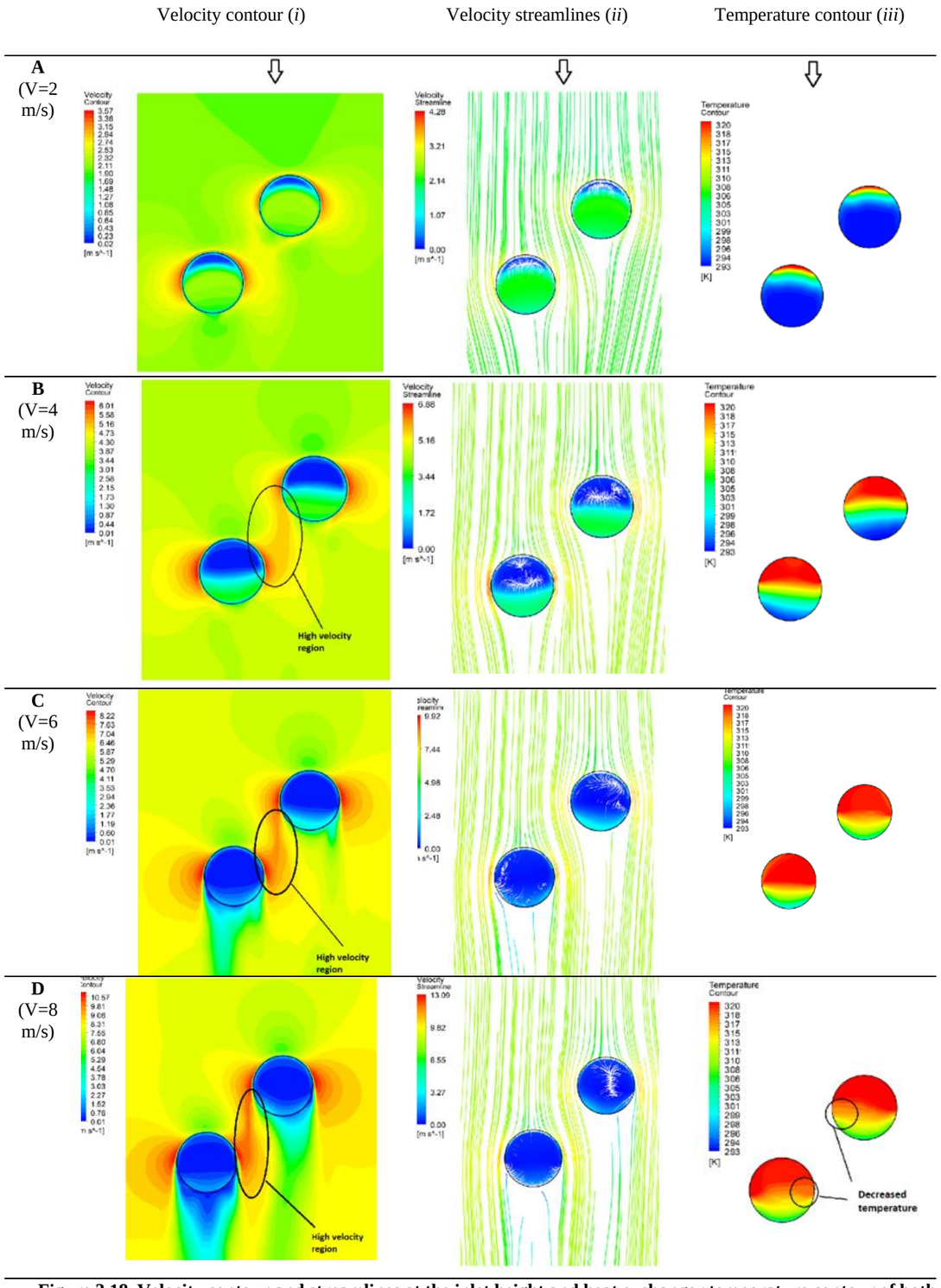

Figure 3.18. Velocity contour and streamlines at the inlet height and heat exchanger temperature contour of both NDDCTs at wind incidence angle of 45°, tower spacing of 1.8D, and wind speeds of 2 m/s (A), 4 m/s (B), 6 m/s (C), and 8 m/s (D)

At 8 m/s, the high-velocity region between the NDDCTs becomes the dominant feature of the flow (Figure 3.18.D.*i*). Now, at a lower wind speed this high-velocity region decreases the thermal performance of the heat exchanger in that region and the temperature increases. Here, the high-velocity region between the towers decreases the heat exchanger temperature (Figure 3.18.D.*iii*). As discussed earlier, at very high wind speeds the forced-convection component increases and compensates the decreased total heat-rejection, due to the negative effect of the crosswind.

To investigate whether, for the NDDCTs, a wind incidence of 45° and tower spacing of 1.8D causes interference at the outlets, the velocity streamlines of the towers' outlets at a wind speed of 4 m/s are displayed in Figure 3.19. The plumes of the towers at this condition do not interfere with each other, hence, at a wind incidence of 45° and tower spacing of 1.8D there is no interaction between the outlets of the towers.

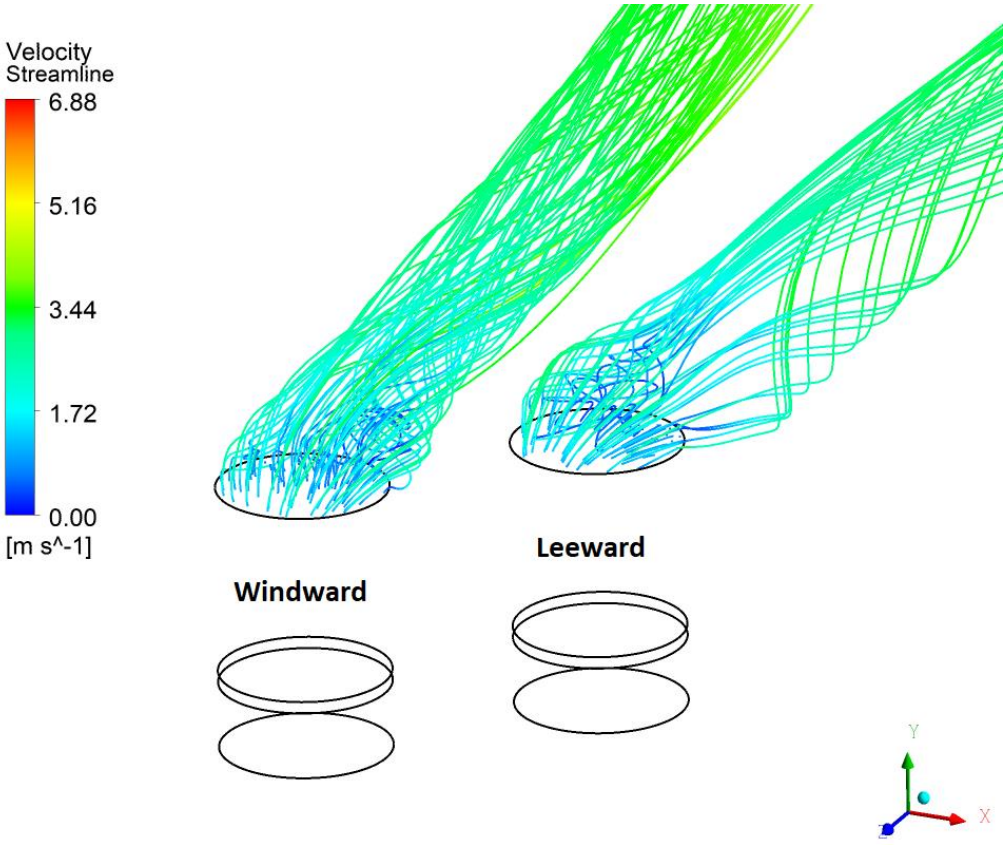

Figure 3.19. Velocity streamline of the NDDCTs' outlets at tower spacing of 1.8D at wind speed 4 m/s (isometric view).

By increasing the tower spacing to 2.6D, at a wind speed of 2 m/s the velocity and temperature field of the two NDDCTs at a wind incidence of 45° is similar (Figure 3.20). The deflected flow of the windward tower moves toward the contractive passage between the towers as shown in Figure 3.20. However, because of the low wind speed and large tower spacing, a high-velocity region does not appear at this region, and the flow fields around the towers becomes similar. At a wind speed of 4 m/s, the high-velocity region between the towers becomes apparent (Figure 3.20.B.i) and, as discussed previously, this higher velocity causes flow instabilities in the NDDCTs. The high-velocity region causes the temperature of the leeward tower at the right side of the heat exchanger to increase as highlighted in Figure 3.20.C.iii. Further, at 6 m/s, the high wind-speed and the high-velocity region between the towers result in a high temperature over most of the heat exchanger for both towers (Figure 3.20.C).

Finally, at wind speed of 8 m/s, the same as for a tower spacing of 1.8D, at this wind speed the high-velocity region increases the forced heat-transfer component and compensates the decreased total heat rejection due to the negative impact of the crosswind (Figure 3.20.D). This result is the same as that found with a 1.8D tower spacing.

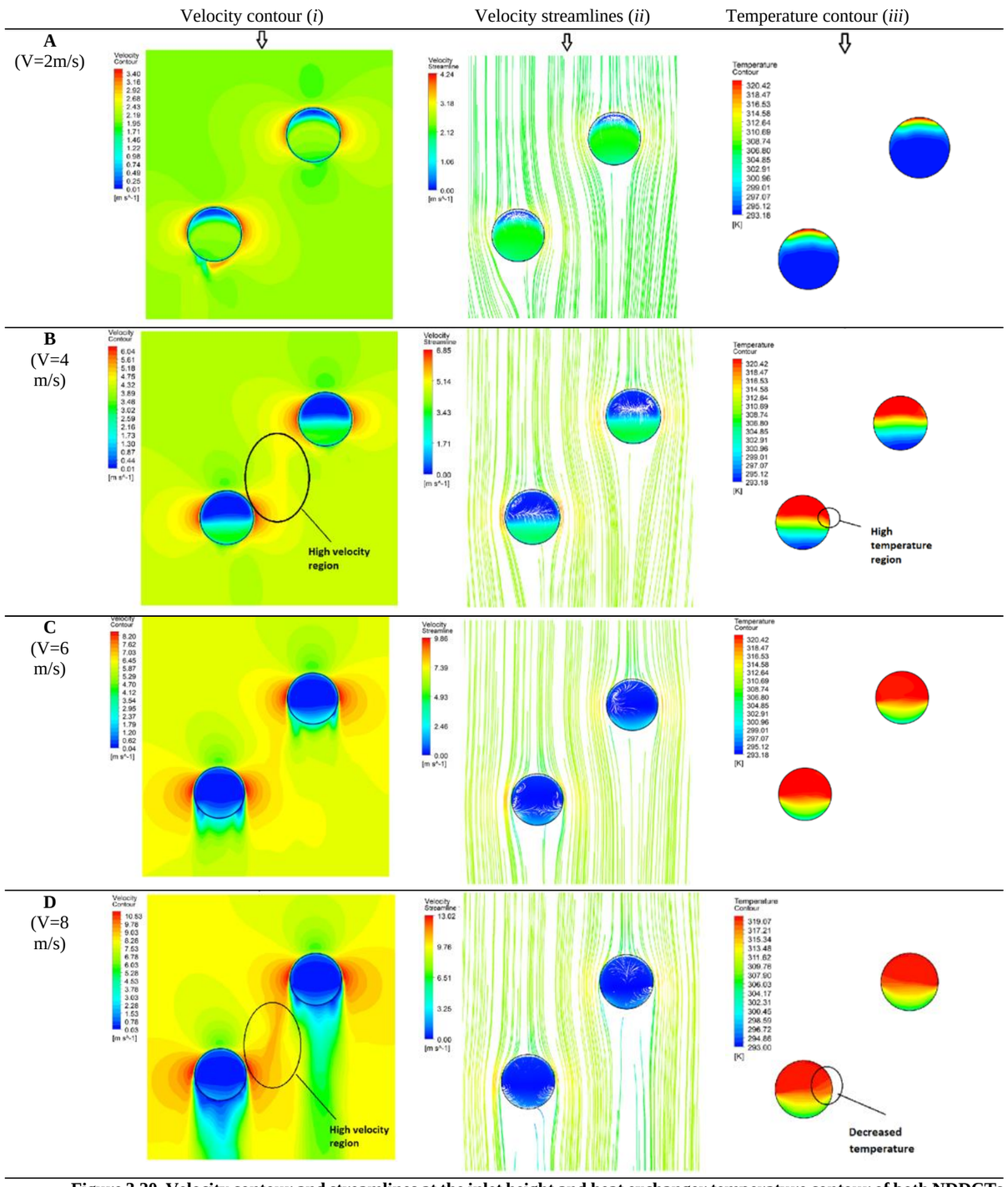

Figure 3.20. Velocity contour and streamlines at the inlet height and heat exchanger temperature contour of both NDDCTs at wind incidence angle of 45°, tower spacing of 2.6D, and wind speeds of 2 m/s (A), 4 m/s (B), 6 m/s (C), and 8 m/s (D).

Based on these observations, it is expected that at a wind incidence of 45° and tower spacing of 2.6D, the towers' will not interfere with each other and is the same result as that found at for the tower spacing of 1.8D. This is clearly shown to be the case as shown by Figure 3.21.

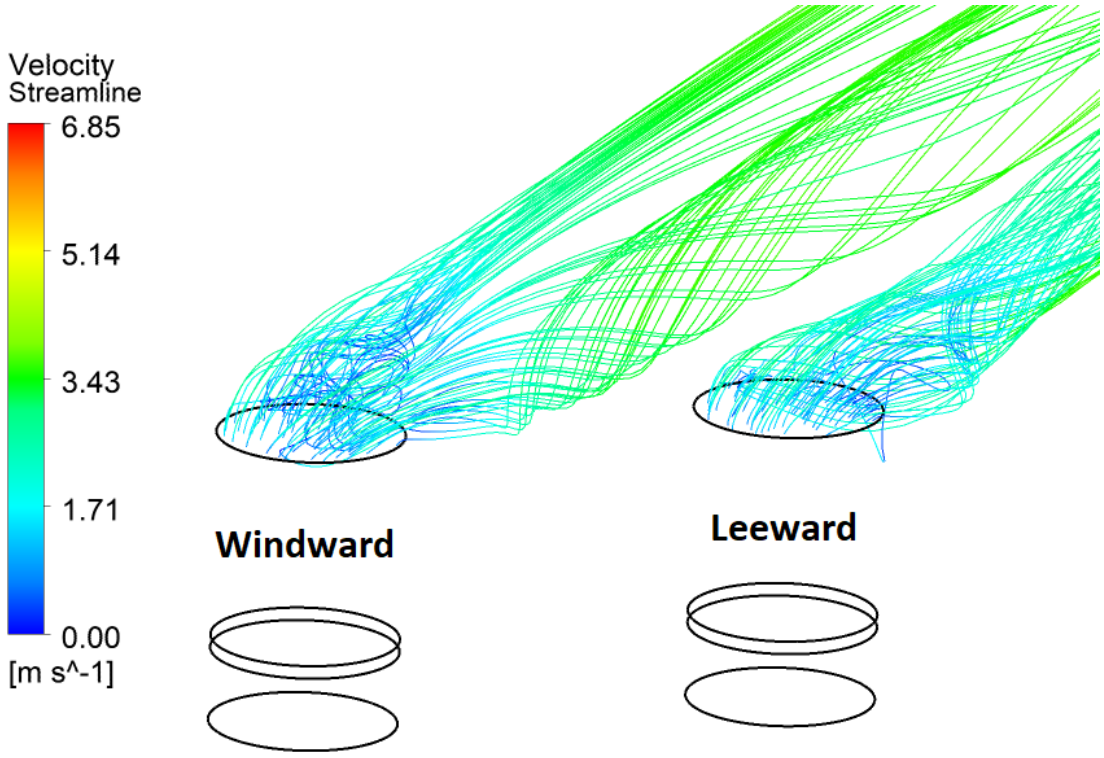

Figure 3.21. Velocity streamlines of the NDDCTs' outlets at tower spacing of 2.6D and wind speed of 4 m/s (isometric view).

Taking this idea to its extreme, Figure 3.22 shows the velocity and temperature fields of the two NDDCTs at a wind incidence of 45°, tower spacing of 4.2D, and wind speeds of 2 m/s, 4 m/s, 6 m/s, and 8 m/s respectively. The velocity and temperature fields show that at a tower spacing of 4.2D, the towers do not interact with each other and the thermo-flow performance of the towers exhibits similar characteristics at all wind speed considered.

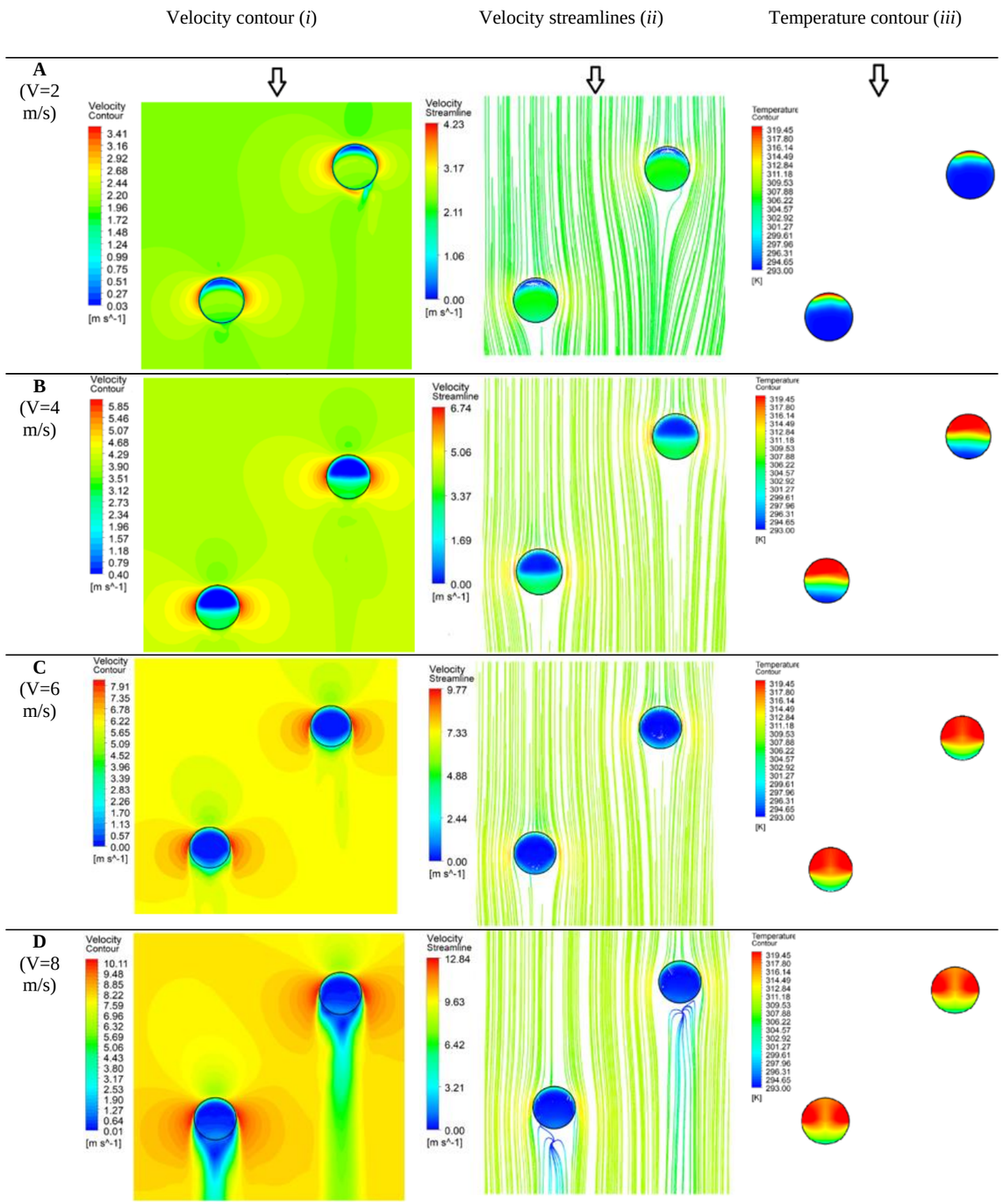

Figure 3.22. Velocity contour and streamlines at the inlet height and heat exchanger temperature contour of both NDDCTs at wind incidence angle of 45°, tower spacing of 4.2D, and wind speeds of 2 m/s (A), 4 m/s (B), 6 m/s (C), and 8 m/s (D).

As with the previous tower spacings, the outflowing plume from each tower do not interfere with each other at tower spacing of 4.2D, as shown in Figure 3.23.

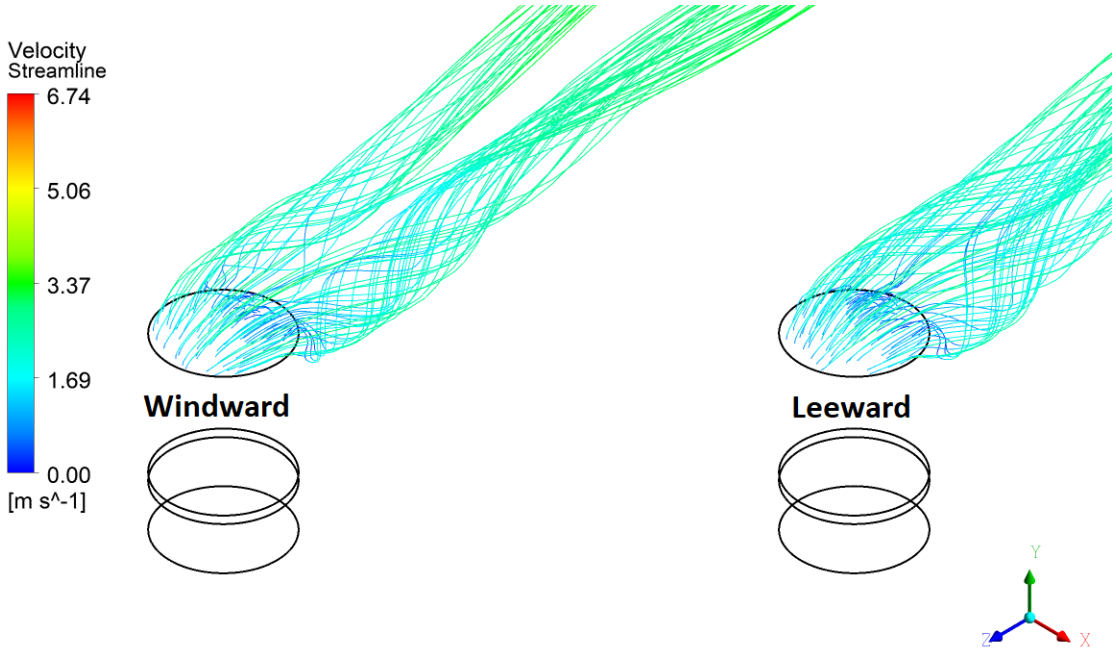

Figure 3.23. Velocity streamlines of the NDDCTs' outlets at tower spacing of 4.2D and wind speed 4 m/s (isometric view).

It is apparent that at a wind incidence angle of 45°, the flow and temperature fields suggest the windward tower does not protect the leeward tower to the same extent as for when the flow is in line with the orientation of the towers. At tower spacings of 1.8D and 2.6D, the contractive passage between the towers causes increased local velocity, which is not beneficial for the NDDCTs. In particular, at a tower spacing of 4.2D, the NDDCTs appear to act as isolated towers and do not interact with each other. Figure 3.24, showing the normalized heat rejection of the two NDDCTs at different tower spacings, supports this assertion. Although the leeward tower's heat rejection is less than that of the windward tower. The heat rejection of both the windward and leeward towers increases beyond a wind speed of 6 m/s. The heat transfer increment of the leeward tower is more than that of the windward tower or of an isolated tower. This is because the high local wind-velocity between the towers at high wind-speeds causes the forced heat transfer component of the total heat rejection for the leeward tower to increase. By increasing the

tower spacing the interaction between the NDDCTs decreases and, at a tower spacing of 4.2D, these towers act as isolated towers.

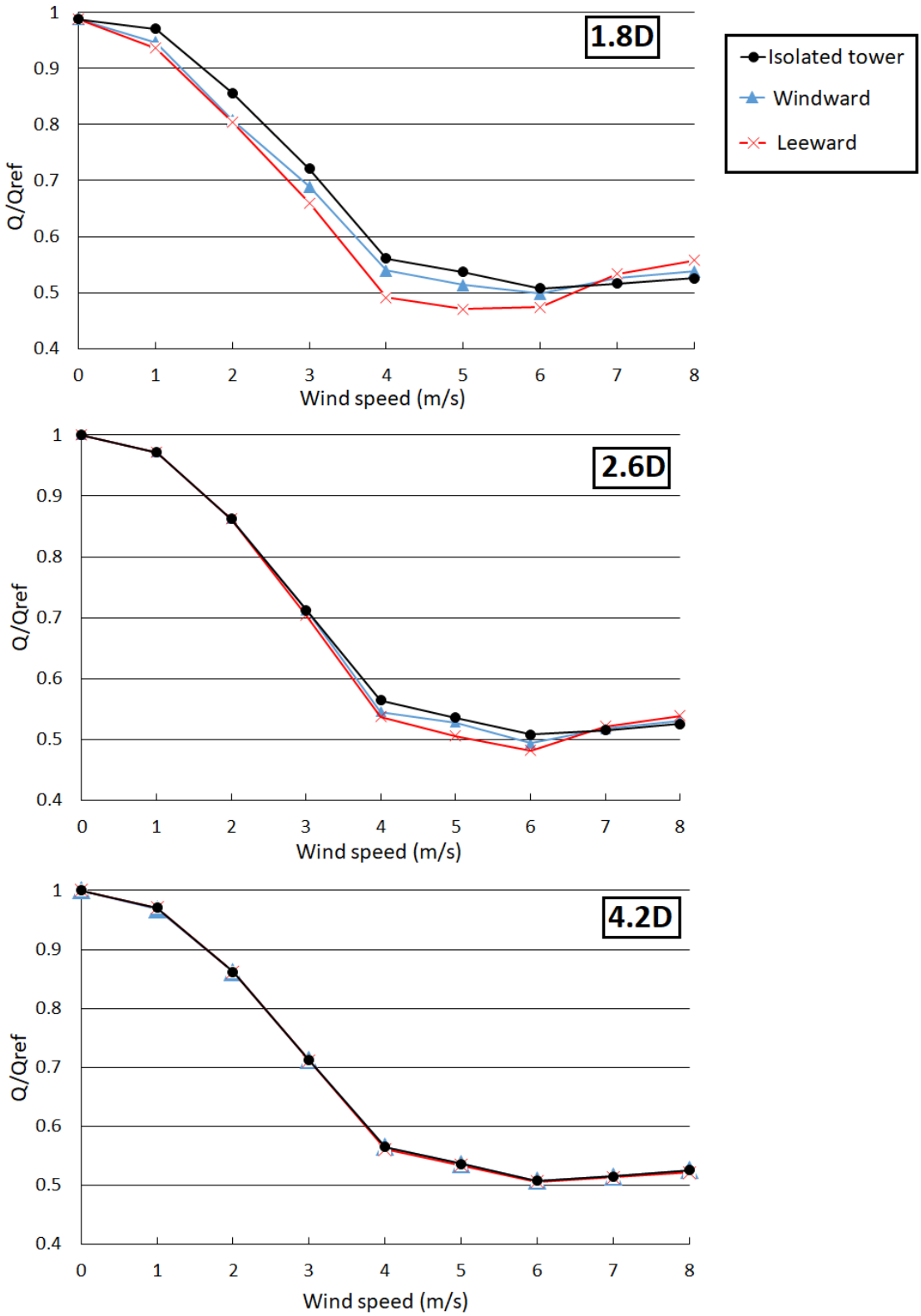

Figure 3.24. The normalized heat rejection of two NDDCTs at wind incidence of 45°.

At tower spacings of 1.8D and 2.6D, the interaction between the towers is not beneficial and the heat rejection of the towers is less than for an isolated tower. This can be attributed to the high-velocity region between the towers. The high velocity region in a contractive passage has been noted previously in Dai et al's (80) study which investigated the effect of wind on multiple buildings. However, the objects considered in their study were rectangular buildings without any interior thermal source.

3.4.3. Wind incidence of 90°

Having observed the effect of 0° and 45° flow, it was decided to explore what happened when the towers were placed beside each other that is at a 90° wind incidence. The velocity streamlines and contours at the inlet height, and heat exchanger temperature contour of the two NDDCTs at a wind incidence of 90°, tower spacing of 1.8D, and wind speed of 2 m/s, are displayed in Figure 3.25.A. As previously discussed, the low-velocity region at the bottom of the NDDCTs shows the flow circulations at the bottom of the towers. Here, the flow circulation has shifted toward the centre of the heat exchanger (Figure 3.25.A.*i* and *ii*). At a tower spacing of 1.8D, the contraction between the towers increases the wind velocity in that region (Figure 3.25.A.*i*), which is not beneficial for the NDDCTs. However, while this small passage between the towers means that little air can flow through the passage between the towers, there is a greater air flows into the windward side of both towers instead. The result of this is that the temperature contour shows a low temperature at the windward tip of the heat exchanger (Figure 3.25.A.*iii*).

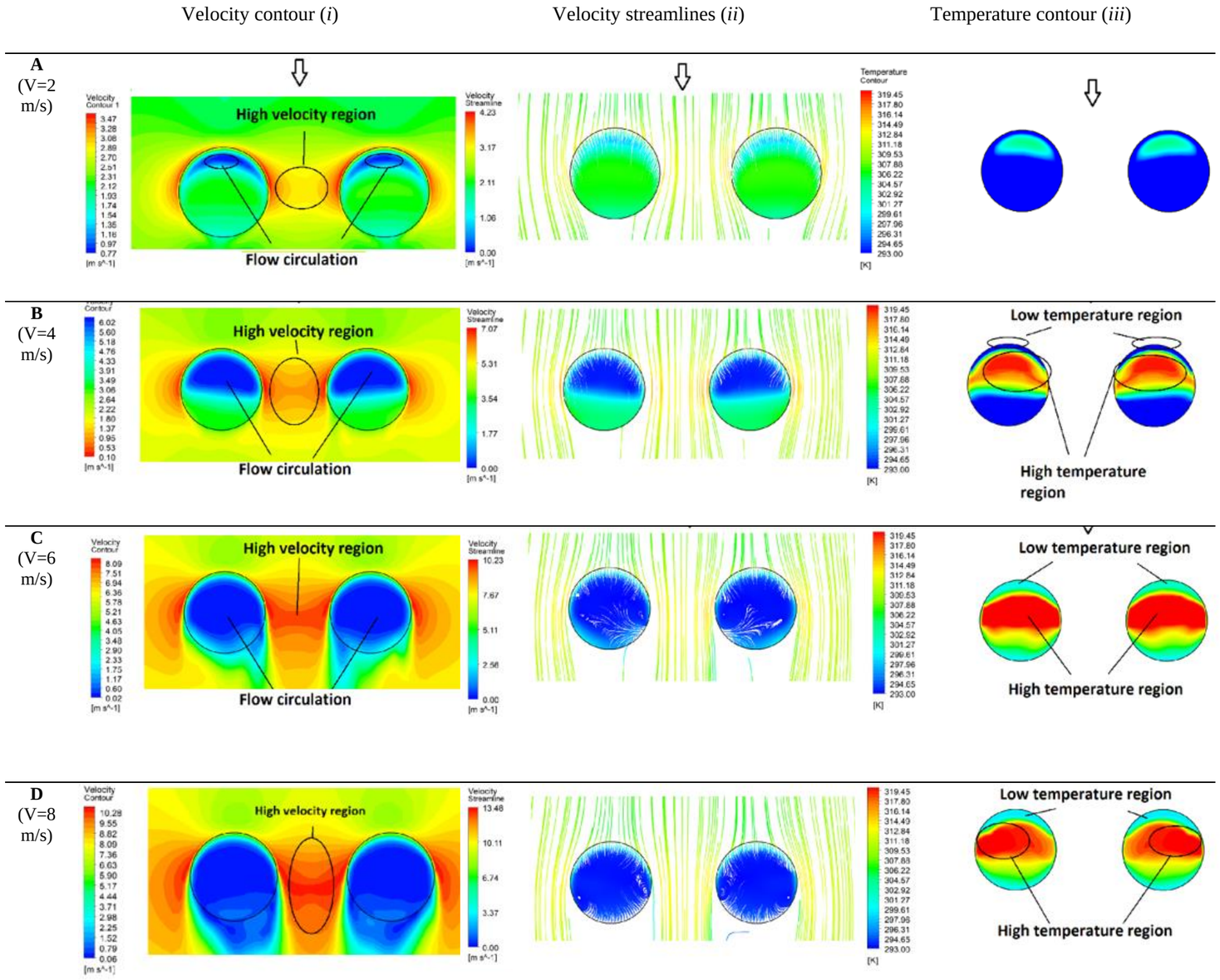

Figure 3.25. Velocity contour and streamlines at the inlet height and heat exchanger temperature contour of both NDDCTs at wind incidence angle of 90°, tower spacing of 1.8D, and wind speeds of 2 m/s (A), 4 m/s (B), 6 m/s (C), and 8 m/s (D).

By increasing the wind speed to 4 m/s, the high-velocity region between the towers becomes more apparent (Figure 3.25.B.*i*). The contraction between the towers means less air can flow through the passage between the towers, which means that more air flows onto the windward side of the towers instead. The flow circulation has again shifted toward the centre of the tower from the tip of the windward side of the towers. The high- and low-velocity regions of the heat exchanger are highlighted (Figure 3.25.B.*i* and *ii*). When the wind speed increases to 6 m/s, the flow circulation at the bottom of the towers becomes larger than that found at lower wind speeds (Figure 3.25.C.*i* and *ii*). However, there is still flow entering the NDDCTs from the windward side. The temperature distribution shows a notable difference between the tip of the windward side and the centre of the heat exchanger (Figure 3.25.C.*iii*).

Finally, at a wind speed of 8 m/s, the flow still enters the towers from the windward side causing the flow circulations to shift toward the leeward side of the tower (Figure 3.25.D.*i*). The temperature contour is the same as other wind speeds, showing a low-temperature region at the windward side of the NDDCTs (Figure 3.25.D.*iii*). As mentioned before, after the turnaround point increases the wind speed increases the total heat rejection of the towers. This is due to an increase in the forced heat transfer component of the total heat transfer.

At a wind incidence of 90° and tower spacing of 1.8D, the NDDCTs outflow plumes do not interfere with each other, as shown in Figure 3.26. The velocity streamlines show that the plume exits each NDDCT without any interaction. At this wind-incidence angle, when the plumes of the towers do not interfere with each other at the tower spacing of 1.8D, by increasing the tower spacing further, the same phenomena will be observed and there will be no interaction from top of the towers at even greater tower spacings. Therefore, the outlet flow fields of the towers for larger tower spacings will not be assessed.

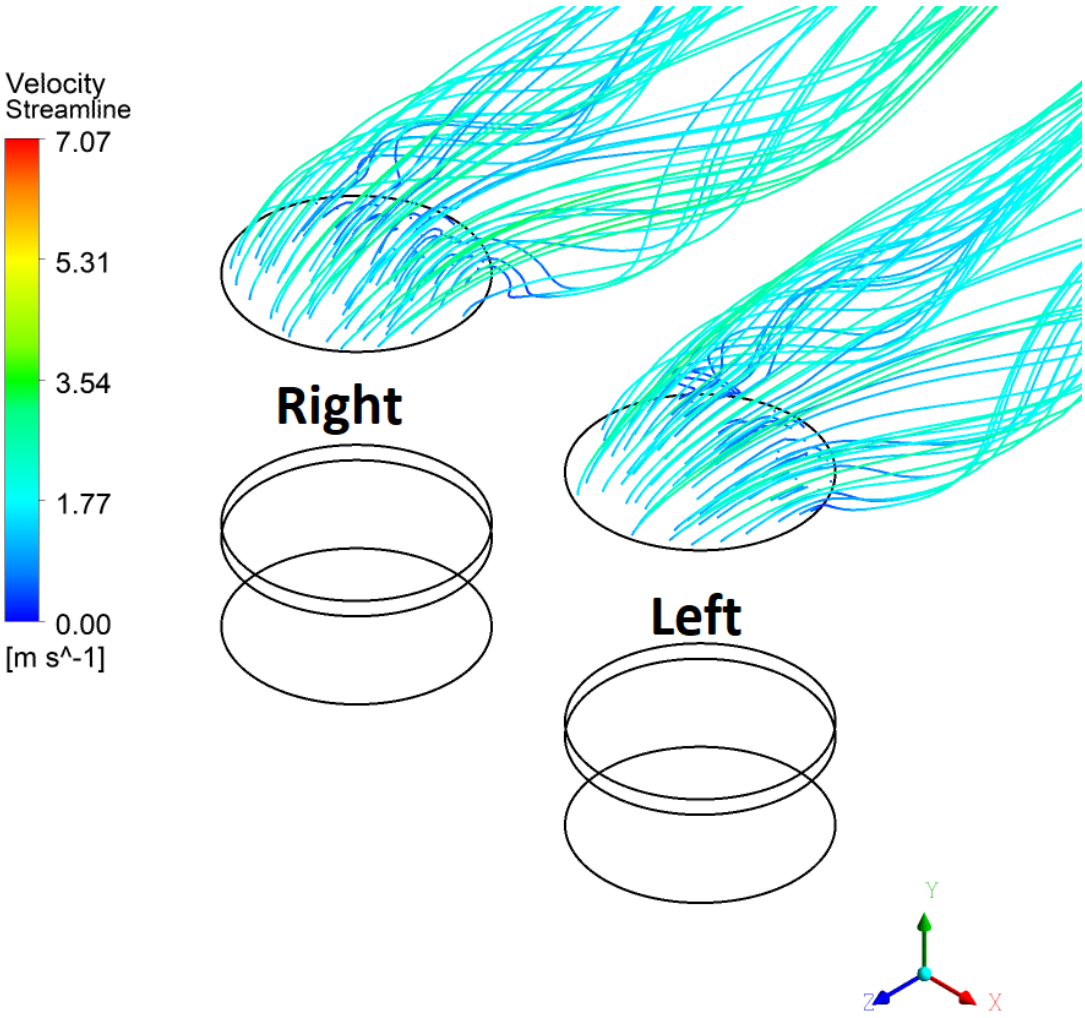

Figure 3.26. Velocity streamline of the NDDCTs' outlets at tower spacing of 1.8D and wind speed of 4 m/s (isometric view).

Exploring the effect of the tower spacing on the other factors, Figure 3.27.A shows the velocity streamlines and contours at the inlet height, and the heat exchanger temperatures, of the two NDDCTs at a wind incidence of 90°, tower spacing of 2.6D, for a wind speed of 2 m/s.

At a tower spacing of 2.6D, the reduced contraction between the towers does not create a low-velocity region and the towers act as two isolated towers. The velocity contour shows that flow circulation occurs at the tip of the heat exchangers (Figure 3.27.A.*i*), and the temperature contour shows a high temperature at this area (Figure 3.27.A.*iii*). Similarly, a wind speed of 4 m/s the flow and temperature fields show that there is no interaction between the towers and the towers act as isolated towers (Figure 3.27.B).

For a wind speed of 6 m/s, however the contraction between the towers causes a high-velocity region. The flow circulation at bottom of the towers has been shifted from the windward side of the towers to the leeward side (Figure 3.27.C.*i*). This change causes less air to flow through the passage between the towers and more air to flows into the windward side of the towers. The resulting temperature contours show that the windward side of the heat exchangers is cooler than the middle and leeward regions of the heat exchangers (Figure 3.27.C.*iii*).

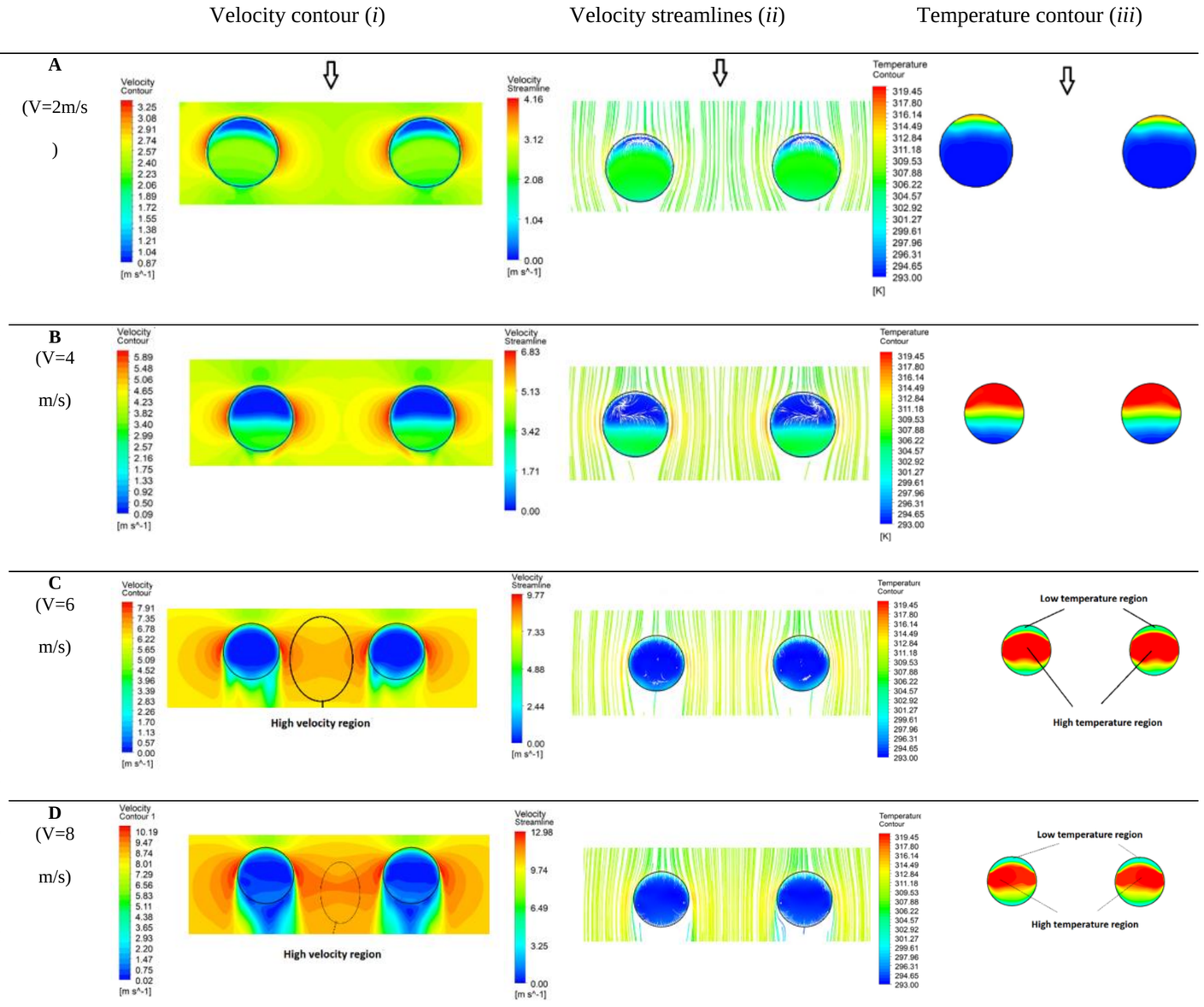

Figure 3.27. Velocity contour and streamlines at the inlet height and heat exchanger temperature contour of both NDDCTs at wind incidence angle of 90°, tower spacing of 2.6D, and wind speeds of 2 m/s (A), 4 m/s (B), 6 m/s (C), and 8 m/s (D).

At a wind speed of 8 m/s, the same flow field can be seen as for a wind speed of 6 m/s (Figure 3.27.D). By comparing the temperature contour of the heat exchangers at wind speeds of 6 m/s and 8 m/s, the temperatures of the NDDCTs at a wind speed of 8 m/s is lower than at 6 m/s (Figure 3.27.D.*iii*). This demonstrates the heat rejection increases after a certain wind speed, which is the turnaround point as discussed earlier in this chapter.

At a wind incidence angle of 90° and tower spacing of 2.6D, it was previously observed that the NDDCTs act as isolated towers at low wind speeds of 2 m/s and 4 m/s. Here, at a tower spacing of 4.2D, the velocity and temperature fields show (Figure 3.28) that the towers do not interact with each other and act as isolated towers at all considered wind speed.

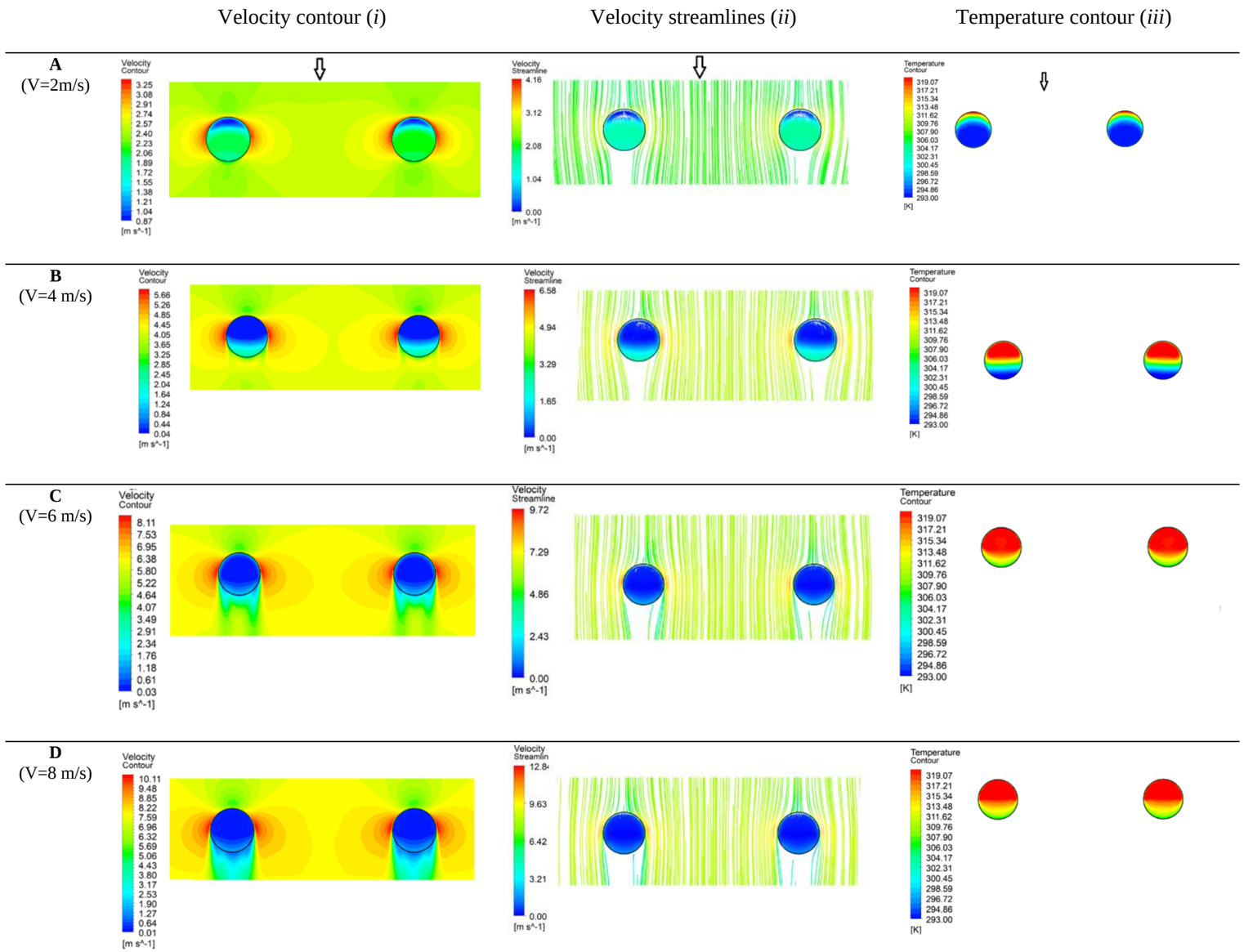

Figure 3.28. Velocity contour and streamlines at the inlet height and heat exchanger temperature contour of both NDDCTs at wind incidence angle of 90°, tower spacing of 4.2D, and wind speeds of 2 m/s (A), 4 m/s (B), 6 m/s (C), and 8 m/s (D).

Figure 3.29 shows the heat rejection of the two NDDCTs at a wind incidence of 90° at different tower spacings. Due to the symmetrical layout of the towers at a wind incidence of 90° the performance of the two towers is similar. The normalized heat rejection of an isolated tower is also shown, to compare the thermal performance of the two NDDCTs with that of a single tower. The blockage of the flow in front of the towers at a tower spacing of 1.8D and 2.6D results in increased air flow onto the windward side of the towers. By increasing the tower spacing, the interaction of the towers decreases, and the normalized heat rejection becomes like that of an isolated tower at a tower spacing of 4.2D.

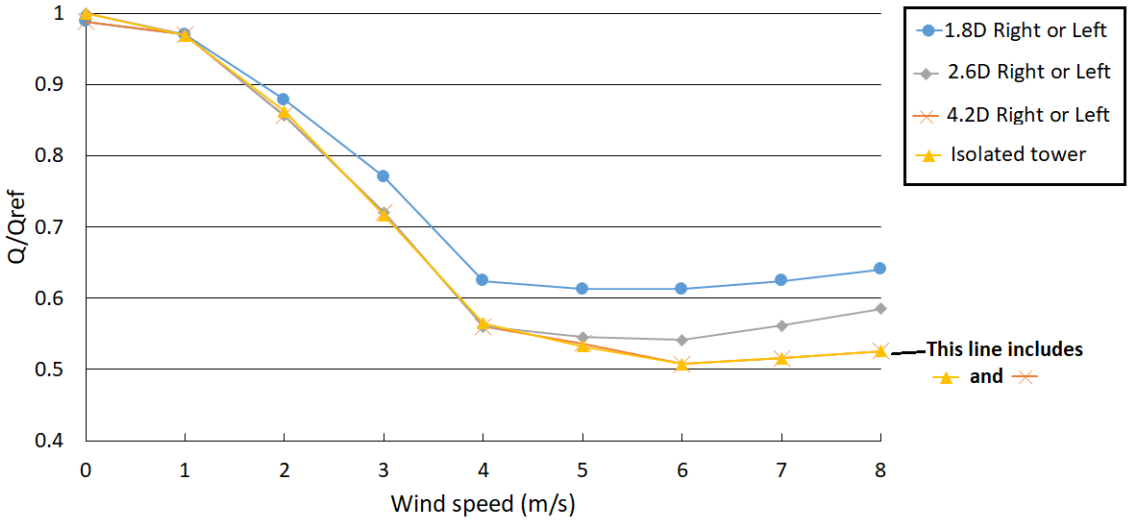

Figure 3.29. The normalized heat rejection of two NDDCTs at wind incidence of 90°.

3.5. Summary of findings

The performance of two NDDCTs was investigated at various wind speeds (0-8 m/s), at different wind incidence angles, and with tower spacing variables from 1.8D to 4.2D. The flow field around the NDDCTs, and heat exchanger temperature distribution at each condition, were presented and discussed. The interactions between the NDDCTs from the bottom and the top were analysed and, finally, the normalized heat rejection of the towers was discussed and compared with the heat rejection of an isolated NDDCT.

The results from this investigation have demonstrated that there is a noticeable interaction between the two towers at different tower-layouts especially at a smallest tower spacing of 1.8D. The results at different wind incidence angles demonstrated that at a wind incidence of 0°, the NDDCTs interact with each other at both the bottom and top level of the towers. The windward tower redirects the wind-flow and reduces the local velocity near the leeward tower. The windward tower also acts as a passive windbreak and protects the leeward tower's outlet. This is more noticeable at low wind-speeds because at high wind-speeds the plume of the tower exits horizontally rather than vertically, which suggests no protection for the leeward tower. The heat rejection of the leeward tower is higher than that of the windward tower at all wind incidence angles and tower spacings. It was observed that by increasing the tower spacing the heat rejection of the leeward tower decreases, which means the protection provided by the windward tower is lower at large tower spacings compared to smaller tower spacings.

At a wind incidence of 45°, the performance of the leeward tower decreases at tower spacings of 1.8D and 2.6D. The interaction between the towers disappears at a tower spacing of 4.2D. The interaction at this wind incidence angle is mainly devoted to the bottom of the towers and the plumes of the towers do not interact with each other.

When the wind is blowing at 90°, there is a performance improvement in both towers at low tower-spacings. However, the performance of both towers is almost the same as for two individual towers at tower spacings of 1.8D and 4.2D. The interaction between the towers is from the bottom of the towers and the plumes of the towers do not interfere with each other the same as for a wind incidence of 45°.

3.6. Chapter conclusions

This chapter was set out to explore the possibility of interaction between two towers during windy conditions at different wind speeds, wind incidence angles, and tower

spacing. It was concluded that the interaction between the towers and the heat rejection of them varies at each wind speed, wind incidence angle, and tower spacing. The interaction between the towers results in an increase or decrease in the heat rejection rate of the towers.

At wind incidence of 0°, the protection of the windward tower results in a better thermal performance of the leeward tower, and this protection decreases by increasing the tower spacing.

When the wind blows at 45° to the towers, the interaction of the towers decreases the heat rejection of the towers especially the windward towers. This interaction is more notable at low tower spacing and it disappears at very large tower spacings.

Finally, at wind incidence of 90°, when the wind blows perpendicular to the towers, the interaction between the towers enhances the heat rejection of the towers at low tower spacing and the interaction vanishes at large tower spacings.

Generally, the performance of the two towers at a wind incidence of 0° is superior to that of the other two wind-incidence angles. These results provide practical insights into the targeted placement of towers in locations with a prevailing wind direction.

Chapter 4: Simulation of multiple in-line NDDCTs under windy conditions

4.1. Introduction

In the previous chapter the effect of wind on two NDDCTs was investigated at different tower spacings and wind-incidence angles. Based on the findings from this investigation, it was concluded that placing the towers in the direction of the prevailing wind maximizes the heat rejection from the towers. This is relevant because there is frequently a predominant wind direction at CST sites; for instance, the wind direction in Zagora was detected as coming mainly from the south-west, and in Missouri the prevailing wind direction is westerly (81). The aim of this chapter is to investigate the effects of wind on three NDDCTs arranged in line with the prevailing wind direction, at various equal tower spacings.

4.2. Method

The same geometry and numerical approach, as explained previously in section 3.2, was used to determine the performance of the three NDDCTs under windy conditions. The cooling towers were placed in a computational domain, as shown in Figure 4.1. The computational domain for three NDDCTs was extended so the outlet boundary did not affect the flow field. The entire computational domain was discretised using 4.8 million structured mesh. At each tower spacing, a grid-independence test was performed, and the resulting (heat-transfer rate) deviation was less than 1% when the number of cells was over 4.8 million, 5.5 million, and 6.2 million, for tower spacings of 1.8D, 2.6D, and 4.2D, respectively. The details of the grid-independence tests can be found in Appendix B.

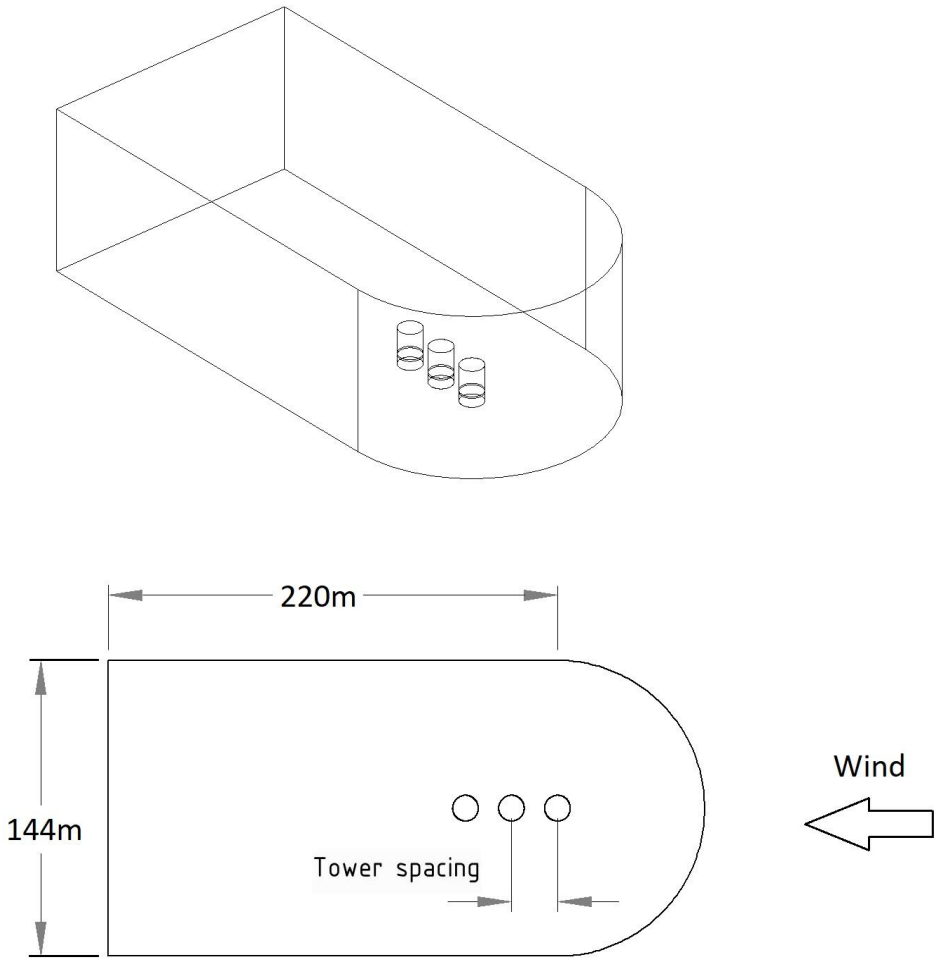

Figure 4.1. Computational domain.

4.3. Flow field analysis for three towers spaced at 1.8D

Figure 4.2 shows the surface velocity streamlines at the inlet height, and the heat exchangers' temperature distribution, at different wind speeds and tower spacing of 1.8D. As the flow passes over the windward tower at 2 m/s, it is redirected due to the blockage the tower presents. The velocity streamlines (Figure 4.2.A.*i*) show that at the windward side of the windward tower, a low-velocity region is formed. This low-velocity region shows the flow circulations at the bottom of the tower. The effect of the flow circulation at the bottom of the windward tower on the heat exchanger temperature is apparent in (Figure 4.2.A.*ii*). It can be observed that at the windward side of the windward tower, the heat exchanger temperature is higher than at the leeward side. The low-velocity region under the middle and leeward towers is smaller than for the windward tower due to the protection provided by the windward tower. The protection of the windward tower for the leeward sections of the middle and leeward tower is similar. However, the redirected flow after the windward tower, impinges on the side of the leeward tower (Figure 4.2.A.*i*). This is evident in the heat exchanger temperature of the leeward tower which shows that the temperature of the windward and side regions of the leeward tower is higher than that of the rest of the heat exchanger's surface area. The heat exchanger temperature of the middle and windward towers is different, and for the middle tower the temperature increases only at the windward side (Figure 4.2.A.*ii*).

At a higher wind speed of 4 m/s, a larger low-velocity region forms at the bottom of the windward tower compared to a wind speed of 2 m/s (Figure 4.2.B.*i*). This results in the expansion of the high-temperature region of the windward tower's exchanger (Figure 4.2.B.*ii*). The low-velocity region at the bottom of the tower is highest at the windward tower and smallest at the leeward tower.

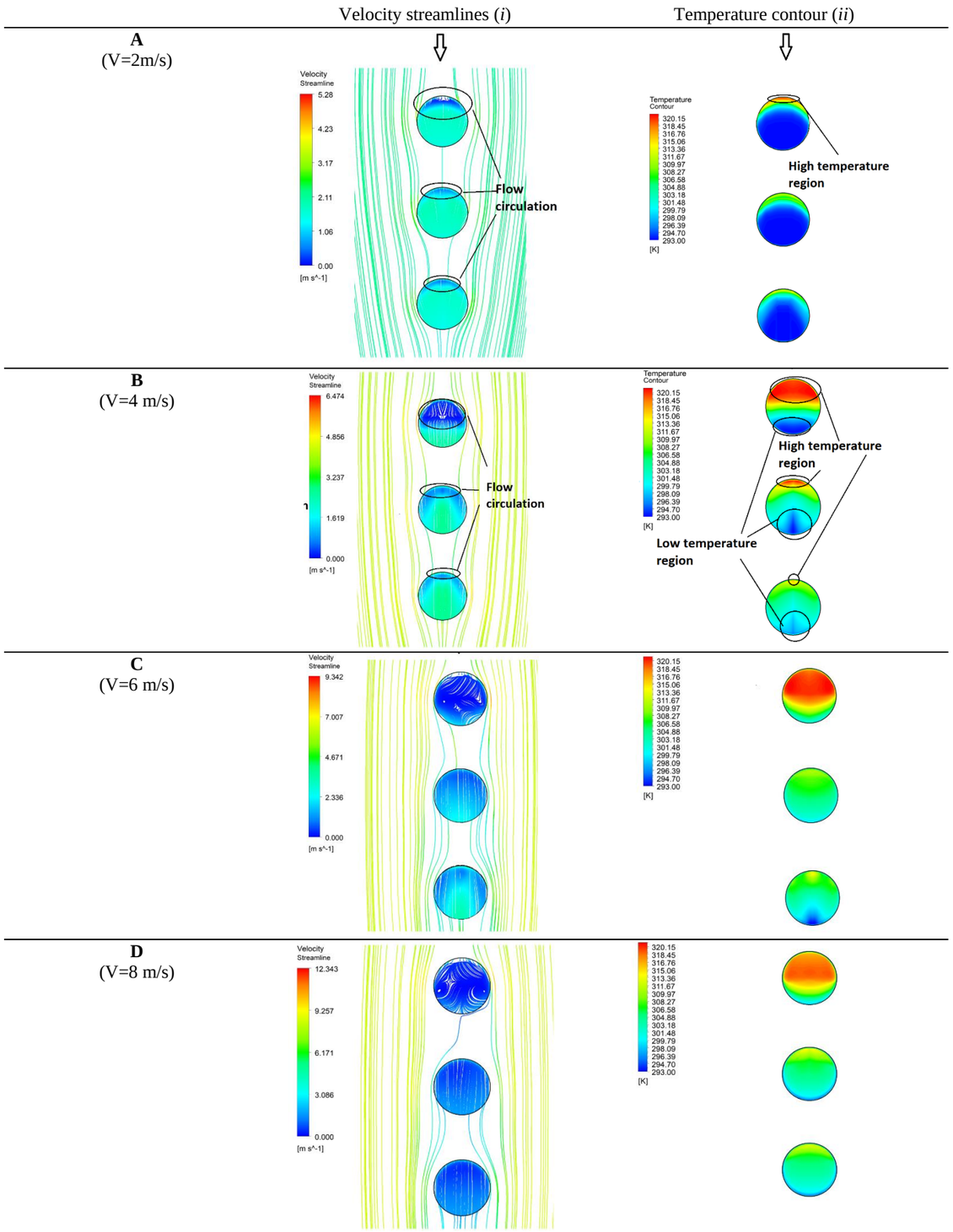

Figure 4.2. Velocity contour and streamlines at the inlet height and heat exchanger temperature contour of three NDDCTs at tower spacing of 1.8D, and wind speeds of 2 m/s (A), 4 m/s (B), 6 m/s (C), and 8 m/s (D).

The heat exchanger temperature of the middle tower is higher than that of the leeward tower. However, the heat exchanger temperature of the leeward section of the leeward tower is higher than that of the middle tower. This is due to the flow convergence at the side regions of the leeward tower creating a high-velocity region in this area.

As the wind speed increases to 6 m/s at a tower spacing of 1.8D, the low-velocity region under the windward tower becomes dominant at the inlet surface (Figure 4.2.C.*i*), which results in a significant temperature increase in the heat exchanger temperature(Figure 4.2.C.*ii*). At this wind speed, the windward and middle towers protect the leeward tower and the flow is deflected before it reaches the leeward tower. At the leeward side of the leeward tower the heat exchanger temperature is lower than that at a wind speed of 4 m/s.

Finally, at 8 m/s, the low-velocity region at the bottom of the windward tower increases to the largest extent observed. At this wind speed the heat taken away by the forced convection has been enhanced, which reduces the heat exchanger temperature of the windward tower compared to a lower wind speed of 6 m/s. The flow is redirected after the windward tower and becomes parallel with the dominant wind direction, and the flow passes the middle and leeward towers. At wind speeds of 6 m/s and 8 m/s the protection of the windward tower for the middle and leeward towers becomes similar (Figure 4.2.D.*i*), with the leeward heat exchanger temperature slightly lower than the middle tower (Figure 4.2.D.*ii*).

To further illustrate the flow characteristics Figure 4.3 shows the velocity streamlines around the NDDCTs at a tower spacing of 1.8D. One may expect that the vortices generated in the wake region of the towers to rise vertically from the ground and interfere with the next tower's outlet. At a wind speed of 2 m/s (Figure 4.3.A) , the outflow plume coming from the windward tower's outlet joins the middle tower's outflow and then moves vertically, which gives protection to the leeward tower. The wake of the middle

tower rises toward the leeward tower's outlet and slightly deflects the plume from the leeward tower.

The deflection of the plume from the windward tower increases as the crosswind speed increases. At a wind speed of 4 m/s (Figure 4.3.B), the windward tower's outlet joins the middle tower's outflow, which covers the outlet of the leeward tower. However, the wake of the middle tower rises toward the leeward tower's outlet and interferes with the upcoming plume from the leeward tower.

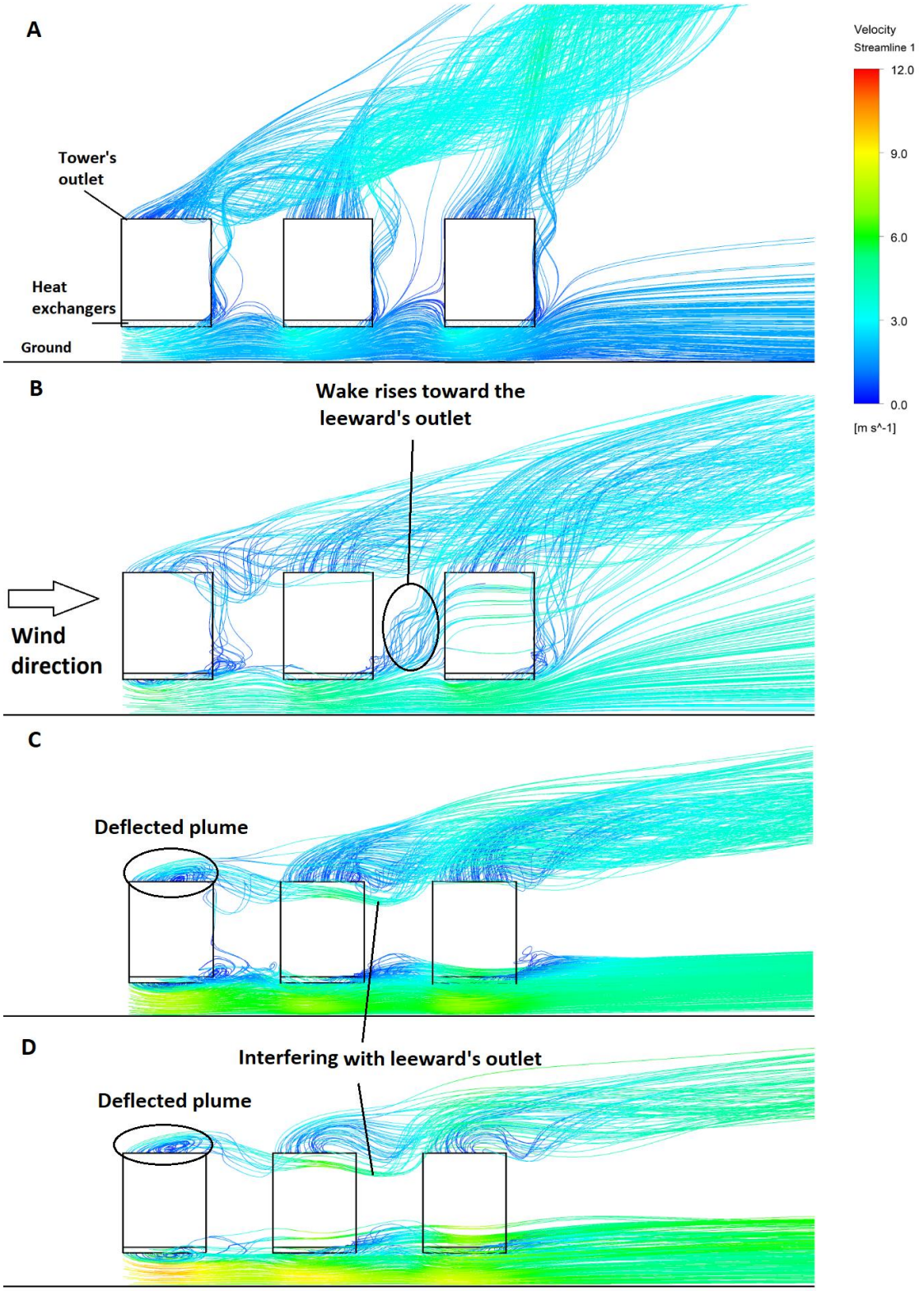

Figure 4.3. Velocity streamlines around NDDCTs and tower spacing of 1.8D at wind speeds of 2 m/s (A), 4 m/s (B), 6 m/s (C), and 8 m/s (D).

At wind speeds of 6 m/s and 8 m/s (Figure 4.3.C and D respectively), the wakes of the windward and middle towers do not rise vertically. Due to the low tower-spacing, the deflected wakes of the windward and middle towers enter the next tower and cause no interference to the tower's outlet. At high crosswind speeds, the plume of the windward tower is deflected and moves lower than the middle tower's outlet and interferes with the outlet of the leeward tower. This results in a flow circulation at the leeward tower's outlet despite the flow protection provided by the windward and middle towers.

The wind passing over the tower's outlet, deflects the exiting plume which causes flow circulation. Figure 4.4 shows the average vorticity at the towers' outlets surface at tower spacing of 1.8D. The vorticity at the windward tower is the same as for an isolated cooling tower. As the wind speed increases, the plume tends to exit the outlet of the tower more horizontally. For 1 m/s < V < 3 m/s the average vorticity of the middle tower is larger than the leeward tower. Figure 4.3 demonstrates the vertically moving plume from the middle tower deflects the wind and protects the leeward tower's outlet. At wind speed greater than 3 m/s the vorticity of the leeward tower becomes larger than the middle tower. The flow exiting the windward tower and middle tower moves horizontally towards the leeward tower. The exiting plume from the windward and leeward towers generates a high velocity zone at the leeward tower's outlet. This causes the vorticity at the leeward tower's outlet to be high compared to the middle and windward tower, shown by Figure 4.4.

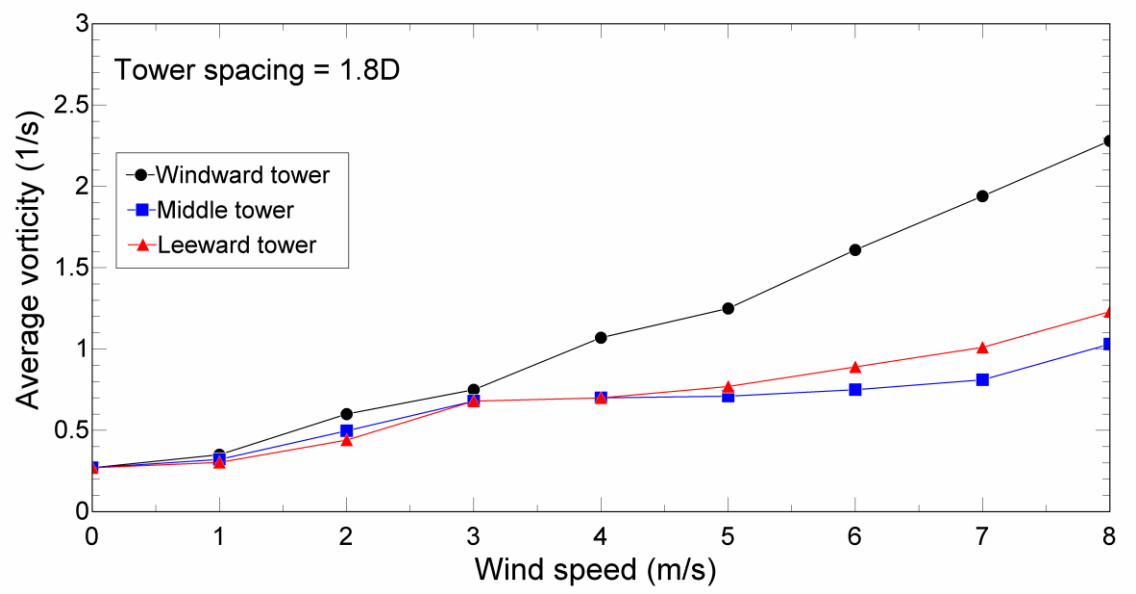

Figure 4.4. Average vorticity at towers' outlets at tower spacing of 1.8D.

The wind passing over a tower's outlet deflects the exiting plume, which causes flow circulation. The warm air is quickly cooled at the tower's outlet by the wind, and some cold air sinks back into the tower, which results in the reduction of the effective draft-height of the cooling tower. This phenomenon is known as cold flow intake.

The effect of wind on the cold flow intake of the NDDCTs can be observed in the temperature distribution on a vertical cross sectional plane at different wind speeds in Figure 4.5. At a wind speed of 2 m/s (Figure 4.5.A), the crosswind deflected the windward tower plume. In the presence of wind, the temperature at the windward side of the towers is higher than the leeward side. By increasing the wind speed the temperature difference between the windward and leeward sides of the towers increases. At wind speed of 4 m/s (Figure 4.5.B), the wind at the top of the tower dampens the plume at the leeward side preventing the hot air exiting the tower. Hence, the plume cools and circulates back into the tower at the leeward side decreasing the temperature. This temperature decrease reduces the draft height which in turn decreases the thermal performance of the towers.

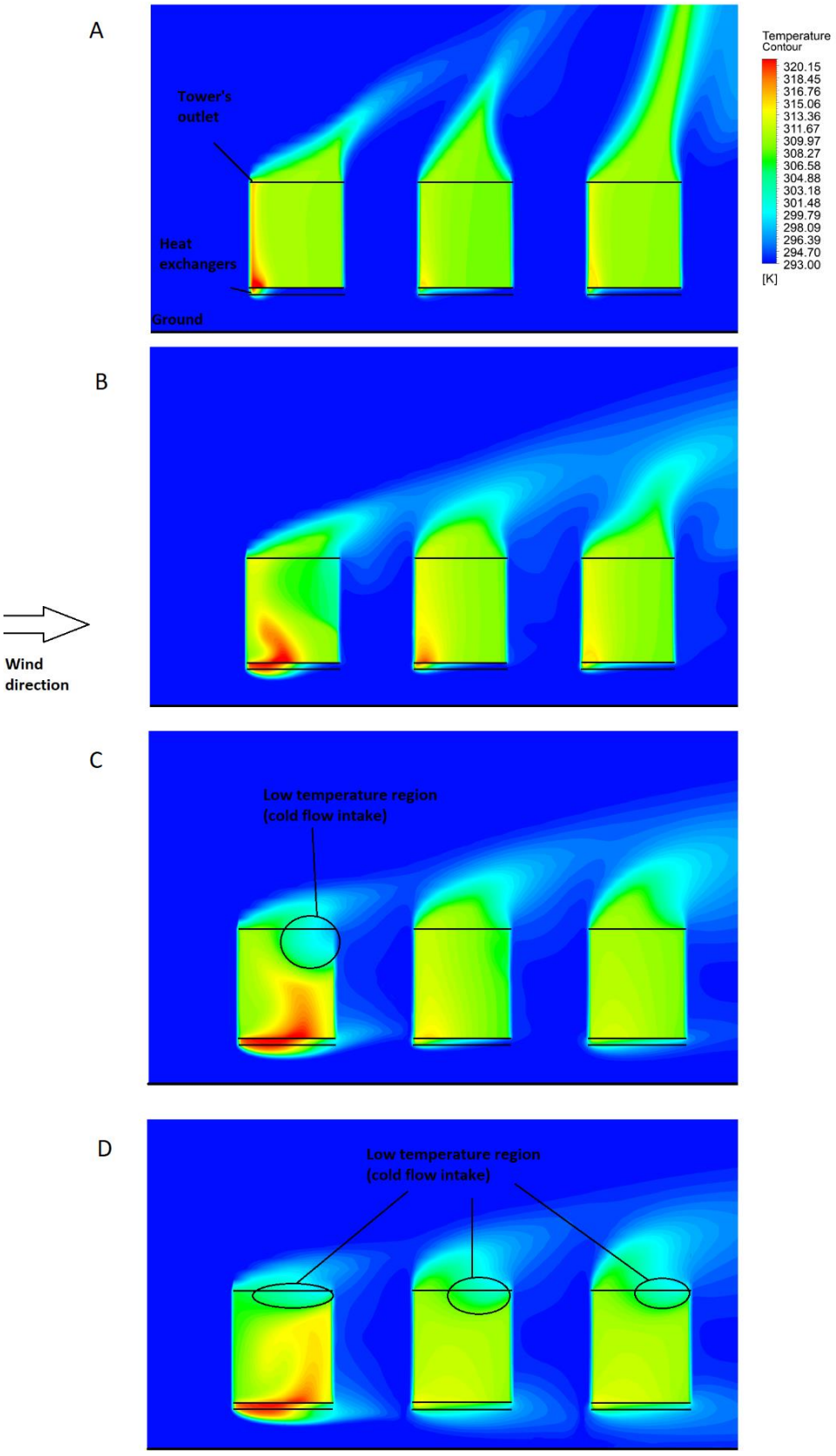

Figure 4.5. Air temperature contour at vertical cross-sectional plane and tower spacing of 1.8D at wind speeds of 2 m/s (A), 4 m/s (B), 6 m/s (C), and 8 m/s (D).

At a wind speed of 6 m/s (Figure 4.5.C), the cold flow intake at the leeward tower is clear, and at wind speed of 8 m/s (Figure 4.5.D) it is evident in all towers. The cold flow intake becomes more significant by increasing the wind speed in towers.

It also can be observed that the warm flow exiting the bottom of windward and middle towers dissipates the heat to the ambient before entering the next tower. This does not reduce the thermal performance of the middle and leeward tower because of warm air draw from the windward towers.

The temperature contour around the windward tower displays similar characteristics of what previously found in Lu et al.'s single-tower study (23).

4.4. Flow field analysis for three towers spaced at 2.6D

Exploring the interaction of three towers further, by increasing the tower spacing to 2.6D (at a wind speed of 2 m/s) the wind passing over the windward tower is deflected and converges around the middle and leeward towers (Figure 4.6.A.*i*). This is because, at low wind speeds the air enters the cooling towers more easily, which creates a low-pressure region around the tower. This draws the wind passing the middle and leeward towers and the flow converges around these towers.

The flow convergence is around the leeward tower which increases the velocity around the side regions of the leeward tower. The consequence of the higher wind velocity around the leeward tower can be seen in the heat exchanger temperature, which shows that the temperature of the side sections is higher than at the leeward section (Figure 4.6.A.*ii*). The temperature at the leeward section of the all towers is higher than at the rest of the heat exchanger sections due to the crosswind mainly entering the tower from the windward section, thus causing the flow to circulate at this region.

Increasing the wind speed to 4 m/s, the flow behaviour around the middle and leeward towers becomes similar (Figure 4.6.B.i). At this wind speed, the flow convergence occurs around the windward side of the leeward tower, where the flow velocity is high. This results in a flow circulation at the windward side of the leeward tower, and a high-temperature region. This flow circulation decreases the heat transfer area, and this flow blockage pushes more air to enter the tower from the leeward side of the tower. This is evident as the velocity at the leeward side of the leeward tower is higher than at the windward side (meaning more air flows into the tower from this section), which results in a lower heat exchanger-temperature (Figure 4.6.B.ii).

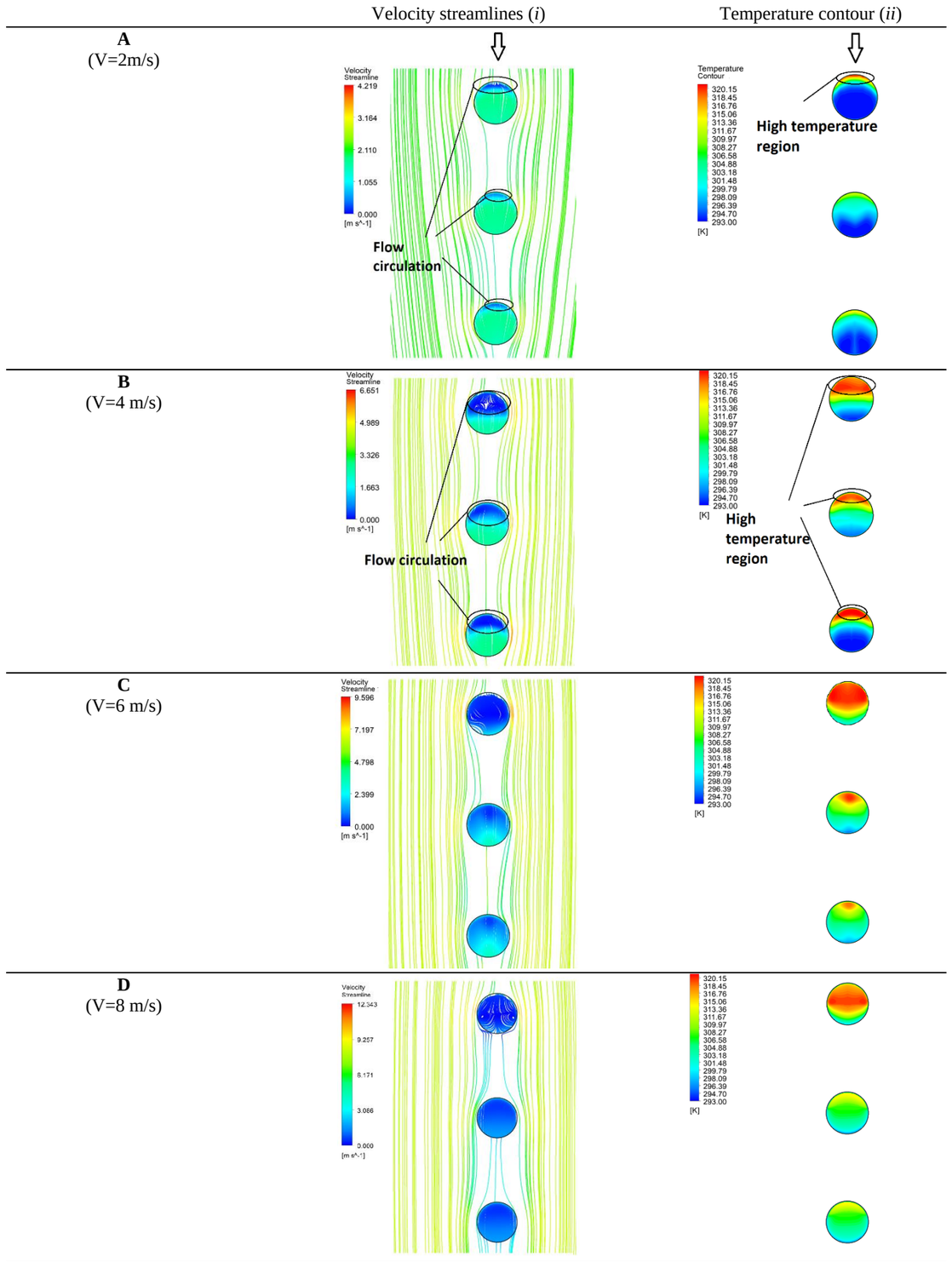

Figure 4.6. Velocity contour and streamlines at the inlet height and heat exchanger temperature contour of three NDDCTs at tower spacing of 2.6D, and wind speeds of 2 m/s (A), 4 m/s (B), 6 m/s (C), and 8 m/s (D).

At a wind speed of 6 m/s, the wind tends to move parallel to the wind direction instead of converging toward the middle and leeward towers (Figure 4.6.C.*i*). The low-velocity region at the bottom of the windward tower, shows that the flow circulation at the bottom is larger than at the middle and leeward towers (Figure 4.6.C.*i*). The windward tower protects the middle and leeward towers, at which the heat exchanger temperature-contours verify the flow field. The temperature at the windward side of the middle tower is larger than that of leeward tower (Figure 4.6.C.*ii*). This means that the leeward tower benefits from the protection of the windward and middle towers, while the middle tower is protected by only the windward tower.

The deflected flow at wind speed of 8 m/s, after the windward tower, reaches around the middle tower and is again slightly deflected and then moves parallel to the wind direction. This provides a protection for the leeward tower (Figure 4.6.D.*i*). This flow deflection, after the windward tower, enhances the thermal performance of the middle and leeward towers (Figure 4.6.D.*ii*). The heat exchanger temperature of the middle and leeward towers is lower than that found at a wind speed of 6 m/s. The same as for a tower spacing of 1.8D, the heat exchanger temperature of the windward tower is lower at a wind speed of 8 m/s compared to at a wind speed of 6 m/s.

Figure 4.7 illustrates the velocity streamlines around the towers at tower spacing of 2.6D at different wind speeds. Although at wind speed of 2 m/s and 4 m/s (Figure 4.7.A and B respectively), the windward and middle towers protect the leeward tower, and the wake of the middle tower rises toward the leeward tower and deflects the plume. At a wind speed greater than 4 m/s, the plumes from the middle and leeward towers' outlets exit vertically (Figure 4.7.C and D respectively). It can be observed that, the same as for tower spacing of 1.8D, the deflected plume of the windward tower interferes with the leeward tower.

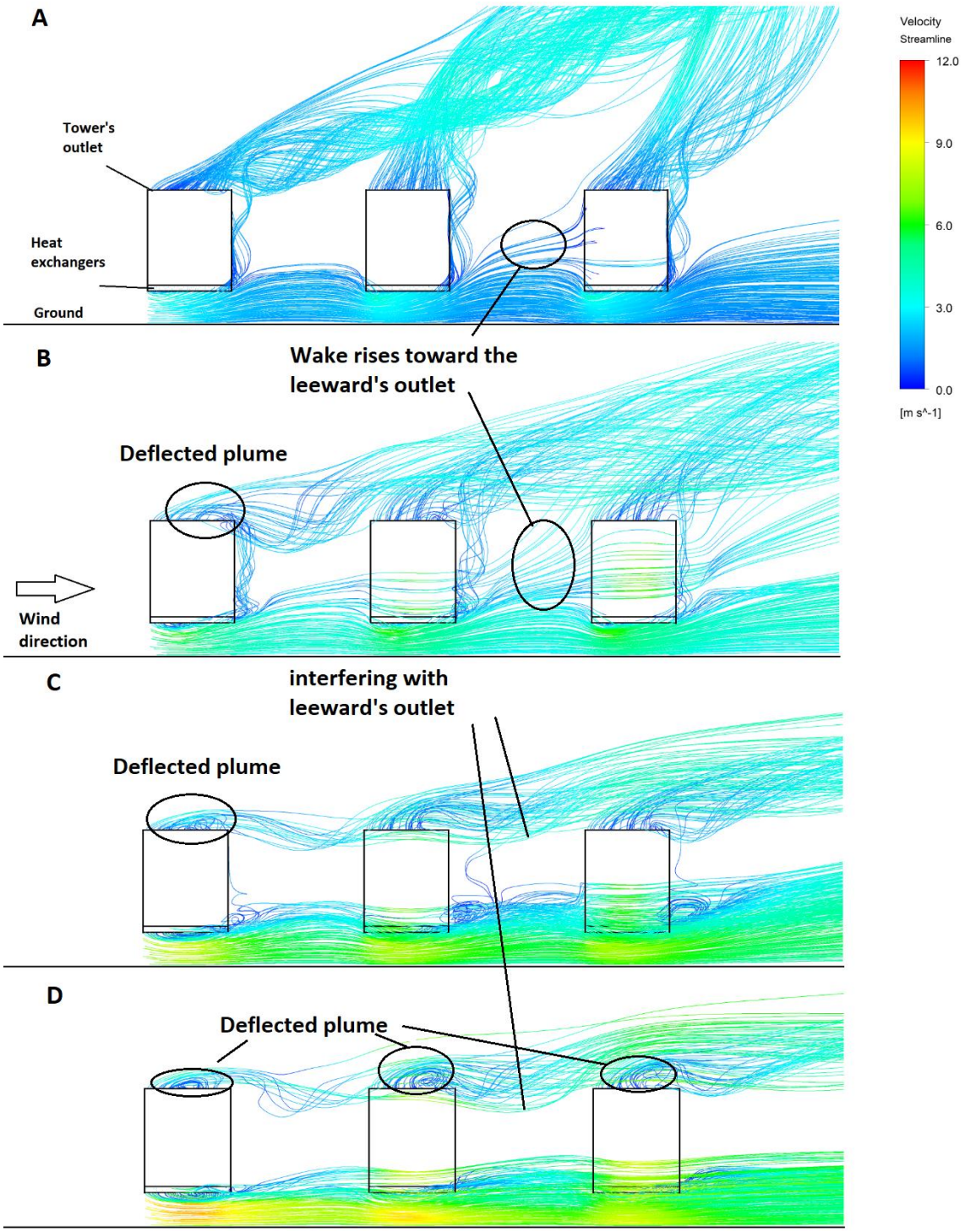

Figure 4.7. Velocity streamlines around NDDCTs and tower spacing of 2.6D at wind speeds of 2 m/s (A), 4 m/s (B), 6 m/s (C), and 8 m/s (D).

To illustrate these points, the average vorticity at the bottom of the heat exchangers at a tower spacing of 2.6D is shown in Figure 4.8. At wind speeds of 1 m/s and 2 m/s, the vortices at the towers' outlets are similar. The vorticity at the windward tower's outlet is the same as for the tower spacing of 1.8D. At wind speeds of 4 m/s and 5 m/s, the vorticity at the middle and leeward towers' outlets is similar, and for wind speeds greater than 5 m/s the vortices at the leeward tower's outlet become larger than at the middle tower.

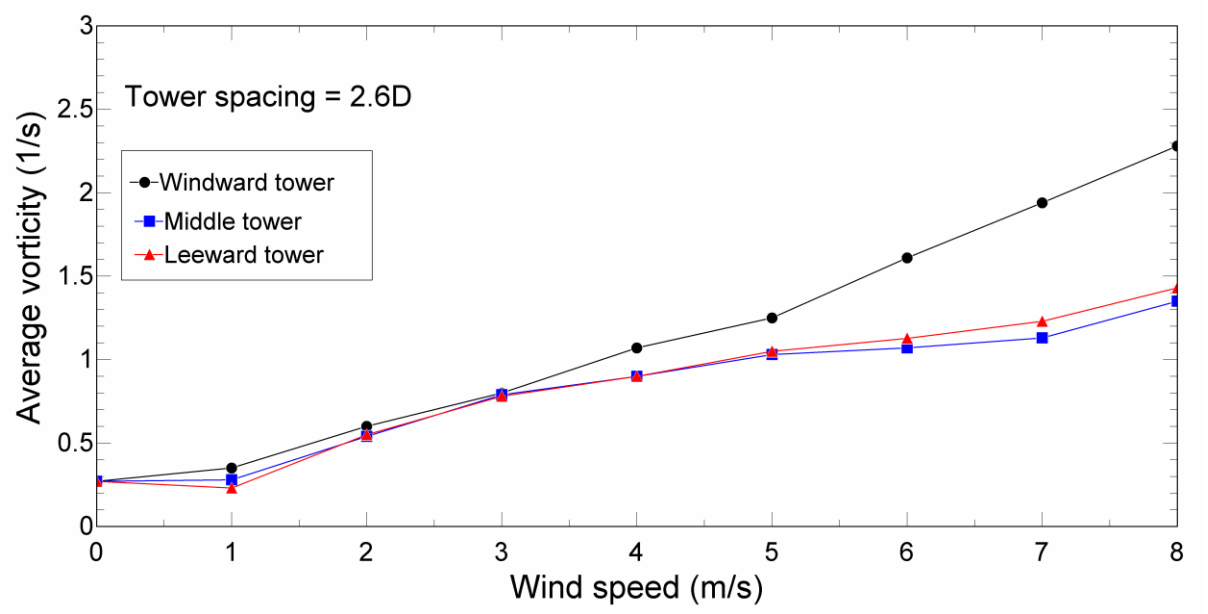

Figure 4.8. Average vorticity at towers' outlets at tower spacing of 2.6D.

The temperature contour at the vertical cross-sectional plane at tower spacing of 2.6D at different wind speeds is displayed in Figure 4.9. At wind speed of 2 m/s (Figure 4.9.A), the plume of the leeward tower deflected more than the middle tower which is due to interference of the middle tower wake with the outlet of the leeward tower's outlet. At wind speed of 6 m/s (Figure 4.9.C), the cold flow intake occurs at the middle tower which can be seen at low temperature region at the middle tower's outlet. By increasing the wind speed to 8 m/s (Figure 4.9.D), the cold flow intake appears at the leeward tower outlet. Although the windward and middle towers provide protection for the leeward tower, at high wind speeds, the leeward tower's plume cannot push the wind at the towers outlet and the air cooled down sink back again into the tower at the leeward section of the leeward tower's outlet.

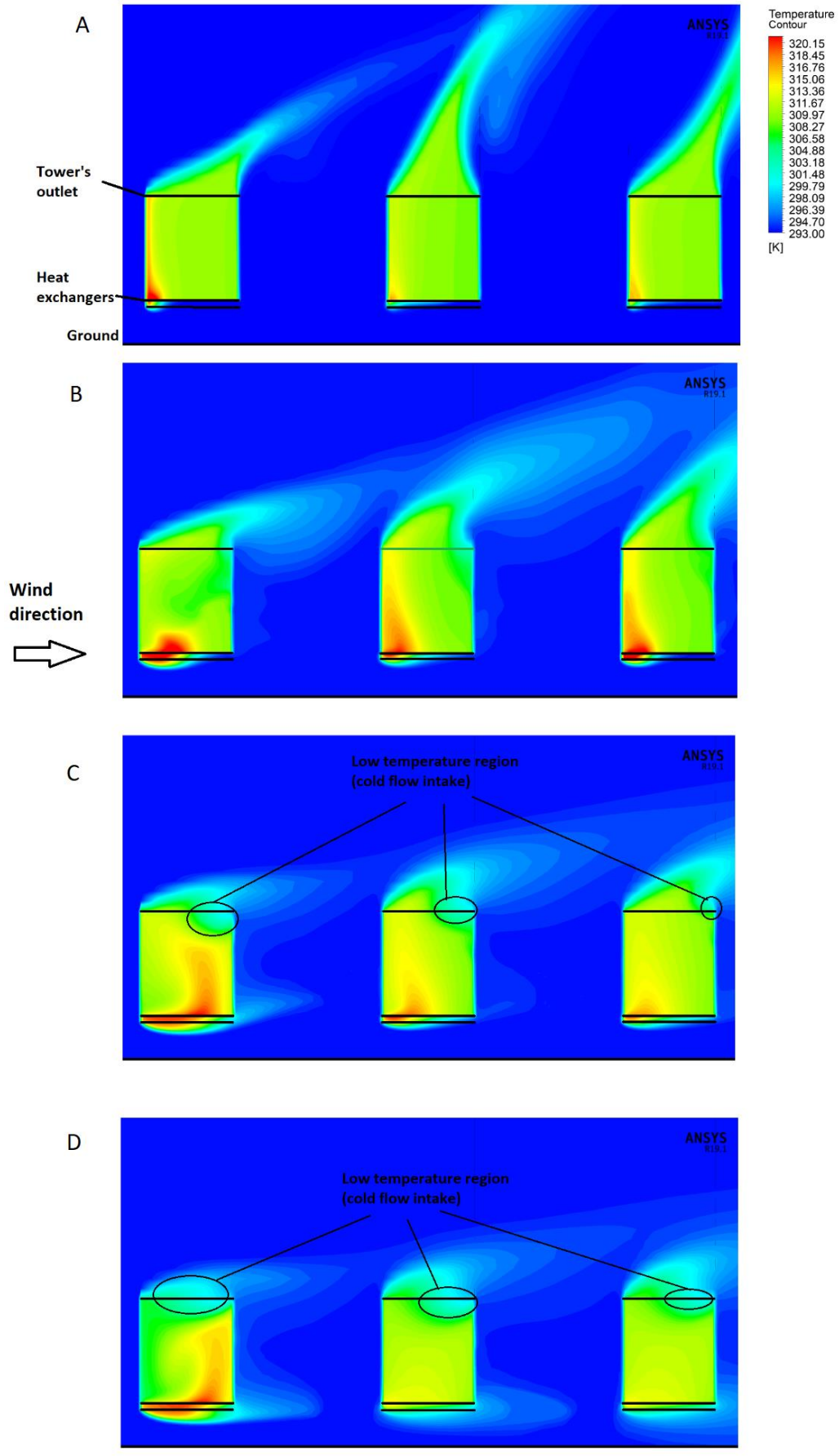

Figure 4.9. Air temperature contour at vertical cross-sectional plane and tower spacing of 2.6D at wind speeds of 2 m/s (A), 4 m/s (B), 6 m/s (C), and 8 m/s (D).

4.5. Flow field analysis for three towers spaced at 4.2D

Taking the tower spacing to it's extreme, the surface velocity streamlines at the inlet height, and heat exchanger temperature contours, at a tower spacing of 4.2D and wind speeds of 2 m/s and 4 m/s are presented in Figure 4.10.A and B respectively. At a tower spacing of 4.2D and wind speed of 2 m/s, the flow around the NDDCTs shows the deflected flow after the windward tower converges around the leeward tower.

With an increase in the wind speed to 4 m/s (Figure 4.10.B.i), the deflected flow after the windward tower cannot converge back to the front of the middle and leeward towers and move alongside the wind direction. The temperature and velocity fields around the middle and leeward towers become similar, with more protection for the leeward tower. This can be seen in the low temperature region at the leeward side of the leeward tower (Figure 4.10.B.ii).

The increase in heat exchanger temperature at a wind speed of 6 m/s and tower spacing of 4.2D can be observed in (Figure 4.10.C.ii), which can be compared to those for wind speeds of 2 m/s and 4 m/s. The spacing between the towers is large, which means the flow after the windward tower becomes uniform and passes over the middle and the leeward towers. This results in less protection provided by the windward tower for the middle and leeward towers compared to at the tower spacing of 1.8D and 2.6D.

At wind speed of 8 m/s, the deflected flow beyond the windward tower moves parallel to the wind direction and doesn't tend to move to the side of the middle and leeward towers (Figure 4.10.D.*i*). This is more evident for the leeward tower than the middle tower. This results in a lower heat exchanger temperature for the middle and leeward towers compared to at the wind speed of 6 m/s (Figure 4.10.D.*ii*).

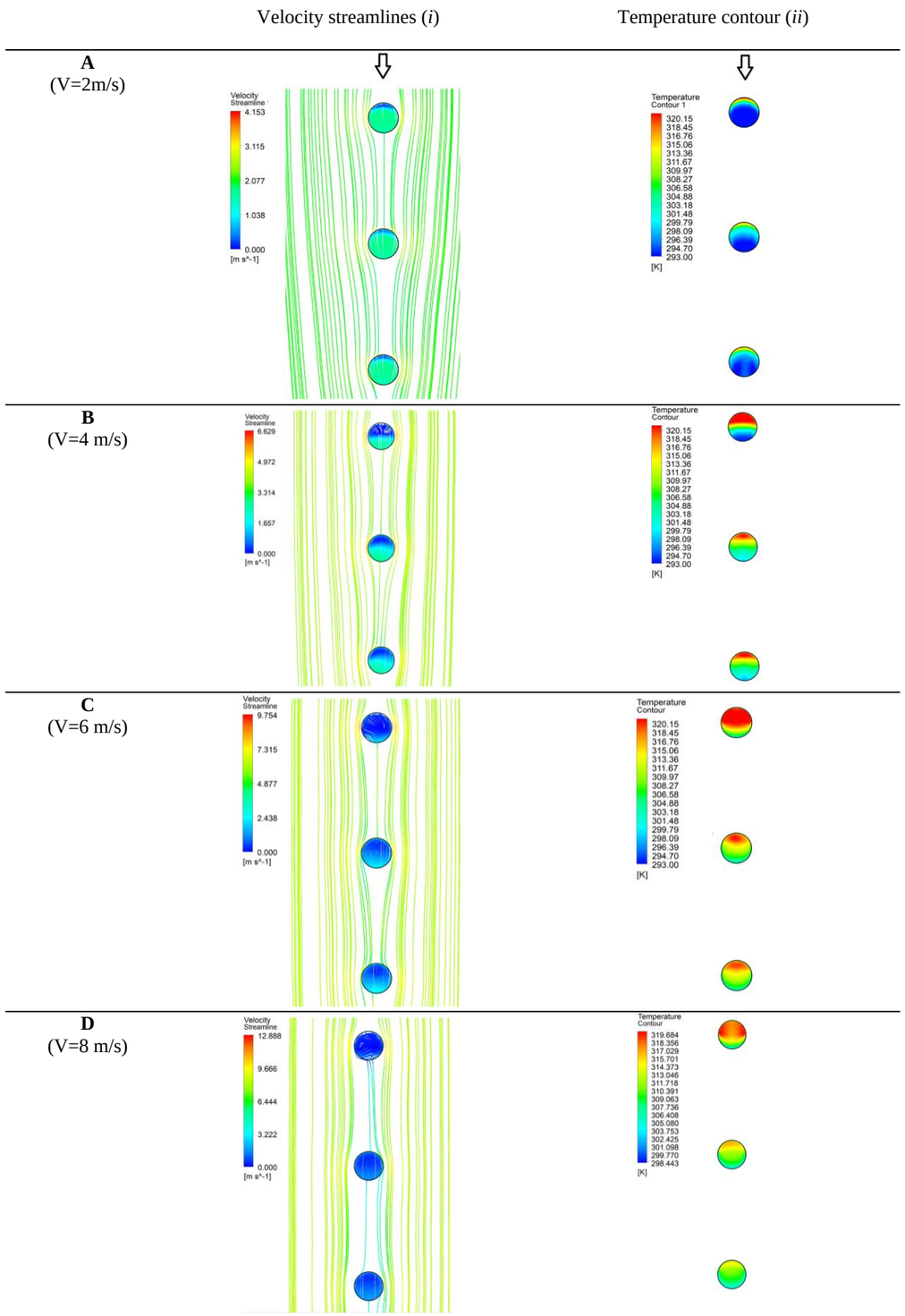

Figure 4.10. Velocity contour and streamlines at the inlet height and heat exchanger temperature contour of three NDDCTs at tower spacing of 4.2D, and wind speeds of 2 m/s (A), 4 m/s (B), 6 m/s (C), and 8 m/s (D).

The same as for the tower spacings of 1.8D and 2.6D, the heat exchanger temperature of the windward tower decreases compared to at a wind speed of 6 m/s, due to enhanced force convection.

The flow patterns from the towers' outlets are represented by 3D streamlines at different wind speeds at tower spacing 4.2D, as shown in Figure 4.11. The windward tower protects the middle and leeward towers by deflecting the upcoming wind. The windward tower redirects the upcoming flow and decreases the local wind-velocity, and this also occurs again by the middle tower. However, the wake of middle tower interferes with the leeward tower's outlet and causes the plume to deflect. The vortices which are generated at the outlets of the middle and leeward towers are similar. At a wind speed of 8 m/s, the wake of the middle tower does not rise vertically and is deflected by the high wind-speed (Figure 4.11.D). Therefore, the leeward tower benefits only from the protection provided by the middle and windward towers.

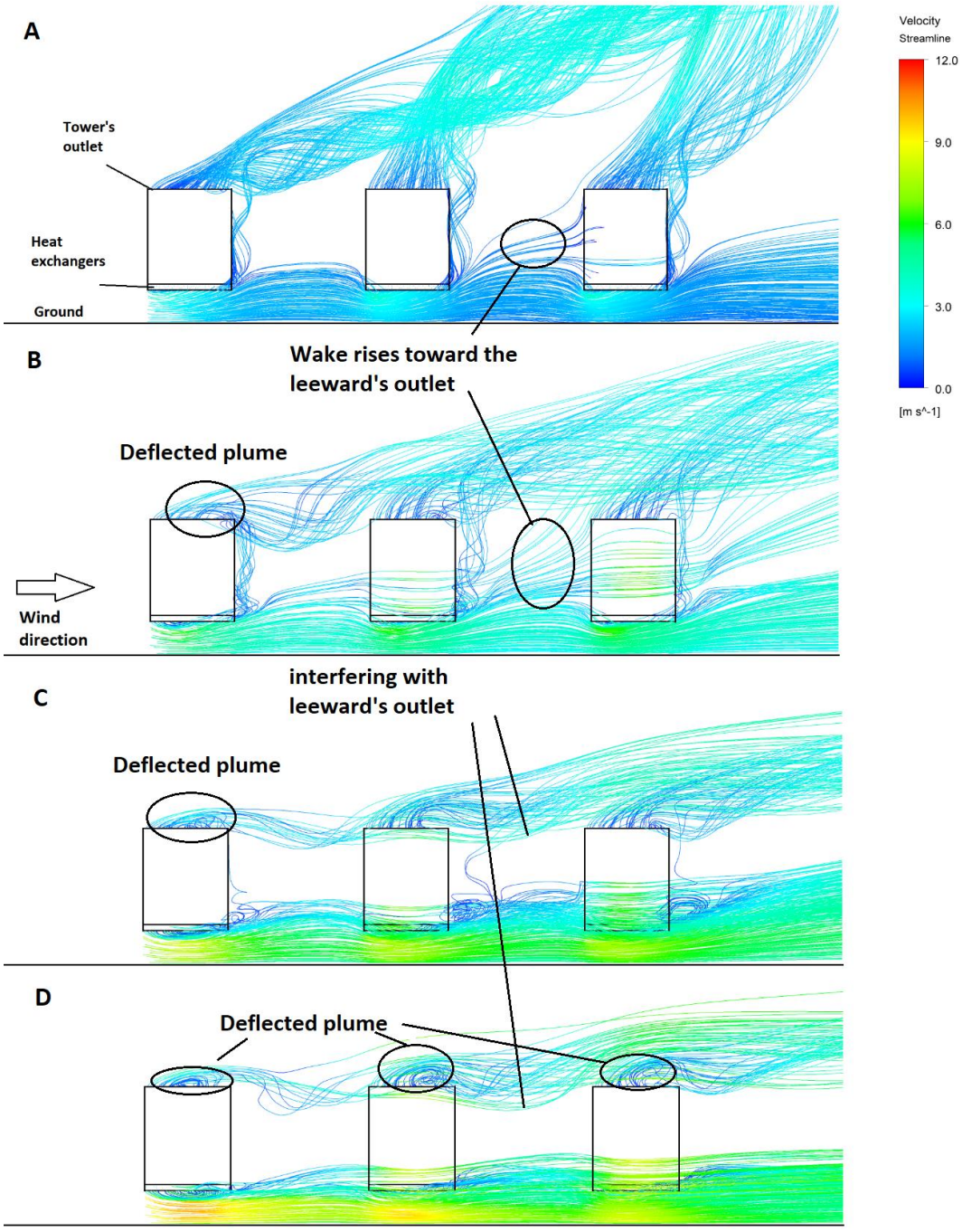

Figure 4.11. Velocity streamlines around NDDCTs and tower spacing of 4.2D at wind speeds of 2 m/s (A), 4 m/s (B), 6 m/s (C), and 8 m/s (D).

The average vorticity at the towers' outlets at a tower spacing of 4.2D is shown in Figure 4.12. For all wind speeds, the vorticity at the outlet of the windward tower is similar to the windward tower at a tower spacing of 1.8D and 2.6D. For wind speeds smaller than 6 m/s, the vorticity of the leeward and middle towers is similar. For wind speeds of 7 m/s

and 8 m/s, the vortices at top of the leeward tower become smaller than at the middle tower.

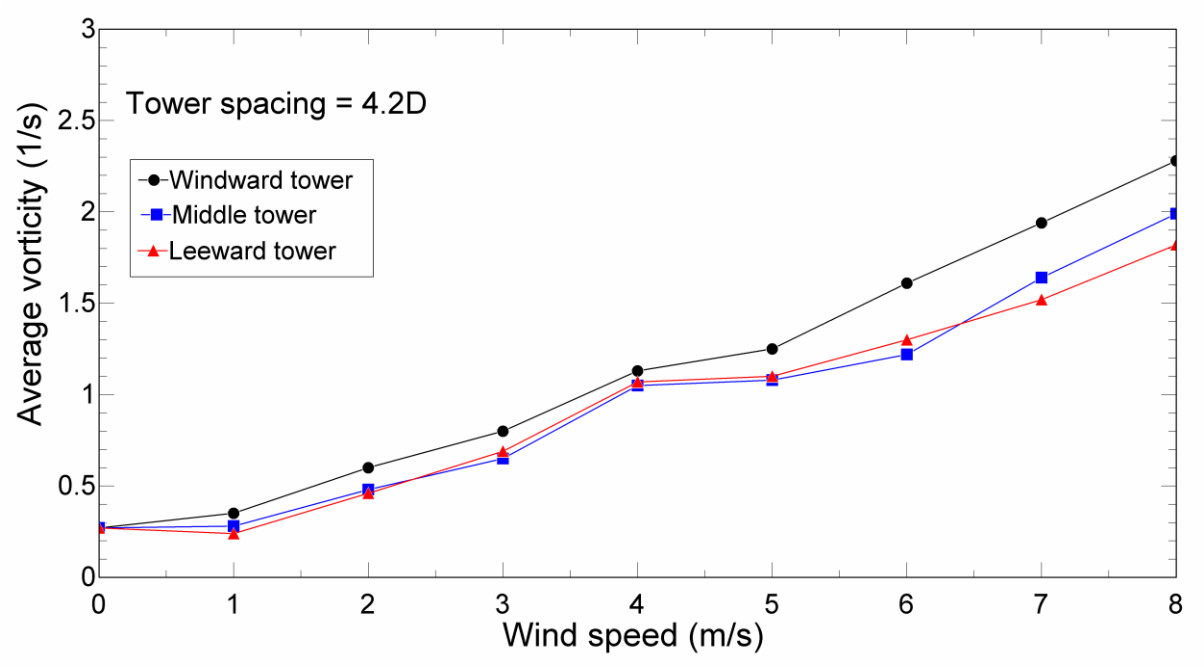

Figure 4.12. Average vorticity at towers' outlets at tower spacing of 4.2D.

The temperature field shown in Figure 4.13 is consistent with the velocity streamlines. The temperature inside the windward tower is always higher than the middle and leeward towers. At tower spacing of 4.2D, the difference between the temperature inside the towers decreases by comparing to the tower spacing of 2.6D and 4.2D.

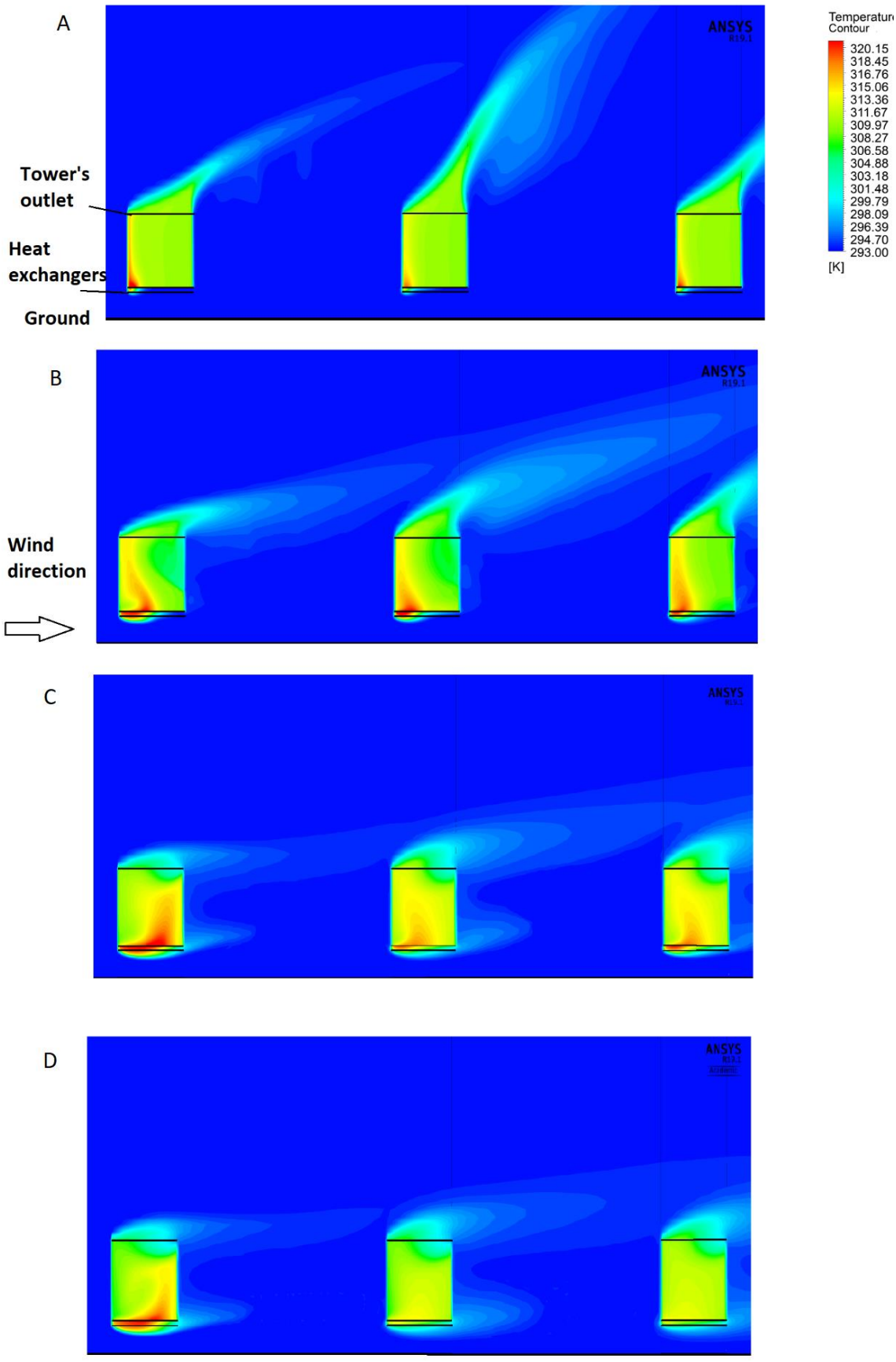

Figure 4.13. Air temperature contour at vertical cross-sectional plane and tower spacing of 4.2D at wind speeds of 2 m/s (A), 4 m/s (B), 6 m/s (C), and 8 m/s (D).

4.6. Summary of the flow field analysis at different tower spacings

It was expected that the leeward tower benefits from the protection provided by the windward and middle towers at all wind speeds. However, the results demonstrated that at different wind speeds the windward tower protection is different for the middle and leeward towers.

At tower spacing of 1.8D, at low wind speeds the deflection of the wind after the windward tower converges around the leeward tower and the middle tower stays in the low-velocity wake of the windward tower. This resulted in a higher heat exchanger temperature of the leeward tower compared to the middle tower. By increasing the wind speeds, the protection provided by the windward and leeward towers enhances.

At tower spacing of 2.6D, the same flow field of the 1.8D was observed, however, the difference between the middle and leeward towers flow field decreased.

At tower spacing of 4.2D, same as the other tower spacings, the windward tower has the highest heat exchanger temperature at all wind speeds. At this tower spacing, the distance between the towers is large and the separated flow from the windward joins around the middle and leeward towers. This means there is less windward tower protection at largee tower spacings.

The results demonstrated at this configuration the outflow plumes of the towers interfere with each other. At all tower spacings, the outflow of the windward tower protects the outlet of the middle and leeward towers especially at low wind speeds due to vertical movement of the plume. This protection decreases by increasing the wind speed as the plume of the windward tower deflects by the crosswind and moves horizontally and can’t provide protection for the middle and leeward towers.

The findings of this study with respect to the development of flow-shear layers from the windward cylinders, and their place of reattachment onto the downstream cylinders, are in agreement with the findings of (82). Igarashi and Suzuki (82) investigated the characteristics of the flow around three circular cylinders arranged in a line, using flow visualization by a smoke-wind tunnel. It was found that by increasing the equal spacing between the towers, the flow field around the second and third towers becomes similar. At low spacing, the reattachment mainly occurs around the third cylinder. This has been shown in the findings of this study: at V=4 m/s, the streamlines around the leeward tower become more similar to the middle tower by increasing the tower spacing.

4.7. Heat rejection analysis at different tower spacings

The heat rejection of the NDDCTs at different tower spacings and various wind speeds was calculated, and the thermal performance of each tower at different conditions was compared with the heat rejection rate of an isolated cooling tower under the no-wind condition (Q_{ref}).

Figure 4.14 shows the normalized heat rejection of the NDDCTs at a tower spacing of 1.8D. The thermal performance of the windward tower is the same as for an isolated tower, it decreases with increasing wind speed, for wind speeds of less than 6 m/s. For wind speeds greater than 6 m/s the heat rejection of the windward tower increases due to the increase of the forced convection at the bottom of the windward tower. At a no-wind condition the normalized heat rejection of the towers is less than 1. It has been explained previously in Chapter 2, that at low tower-spacings the performance of the towers is exacerbated by the interference of the towers.

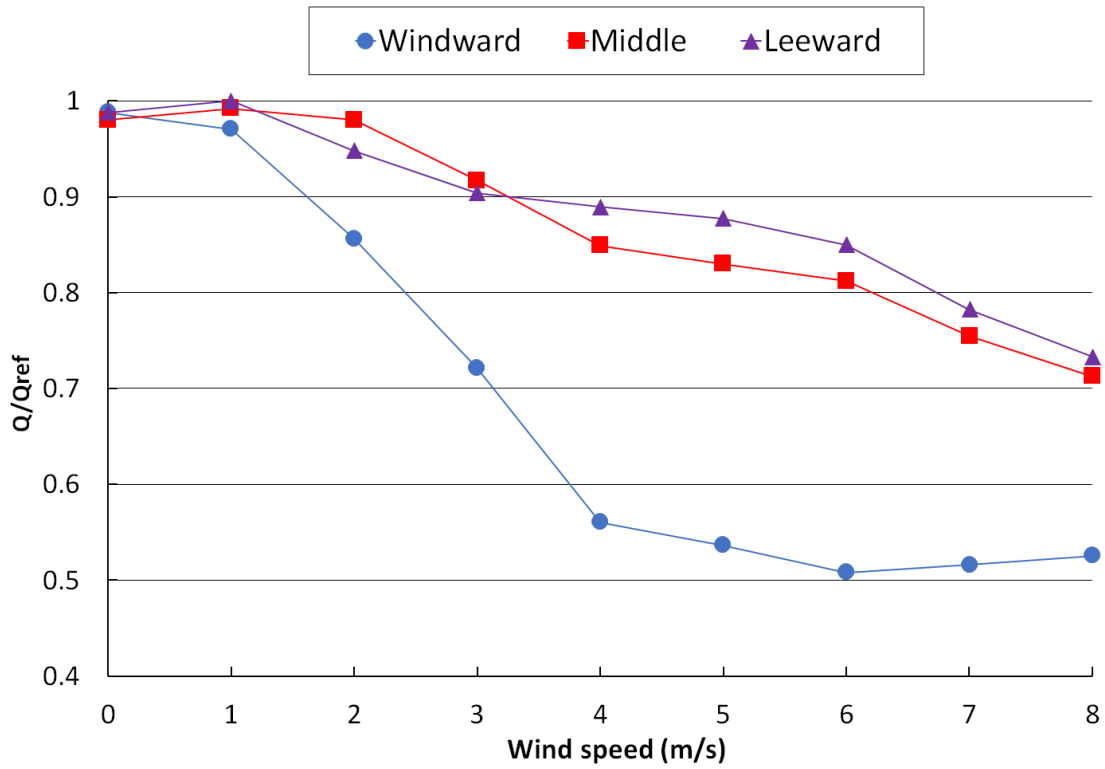

Figure 4.14. Normalized heat rejection of NDDCTs at tower spacing of 1.8D.

In the flow field analysis, it was shown that at wind speed of 2 m/s, the crosswind moves toward the leeward tower after passing the windward tower. At wind speeds greater than 4 m/s, the flow deflected after the windward tower does not converge back to the middle and leeward towers. The leeward tower benefits from the protection of the middle and windward towers, thus the heat rejection of the leeward tower is higher than that of the middle tower. It is clear that due to there being no protection for the windward tower, the heat rejection of this tower is less than that of the other downstream towers for all wind speeds.

As for a tower spacing of 1.8D, the normalized heat rejection of the NDDCTs at tower spacing of 2.6D is shown in Figure 4.15. Again, the windward tower's heat rejection is similar to that of an isolated tower. The heat rejection of the middle tower decreases as the wind speed increases, until a wind speed of 5 m/s is reached, and for wind speeds greater than 5 m/s the heat rejection increases. It was observed in the flow field analysis, the separated flow from the windward tower moves alongside the wind direction, which

decreases the local wind-velocity in front of the middle tower. This can be seen in the heat rejection of the leeward tower.

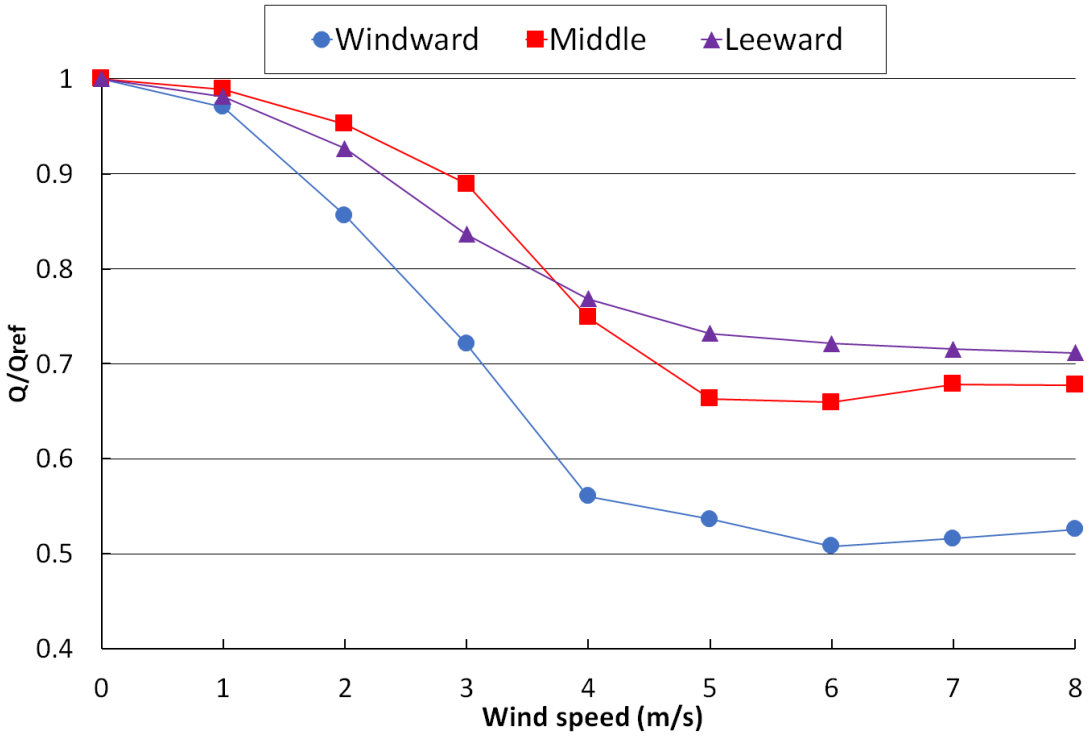

Figure 4.15. Normalized heat rejection of NDDCTs at tower spacing of 2.6D.

Finally, the heat rejection of the NDDCTs at a tower spacing of 4.2D and at different wind speeds is illustrated in Figure 4.16. By comparing Figure 4.14, Figure 4.15, Figure 4.16, it can be seen that the heat rejection of the towers becomes similar by increasing the tower spacing. This shows that increasing the tower spacing decreases the protection of the windward tower for the middle and leeward towers.

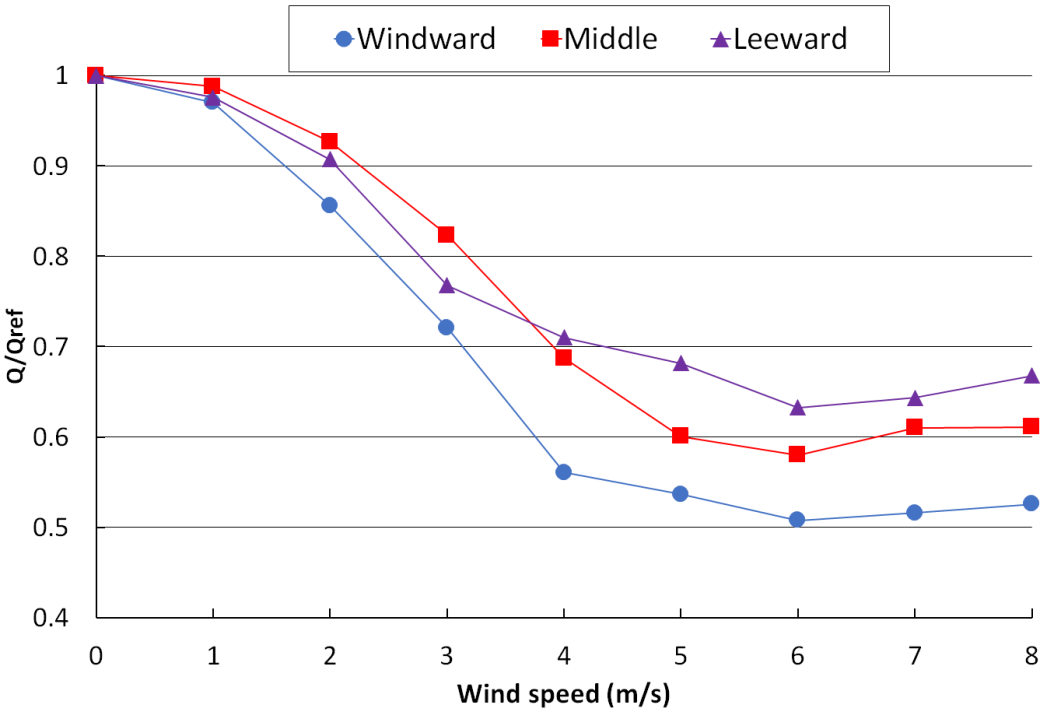

Figure 4.16. Normalized heat rejection of NDDCTs at tower spacing of 4.2D.

4.8. Chapter conclusions

The influence of wind speed and tower spacing on the heat-transfer performance of three NDDCTs arranged in a line with respect to the prevailing wind direction has been studied. The flow and temperature fields were examined and the effects of tower spacing on each tower at various wind speeds was discussed. The interaction of the towers from the bottom and top of the towers were identified at different tower spacings and wind speeds. At all tower spacings, the windward tower protects the middle and leeward towers by deflecting the upcoming wind. It was observed that the windward tower acts as a windbreak and protects the middle and leeward towers. This investigation has found that this protection is more significant at low wind speeds. Further, the protection of the windward tower for the middle and leeward towers decreases by increasing the tower spacing.

Chapter 5: Influences of varying NDDCT dimensions upon the performance of a multi-tower system

5.1. Introduction

In the previous chapters, it was shown that wind had a significant effect on short NDDCTs. Furthermore, it was shown that orienting these towers in line with the prevailing wind would improve the performance. Of course, this raises the question of the generalisability of this finding to cooling towers of different geometries. Although some studies (65, 68) have examined this, they have not undertaken any systematic investigation of varying geometry of the tower. For different sizes and shapes of the cooling towers, the crosswind effects are different. In order to better compare the crosswind effect on the different size (height and diameter) of the cooling tower in a multi-tower system, this chapter explores the thermo-flow performance of three NDDCTs in an in-line arrangement with different sizes. The aim of this chapter is to find a relationship and generalize findings of this study which was found for Tower 1 placed in a multi-tower system with different tower dimensions The results of this chapter will provide an understanding of how the findings of short NDDCTs can be related to larger ones.

5.2. Performance of a single NDDCT with varying height

5.2.1. Method

To help understand the effect of size variation on the interaction and performance of NDDCTs in a multi-tower system, the cooling performance of four cooling towers of varying size (including the tower dimensions of previous chapters) with the same aspect ratio (height/diameter) and air-cooled heat exchanger were investigated. The cooling tower dimensions are listed in Table 5.1. The aspect ratio used in these towers (1.6) was

kept constant to understand the effect that varying only height and diameter has on their cooling performance.

Table 5.1. Tower geometry parameters.

Tower number	Height (m)	Diameter (m)
1	20	12.5
2	40	25
3	60	37.5
4	90	56.25

In doing this the same numerical method of simulation, described in Chapter 2 and 3 was used in this chapter to simulate the airflow and thermal performance. Similarly, the dimensions of the domain were modified based on the dimensions of the simulated tower. Hence, the number of elements to mesh the NDDCT and domain were increased for different tower sizes. The domain sizes and final number of elements for each tower are listed in Table 5.2. A separate mesh sensitivity analysis was performed for each tower configuration, details are summarized in Appendix B. The simulations of a single tower with different sizes were carried out for wind speed range of 0-8 m/s.

Table 5.2. Boundary domain dimensions and finial number of elements for different towers.

Tower number	Computational domain Height x breadth x length (m)	Number of elements (million)
1	90 x 144 x 150	3.2
2	180 x 288 x 300	5.4
3	270 x 430 x 450	7.2
4	400 x 620 x 650	8.8

5.2.2. Results and discussion

The airflow streamlines shown in Figure 5.1 demonstrate that that the air flow recirculation at the heat exchanger is reduced as the tower height is increased. In chapter 3 it was noted that vortices formed at the bottom of the 20m cooling tower and that these vortices could make the hot air return into the heat exchangers which reduced the heat transfer. However, as the height of the tower size increases the airflow inside the cooling tower becomes more uniform, as shown in Figure 5.1. This is due to the natural draft effect becoming stronger for taller cooling towers, which is apparent in the flow circulation at the bottom of the cooling tower becoming smaller.

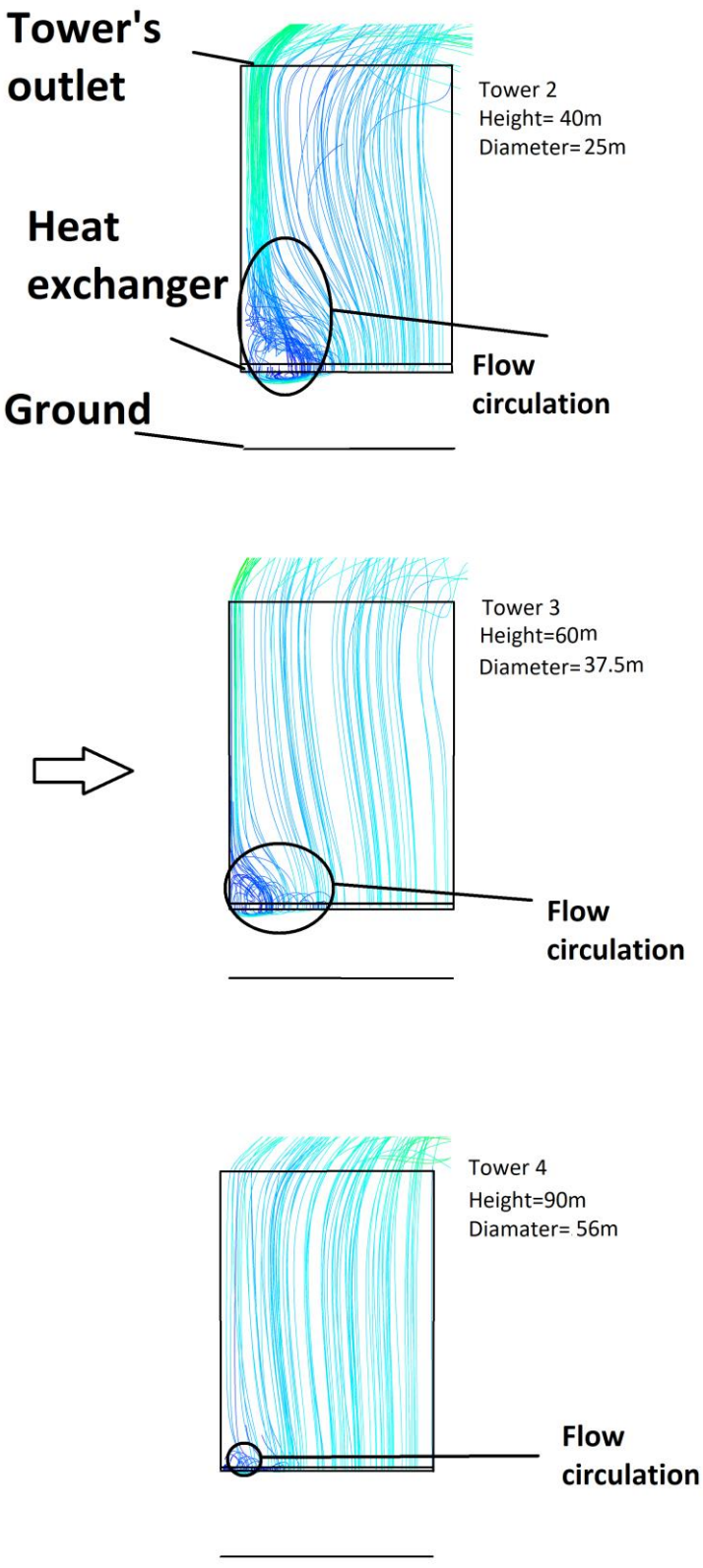

Figure 5.1. Streamlines of the cooling towers at crosswind 4 m/s.

By enlarging the NDDCT, the vertical velocity in the cooling towers increases. The vertical velocity in towers is 0.98 m/s, 1.1 m/s, 1.3 m/s, and 1.54 m/s for towers 1 to 4 respectively. By increasing the vertical velocity inside a cooling tower, the deflection of the exiting plume by the crosswind decreases. The consequence of this is apparent in the normalized heat rejection of a single NDDCT of varying height and similar aspect ratios shown in Figure 5.2. The heat rejection of all towers decreases with increasing crosswind speed, however, the shortest tower (Tower 1) sees an increase in heat rejection for wind speeds above 6 m/s.

It was previously noted in Chapter 3 that the heat rejection of a cooling tower is composed of natural convection term and forced convection term, hence, when the heat rejection of a cooling tower increases after the “turnaround “ point, this means that forced convection is the predominant heat transfer mechanism. The forced convection is the amount of heat taken away from flow circulations at the bottom of the tower. Therefore, the heat rejection of Towers 2, 3, and 4 is mainly controlled by the natural convection (flow moving vertically inside a tower towards the outlet). This effect has been shown in Figure 5.2, where the flow inside the cooling tower becomes more uniform by increasing the tower dimensions. This means that by increasing tower height the cooling effect becomes less vulnerable to the crosswind suppressing heat loss.

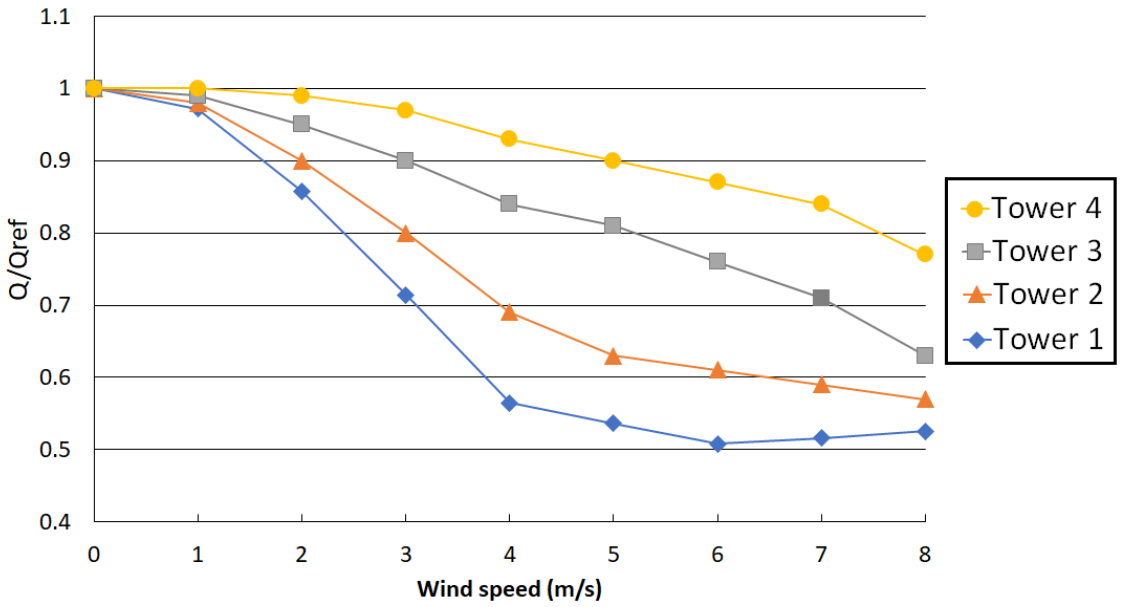

Figure 5.2. Normalized heat rejection of the towers.

5.3. Performance of multi-tower systems with different tower heights

5.3.1. Method

In modelling the multiple tower situation, the same numerical method as described in section 5.2 was used with the same range of tower heights and fixed aspect ratio. In line with the previous chapters, simulations were carried out for three tower spacings of 1.8D, 2.6D, and 4.2D. The parameters of the horizontal arranged heat exchanger were the same for all towers.

The dimensions of the computational domain were modified based on the dimensions of the simulated tower and tower spacing. Hence, the number of elements to mesh the NDDCTs and domain was different at each condition. The computational domain sizes and final number of mesh elements for different tower sizes and tower spacings are listed in Table 5.3.

Table 5.3. Computational domain size and final number of mesh elements.

Tower	Tower spacing	Computational domain Height x breadth x length (m)	Number of elements (million)
1	1.8D	90 x 144 x 220	4.8
1	2.6D	90 x 144 x 240	5.5
1	4.2D	90 x 144 x 260	6.2
2	1.8D	180 x 288 x 240	5.2
2	2.6D	180 x 288 x 320	5.8
2	4.2D	180 x 288 x 400	6.9
3	1.8D	270 x 430 x 320	7.7
3	2.6D	270 x 430 x 440	6.5
3	4.2D	270 x 430 x 520	8.5
4	1.8D	400 x 620 x 500	7
4	2.6D	400 x 620 x 540	8.5
4	4.2D	400 x 620 x 800	9.6

5.3.2. Results and discussion

To illustrate how multiple tower systems respond to the wind, the normalized heat rejection of three NDDCTs of varying sizes (Towers 1-4) at tower spacings of 1.8D is

shown in

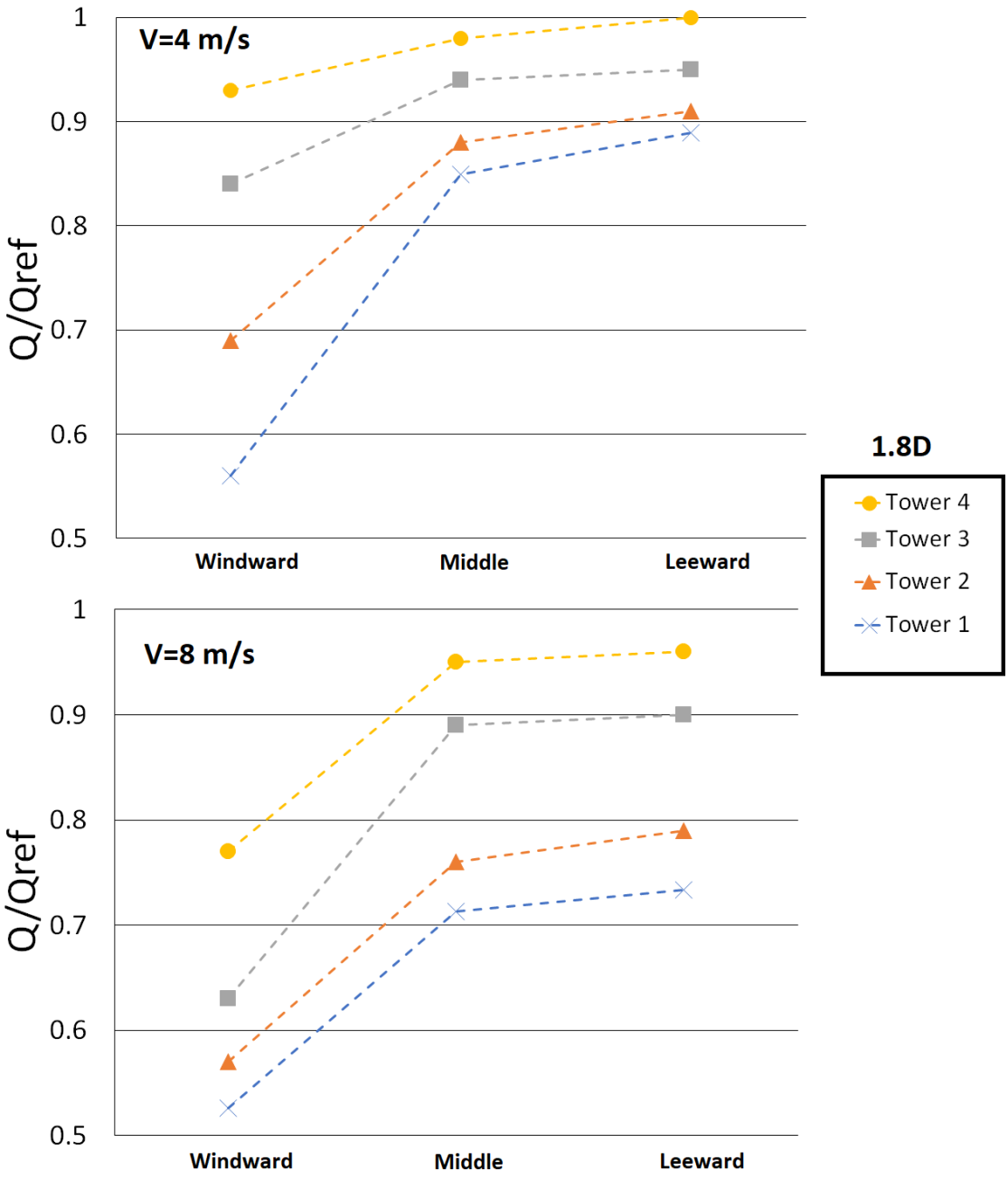

Figure 5.3. The normalized heat rejection of the windward tower increases with an increase in the dimensions of the tower. By increasing the size (height and diameter) of the cooling tower, the natural draft effect is enhanced, so the air flow inside the cooling tower is controlled by the stack effect. The normalized heat rejection of the Towers 1 to 4 as the windward tower at wind speed of 4 m/s is 0.56, 0.66, 0.84, and 0.93. This result reinforces the previous finding of the windward towers sheltering the down-wind towers.

The results show that for all tower sizes, the normalized heat rejection of the windward tower is the minimum and the leeward tower is the maximum. This means that the leeward tower benefits from the protection provided by the middle and the windward towers. By increasing the tower dimensions, the protection provided by the windward tower increases for the middle and leeward towers. Furthermore, at wind speed of 4 m/s, the heat normalized heat rejection of the leeward Tower 4 is almost 1, which means the crosswind does not have any impact on the performance of this tower. Essentially the windward and leeward towers provide significant protection at this tower spacing with this tower size. When wind speed is 4 m/s, the difference between normalized heat rejection of the windward tower and leeward towers increases from Tower 4 to Tower 1. It is also notable that by increasing the wind speed the normalized heat rejection of the Tower 4 does not change significantly compared to the smaller towers. This means at this tower spacing, the impact of increasing crosswind on the leeward and middle tower is small for larger towers.

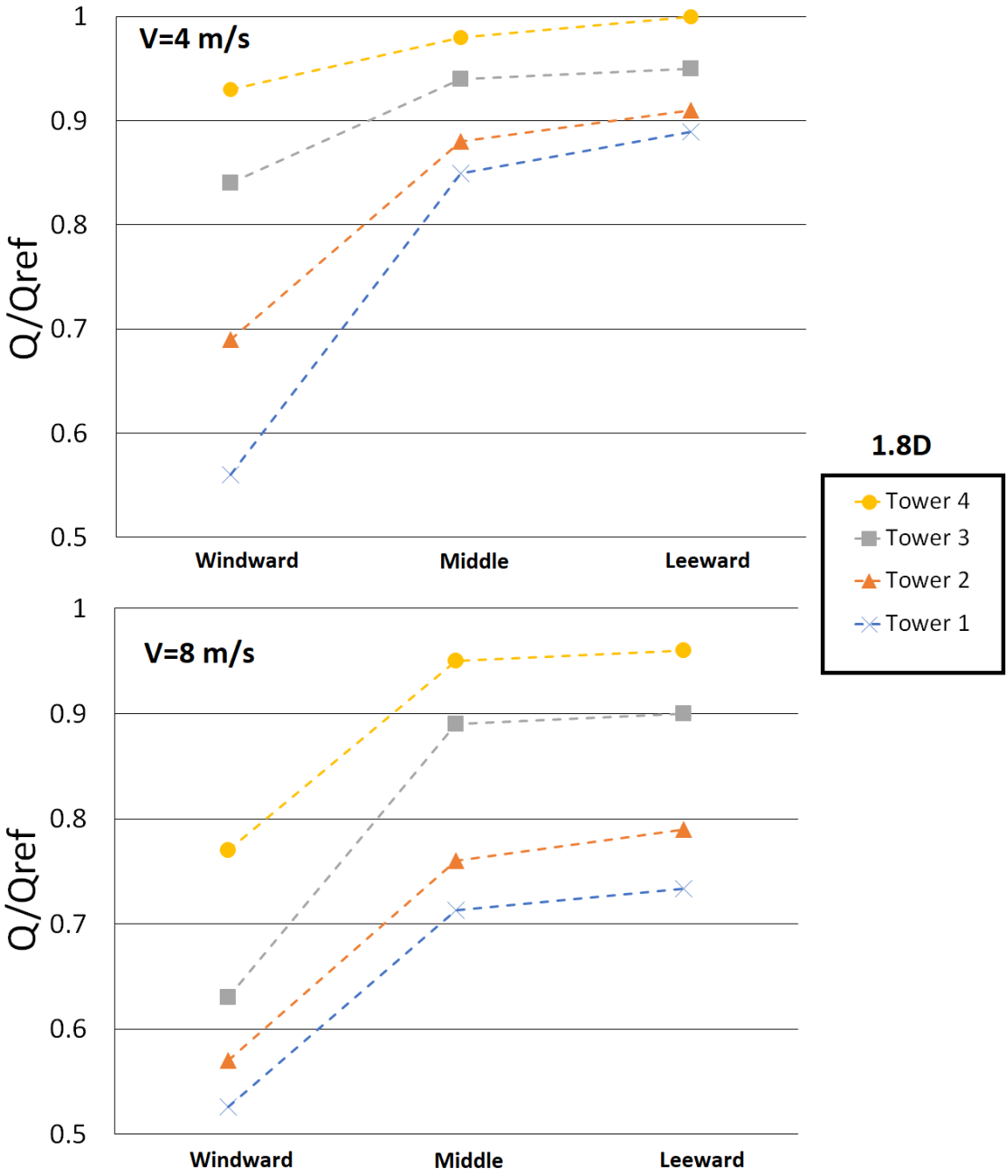

Figure 5.3. Normalized heat rejection of the NDDCTs at different sizes and tower spacing of 1.8D.

Following on from this, Figure 5.4 displays the normalized heat rejection of the NDDCTs with different sizes at tower spacing of 2.6D. The normalized heat rejection of the windward tower at tower spacing of 2.6D is the same as with a tower spacing of 1.8D. Further, the normalized heat rejection of the middle and leeward towers decreases when increasing the tower spacing of all tower sizes. This reduction is caused by increased tower spacing reducing the windward sheltering effect.

At a tower spacing of 2.6D, the thermal performance of the leeward tower is superior to the middle and windward towers for both wind speeds of 4 m/s and 8 m/s. The normalized heat rejection of windward, middle, and leeward towers is 0.93, and 0.98, and 0.99, which shows protection provided by the windward tower for the middle and leeward towers. Moreover, by increasing the diameter of the tower, the size the heat exchanger area will be increased which results in a higher mass flow rate into the cooling tower. The crosswind comes around the windward tower, gets into the cooling tower and decreases the local wind speed in front of the middle and leeward towers. This may provide a calm condition for the middle and leeward towers and air can easily get into these towers without any disturbance. Same as tower spacing of 1.8D, the middle and leeward towers of Tower 4 is less vulnerable to the crosswind effect compared to smaller towers (Towers 3, 2, and 1).

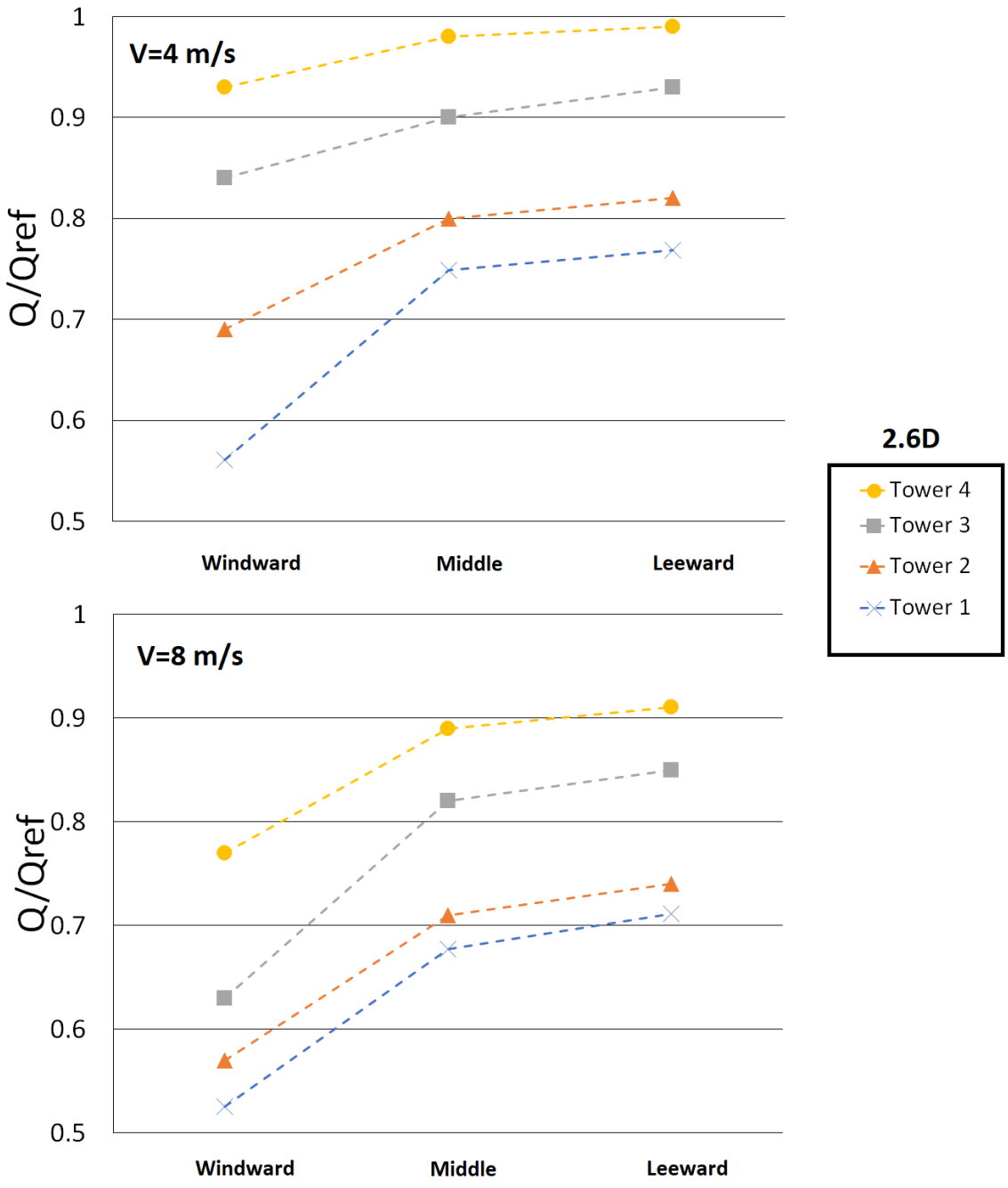

Figure 5.4. Normalized heat rejection of the NDDCTs at different sizes and tower spacing of 2.6D.

Finally, at a tower spacing of 4.2D, similar performance behaviour for the cooling towers can be observed, as shown in Figure 5.5. As shown previously, the normalized heat rejection of the towers decreases by increasing the wind speed, and again, the normalized heat rejection of the towers decreases by increasing the tower spacing from 1.8D to 4.2D (comparing with Figure 5.3). Despite the large tower spacing 4.2D, the performance of the leeward tower (tower 4) at a wind speed of 4 m/s is still close to the no wind heat

rejection, while at a wind speed of 8 m/s, the performance of all towers has dropped compared to a wind speed of 4 m/s.

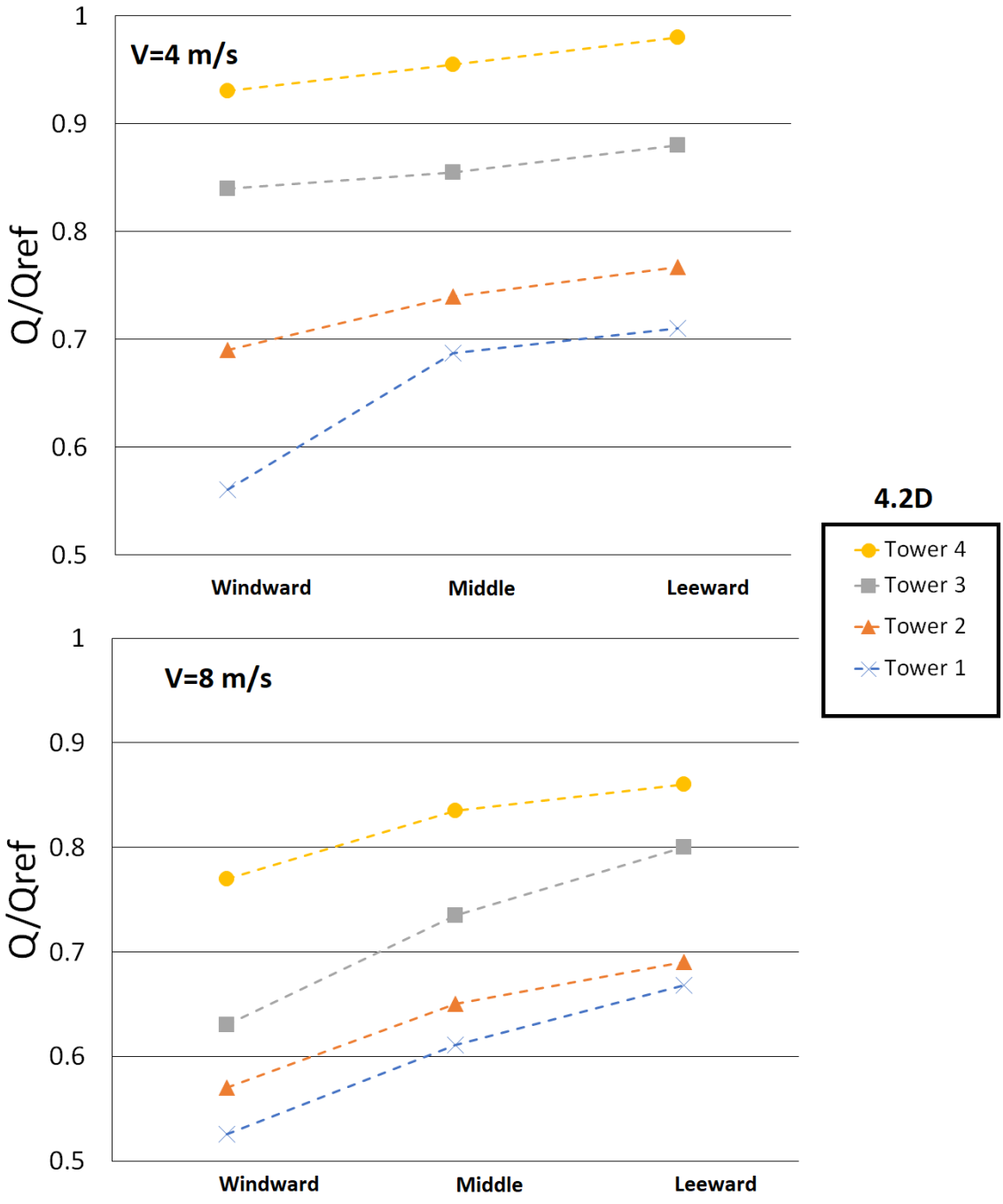

Figure 5.5. Normalized heat rejection of the NDDCTs at different sizes and tower spacing of 4.2D.

This chapter aimed to find a relationship and generalize findings of this study which was found for Tower 1 placed in a multi-tower system with different tower dimensions. The main connection could be found between different tower dimensions was that the

windward tower protects the leeward towers despite of the size. The height of towers was increased from Tower 1 to Tower 4 and it was found out that larger towers are less susceptible to the crosswind effects. This means that middle and leeward towers normalized heat rejection remain almost unaffected for very large towers (Tower 4). The results demonstrated that at low tower spacing, large towers (Towers 3 and 4) becomes independent of the wind speed since by increasing the wind speed from 4 m/s to 8 m/s, the normalized heat rejection of these towers did not change significantly.

The normalized heat rejection of the Tower 4 as the middle and leeward tower did not change by increasing the tower spacing when the wind speed was 4 m/s (at wind speed of 4 m/s, the normalized heat rejection was above 0.9). However, the normalized heat rejection of the middle and leeward of short towers (Tower 1 and 2) changes significantly by increasing the tower spacing when the wind speed is 4 m/s. Overall, for all cooling towers, the smaller tower spacing provides a better protection for the leeward towers.

5.4. Chapter conclusions

In this chapter, the thermal performance of three NDDCTs at a wind incidence of 0° was investigated for various tower dimensions over a fixed height/diameter ratio. For each simulation of different tower spacings, the dimensions of the windward, middle, and leeward towers were identical. The height of towers ranged from 20m to 40, 60m, and 90, with the aspect ratio maintained at 1.6. The simulations were performed for the four heights individually, and it was concluded that by increasing the tower dimensions, the relative cooling performance of the towers decreased for wind speed range of 0-8 m/s.

Furthermore, in agreement with the findings in preceding chapters, the normalized heat rejection is highest for the leeward tower and lowest for the windward tower. However, the larger cooling towers appeared to provide a higher degree of protection for the middle and leeward towers provided by the windward tower.

It is suggested that the ability of larger cooling towers to the draw more air into the cooling tower, may decrease the local velocity in front of the middle and leeward towers. This will result a calm condition for the leeward towers and increase the drafting capability of the middle and leeward towers.

The heat rejection of the very large cooling towers, when placed as the middle and leeward towers, are not influenced by the tower spacing significantly and at low tower spacing crosswind effect on the heat rejection of these towers is not notable. The overall relationship between all of these towers is that the windward tower protects the middle and leeward towers and this protection is higher at lower tower spacings.

Chapter 6: Conclusions, recommendations, and future work

6.1. Conclusions

Over the course of this study the thermal performance of a single and multiple natural draft dry cooling towers (NDDCTs) located on a common site were investigated under both no-wind and windy conditions using CFD simulations. The simulated NDDCT for this study was a cylindrical tower with a horizontally arranged air-cooled heat exchanger, similar to that developed by the University of Queensland. The effects of different wind speeds, tower spacings, and wind-incidence angles on velocity and temperature fields, and on the heat rejection of the towers, were investigated. The model developed for a standalone tower was validated against computational and test results obtained from studies of the University of Queensland test cooling tower. Once the methodology was validated, it was then applied to a multi-tower configuration, for which no precedent results could be found in the literature.

From this a number of interesting conclusions can be drawn which answer the research question of this study and will inform the design of dry cooling systems for expanding CSP plants. In particular, it was found that when two towers were placed more than 2D (diameter of the tower) apart, on a site with still conditions (i.e. no wind), both towers act as an isolated NDDCT and the flow characteristics are symmetrical. Smaller spacings led to a reduction in the scavenge area between the two towers limiting the air supply for both towers. This results in non-uniform temperature and velocity distributions within them. Further, the results obtained from three-tower simulations showed that the middle tower heat rejection decreases by 15% at small tower spacings. This interaction between towers at low tower-spacing decreases the performance of all towers.

Conversely, the situation for sites with multiple towers and windy conditions are far more complex. Put simply, it was found that the flow fields around the NDDCTs are completely different at various wind-incidence angles. At a wind incidence of 0°, the windward tower protects the leeward tower from the upcoming wind, which enhances the cooling performance of the leeward tower. By increasing the tower spacing, the heat rejection of the leeward tower decreases, which means the protection provided by the windward tower is lower at large tower spacings compared to small tower spacings. At this wind-incidence angle, the performance of the windward tower does not change at different tower spacings and it acts like an isolated tower. Velocity field showed that the towers interact with each other at both the bottom and top of the towers. However, the overall outcome is that the windward tower act like a windbreak for the leeward towers.

When the wind is blowing at an incidence angle of 45°, the velocity field indicated that the towers interfere only from bottom of the towers and there was no interference between the towers' outlet. Interaction of the towers at either the bottom or top results in a reduction in the towers' heat rejection compared to an isolated tower. The small tower-spacing creates a contractive passage which accelerates the flow between the towers. The flow acceleration around the towers decreases the heat rejection of the towers, especially the leeward tower. The interaction between the towers decreases by increasing the tower spacing and the towers act as isolated towers at a tower spacing of 4.2D.

When towers are placed beside each other (wind incidence of 90°), the interaction between the towers exists only at a tower spacing of 1.8D, and for tower spacings of 2.6D and 4.2D the interaction between them is negligible. The small passage between the towers means that little air can flow through the passage between the towers, which means more air flows onto the windward side of the towers instead. The temperature fields demonstrated that the windward side of the heat exchanger is cooler than the middle and leeward side of the heat exchanger. At this wind incidence angle, the towers interact only

from bottom of the towers and the velocity field suggested that there is no interaction between the outlets of the towers.

Furthermore, there was a consistency in thermal performance of the cooling towers with different dimensions. However, it was found out that larger towers are less vulnerable to crosswinds, which may be due their ability to draw more air into themselves. Also, it was observed that under windy conditions, the protection offered by the windward tower increased by enlarging the towers.

Overall, perhaps the most important conclusion to be reached, and considered in deploying multiple cooling towers on a common site is that the NDDCTs should be aligned with the respect to the prevailing wind.

6.2. Suggestions for future work

Future investigation could be performed on the power cycle analysis of systems cooled down by multiple short NDDCTs under "real world" conditions, i.e. varying wind speeds and wind directions. The objective of this modelling will be to determine the influence of multi-tower parameters variation on power output of the plant. It has been previously found that optimizing the water mass flow rate into the air-cooled heat exchanger bundles increases the performance of the NDDCT. The optimization of the water mass flow rate into the multiple NDDCTs can be achieved with respect to different wind speeds and incidence angles with objective function of maximizing the heat rejection of the entire multi-tower system.

Also, since the collapse of cooling towers at the Ferrybridge Power Plant, interference effects among grouped buildings have attracted much attention. However, no research has been conducted to investigate the interference factor (IF) which is commonly used to envelop the multiple complex static wind pressure distributions for multiple short NDDCTs. It was shown in this study that towers are interfering with each other and it has

been previously shown that interference effects influence average and fluctuating wind pressure simultaneously. It would be beneficial to perform finite element analysis to calculate the structure responses and shell reinforcements of the current NDDCTs with the tower spacings, wind incidence angles, and wind speeds used in this study. Further, previous studies mainly investigate the interference factor just by modelling the cooling tower's shell. Hence, it is highly recommended that the structural responses of the cooling towers interfering with each other will be examined including the heat exchanger and energy equation due to the strong relationship between the flow and thermal source in the cooling towers.

The findings of this study can be applied in the analysis of the effect of wind on multiple buildings. Previous studies regarding the flow analysis over multiple buildings were considered the geometry of the buildings as a solid without the interaction of the wind on the interior area of the building. This study has the potential to provide better understating of flow over buildings while considering the internal air flows.

This study could also be a guideline for flow analysis over objects with the presence of thermal sources and internal flows and future investigations can be performed on them by considering the findings of this work.

REFERENCES

1. Besarati SM, Goswami DY. Supercritical CO2 and other advanced power cycles for concentrating solar thermal (CST) systems. Advances in Concentrating Solar Thermal Research and Technology. 2016. p. 157-78.
2. Zhu HH, Wang K, He YL. Thermodynamic analysis and comparison for different direct-heated supercritical CO2 Brayton cycles integrated into a solar thermal power tower system. Energy. 2017;140(1):144-57.
3. Budenholzer RJ, Hauser LG, Oleson KA. Slecting heat rejection systems for future steam-electric power plants Combustion. 1972;44(4):30-7.
4. Konak AR. Treatment of once-through cooling systems effectively and economically. Anti-Corrosion Methods and Materials. 1979;26(9):5-7.
5. Porter RW, Weinstein H, Chaturvedi SK. Heat and mass transfer to the atmospher from spray cooling systems. International Heat Transfer Conference. 2017.
6. Macknick J, Newmark R, Heath G, Hallett KC. Operational water consumption and withdrawal factors for electricity generating technologies: a review of existing literature. Environmental Research Letters. 2012;7(4):045802.
7. Madden N, Lewis A, Davis M. Thermal effluent from the power sector: an analysis of once-through cooling system impacts on surface water temperature. Environmental Research Letters. 2013;8(3):035006.
8. Elgawhary AM. Spray pond mathematical model for cooling fresh water and brine: Oklahoma State University; 1971.
9. Bowman CF. Oriented spray cooling system ultimate heat sink for future nuclear plants. 16th International Conference on Nuclear Engineering: American Society of Mechanical Engineers; 2008. p. 383-7.
10. Stanford HW. HVAC Water Chillers and Cooling Towers: Fundamentals, Application, and Operation. HVAC Water Chillers and Cooling Towers: Fundamentals, Application, and Operation. 2011.
11. Kröger DG. Air-cooled Heat Exchangers and Cooling Towers. 2004.
12. Duniam S, Gurgenci H. Annual performance variation of an EGS power plant using an ORC with NDDCT cooling. Applied Thermal Engineering. 2016;105:1021-9.
13. He S. Performance improvement of natural draft dry cooling towers using wetted-medium evaporative pre-cooling: The University of Queensland; 2015.
14. Lu Y. Small natural draft dry cooling towers for renewable power plants: The University of Queensland; 2015.
15. Kröger DG. Air-Cooled Heat Exchangers and Cooling Towers. II, Pennwell Corp,; Tulsa2004. p. 38-91.
16. Goodarzi M. A proposed stack configuration for dry cooling tower to improve cooling efficiency under crosswind. Journal of Wind Engineering and Industrial Aerodynamics. 2010;98(12):858-63.
17. Zhao YB, Long G, Sun F, Li Y, Zhang C. Numerical study on the cooling performance of dry cooling tower with vertical two-pass column radiators under crosswind. Applied Thermal Engineering. 2015;75:1106-17.
18. Alkhedhair A, Gurgenci H, Jahn I, Guan Z, He S. Numerical simulation of water spray for pre-cooling of inlet air in natural draft dry cooling towers. Applied Thermal Engineering. 2013;61(2):416-24.
19. Al-Waked R, Behnia M. The performance of natural draft dry cooling towers under crosswind: CFD study. International Journal of Energy Research. 2004;28(2):147-61.
20. Ardekani MA, Farhani F, Mazidi M, Ranjbar MA. Study of degradation of dry cooling tower performance under wind conditions and method for tower efficiency enhancement. International Journal of Engineering, Transactions A: Basics. 2015;28(3):460-6.
21. Du Preez AF, Kröger DG. Effect of wind on performance of a dry-cooling tower. Heat Recovery Systems and CHP. 1993;13(2):139-46.

22. Hooman K. Theoretical prediction with numerical and experimental verification to predict crosswind effects on the performance of cooling towers. Heat Transfer Engineering. 2015;36(5):480-7.
23. Lu Y, Guan Z, Gurgenci H, Zou Z. Windbreak walls reverse the negative effect of crosswind in short natural draft dry cooling towers into a performance enhancement. International Journal of Heat and Mass Transfer. 2013;63:162-70.
24. Li X, Gurgenci H, Guan Z, Wang X, Xia L. A review of the crosswind effect on the natural draft cooling towers. Applied Thermal Engineering. 2019;150:250-70.
25. Zhang Z, Gao M, Wang M, Guan H, Dang Z, He S, et al. Field test study on thermal and ventilation performance for natural draft wet cooling tower after structural improvement. Applied Thermal Engineering. 2019:305-12.
26. Wei Q-d, Zhang B-y, Liu K-q, Du X-d, Meng X-z. A study of the unfavorable effects of wind on the cooling efficiency of dry cooling towers. Journal of Wind Engineering and Industrial Aerodynamics. 1995;54-55:633-43.
27. Du X, Beyers M, editors. Numerical Studies on Wind Effects on the Cooling Efficiency of Dry Cooling Towers. The Fifth International Symposium on Computation Wind Engineering (CWE2010); 2010.
28. Chen YL, Shi YF, Hao JG, Chang H, Sun FZ, editors. Experimental research on optimizing inlet airflow of wet cooling towers under crosswind conditions. IOP Conference Series: Earth and Environmental Science; 2018.
29. Alavi SR, Rahmati M. Experimental investigation on thermal performance of natural draft wet cooling towers employing an innovative wind-creator setup. Energy Conversion and Management. 2016;122:504-14.
30. Gao M, Sun F-z, Turan A. Experimental study regarding the evolution of temperature profiles inside wet cooling tower under crosswind conditions. International Journal of Thermal Sciences. 2014;86:284-91.
31. Su MD, Tang GF, Fu S. Numerical simulation of fluid flow and thermal performance of a dry-cooling tower under cross wind condition. Journal of Wind Engineering and Industrial Aerodynamics. 1999;79(3):289-306.
32. Chen X, Sun F, Chen Y, Gao M. Novel method for improving the cooling performance of natural draft wet cooling towers. Applied Thermal Engineering. 2019;147:562-70.
33. Blain N, Belaud A, Miolane M. Development and validation of a CFD model for numerical simulation of a large natural draft wet cooling tower. Applied Thermal Engineering. 2016;105:953-60.
34. Hyhlik T, editor Concept of CFD model of natural draft wet-cooling tower flow. EPJ Web of Conferences; 2014.
35. Klimanek A. Numerical Modelling of Natural Draft Wet-Cooling Towers. Archives of Computational Methods in Engineering. 2013;20(1):61-109.
36. Klimanek A, Cedzich M, Białecki R. 3D CFD modeling of natural draft wet-cooling tower with flue gas injection. Applied Thermal Engineering. 2015;91:824-33.
37. Sadafi MH, Ruiz J, Lucas M, Jahn I, Hooman K. Numerical and experimental study on a single cone saline water spray in a wind tunnel. International Journal of Thermal Sciences. 2017;120:190-202.
38. Zheng S, Jin T, Luo K, Tang L, Yi C, Fan J. Three-dimensional numerical simulation on thermal performance in counter flow natural draft cooling tower. Journal of Central South University (Science and Technology). 2013;44(9):3898-903.
39. Ma H, Si F, Kong Y, Zhu K, Yan W. Wind-break walls with optimized setting angles for natural draft dry cooling tower with vertical radiators. Applied Thermal Engineering. 2017;112:326-39.
40. Yang L, Wu X, Du X, Yang Y. Dimensional characteristics of wind effects on the performance of indirect dry cooling system with vertically arranged heat exchanger bundles. International Journal of Heat and Mass Transfer. 2013;67:853-66.

41. Wang W, Zhang H, Liu P, Li Z, Lv J, Ni W. The cooling performance of a natural draft dry cooling tower under crosswind and an enclosure approach to cooling efficiency enhancement. Applied Energy. 2017;186:336-46.
42. Wang W, Wang Y, Zhang H, Lin G, Lu J, Yue G, et al. Fresh breeze cuts down one-third ventilation rate of a natural draft dry cooling tower: A hot state modelling. Applied Thermal Engineering. 2018;131:1-7.
43. Wang W, Lv J, Zhang H, Liu Q, Yue G, Ni W. A quantitative approach identifies the critical flow characteristics in a natural draft dry cooling tower. Applied Thermal Engineering. 2018;131:522-30.
44. Wang W, Lyu J, Zhang H, Liu Q, Yue G, Ni W. A performance enhancement of a natural draft dry cooling tower in crosswind via inlet flow field reconstruction. Energy and Buildings. 2018;164:121-30.
45. Goodarzi M, Keimanesh R. Heat rejection enhancement in natural draft cooling tower using radiator-type windbreakers. Energy Conversion and Management. 2013;71:120-5.
46. Moore FK. Dry Cooling Towers. Advances in Heat Transfer1976. p. 1-75.
47. Du Preez AF. The influence of cross-winds on the performance of natural draft dry-cooling towers: University of Stellenbosch; 1992.
48. Du Preez AF, Kröger DG. The effect of the heat exchanger arrangement and wind-break walls on the performance of natural draft dry-cooling towers subjected to cross-winds. Journal of Wind Engineering and Industrial Aerodynamics. 1995;58(3):293-303.
49. Wu XP, Yang LJ, Du XZ, Yang YP. Flow and heat transfer characteristics of indirect dry cooling system with horizontal heat exchanger A-frames at ambient winds. International Journal of Thermal Sciences. 2014;79:161-75.
50. Bejan A. Advanced engineering thermodynamics. 3rd ed. NewYork: Wiley; 1997.
51. Macknick J, Newmark R, Heath G, Hallett KC. Operational water consumption and withdrawal factors for electricity generating technologies: A review of existing literature. Environmental Research Letters. 2012;7(4).
52. Colmenar-Santos A, Borge-Diez D, Molina CP, Castro-Gil M. Water consumption in solar parabolic trough plants: Review and analysis of the southern Spain case. Renewable and Sustainable Energy Reviews. 2014;34:565-77.
53. Lu Y, Gurgenci H, Guan Z, He S. The influence of windbreak wall orientation on the cooling performance of small natural draft dry cooling towers. International Journal of Heat and Mass Transfer. 2014;79:1059-69.
54. Lu Y, Guan Z, Gurgenci H, Hooman K, He S, Bharathan D. Experimental study of crosswind effects on the performance of small cylindrical natural draft dry cooling towers. Energy Conversion and Management. 2015;91:238-48.
55. Li X, Guan Z, Gurgenci H, Lu Y, He S. Simulation of the UQ Gatton natural draft dry cooling tower. Applied Thermal Engineering. 2016;105:1013-20.
56. Li X, Xia L, Gurgenci H, Guan Z. Performance enhancement for the natural draft dry cooling tower under crosswind condition by optimizing the water distribution. International Journal of Heat and Mass Transfer. 2017;107:271-80.
57. Li X, Duniam S, Gurgenci H, Guan Z, Veeraragavan A. Full scale experimental study of a small natural draft dry cooling tower for concentrating solar thermal power plant. Applied Energy. 2017;193:15-27.
58. Li X, Gurgenci H, Guan Z, Wang X, Duniam S. Measurements of crosswind influence on a natural draft dry cooling tower for a solar thermal power plant. Applied Energy. 2017;206:1169-83.
59. Li X, Gurgenci H, Guan Z, Sun Y. Experimental study of cold inflow effect on a small natural draft dry cooling tower. Applied Thermal Engineering. 2018;128:762-71.
60. Dong P, Li X, Guan Z, Gurgenci H. The transient start-up process of natural draft dry cooling towers in dispatchable thermal power plants. International Journal of Heat and Mass Transfer. 2018;123:201-12.

61. Dong P, Li X, Hooman K, Sun Y, Li J, Guan Z, et al. The crosswind effects on the start-up process of natural draft dry cooling towers in dispatchable power plants. International Journal of Heat and Mass Transfer. 2019;135:950-61.
62. Liu Q, Xia L, Hu M, Li X, Mi Z, Jia J. Positive impact of a tower inlet cover on natural draft dry cooling towers under crosswind conditions. Applied Thermal Engineering. 2018;139:283-94.
63. Lu Y, Klimenko A, Russell H, Dai Y, Warner J, Hooman K. A conceptual study on air jet-induced swirling plume for performance improvement of natural draft cooling towers. Applied Energy. 2018;217:496-508.
64. Laboratory NRE. Concentrating solar power projects [Available from: https://solarpaces.nrel.gov/projects.
65. Zhai Z, Fu S. Improving cooling efficiency of dry-cooling towers under cross-wind conditions by using wind-break methods. Applied Thermal Engineering. 2006;26(10):1008-17.
66. Irtaza H, Ahmad S, Pandey T. 2D study of wind forces around multiple cooling towers using computational fluid dynamics. International Journal of Engineering, Science and Technology. 2011;3(6):116-34.
67. Wu FHY, Koh RCY. Mathematical Model for Multiple Cooling Tower Plumes: W. M. Keck Lab. of Hydraulics and Water Resources; 1977.
68. Liao HT, Yang LJ, Wu XP, Du XZ, Yang YP. Impacts of tower spacing on thermo-flow characteristics of natural draft dry cooling system. International Journal of Thermal Sciences. 2016;102:168-84.
69. Yang LJ, Chen L, Du XZ, Yang YP. Effects of ambient winds on the thermo-flow performances of indirect dry cooling system in a power plant. International Journal of Thermal Sciences. 2013;64:178-87.
70. Ming G, Huang P, Tao L, Zhou X, Fan Z. Experimental study on wind loading on a complicated group-tower. Journal of Fluids and Structures. 2010;26(7-8):1142-54.
71. Niemann HJ, Köpper HD. Influence of adjacent buildings on wind effects on cooling towers. Engineering Structures. 1998;20(10):874-80.
72. Orlando M. Wind-induced interference effects on two adjacent cooling towers. Engineering Structures. 2001;23(8):979-92.
73. Sun TF, Gu ZF. Interference between wind loading on group of structures. Journal of Wind Engineering and Industrial Aerodynamics. 1995;54-55(C):213-25.
74. Zhao L, Chen X, Ge Y. Investigations of adverse wind loads on a large cooling tower for the six-tower combination. Applied Thermal Engineering. 2016;105:988-99.
75. Zhao L, Chen X, Ke S, Ge Y. Aerodynamic and aero-elastic performances of super-large cooling towers. Wind and Structures, An International Journal. 2014;19(4):443-65.
76. Melcer J, editor Important moments in the history of structural aerodynamics. MATEC Web of Conferences; 2017: EDP Sciences.
77. Li X, Gurgenci H, Guan Z, Wang X, Duniam S. Measurements of crosswind influence on a natural draft dry cooling tower for a solar thermal power plant. Applied Energy. 2017.
78. Yang LJ, Du XZ, Yang YP. Space characteristics of the thermal performance for air-cooled condensers at ambient winds. International Journal of Heat and Mass Transfer. 2011;54(15-16):3109-19.
79. Li X. Performance Comparison of the Crosswind Effect on Different Size of Natural Draft Dry Cooling Towers. International Symposium on Industrial Chimneys and Cooling Towers. 2016.
80. Dai YW, Mak CM, Ai ZT. Computational fluid dynamics simulation of wind-driven inter-unit dispersion around multi-storey buildings: Upstream building effect. Indoor and Built Environment. 2017;28(2):217-34.
81. Wiesinger F, Sutter F, Wolfertstetter F, Hanrieder N, Fernández-García A, Pitz-Paal R, et al. Assessment of the erosion risk of sandstorms on solar energy technology at two sites in Morocco. Solar Energy. 2018;162:217-28.
82. Igarashi T, Suzuki K. CHARACTERISTICS OF THE FLOW AROUND THREE CIRCULAR CYLINDERS ARRANGED IN LINE. Bulletin of the JSME. 1984;27(233):2397-404.

83. Zhao Y, Sun F, Li Y, Long G, Yang Z. Numerical study on the cooling performance of natural draft dry cooling tower with vertical delta radiators under constant heat load. Applied Energy. 2015;149:225-37.
84. Goodarzi M, Keimanesh R. Numerical analysis on overall performance of Savonius turbines adjacent to a natural draft cooling tower. Energy Conversion and Management. 2015;99:41-9.
85. Darbandi M, Behrouzifar A, Mirhashemi A, Salemkar H, Schneider GE, editors. Details study of ambient wind effect on heat dissipation capacity of thermal-powerplant dry cooling-towers. American Society of Mechanical Engineers, Fluids Engineering Division (Publication) FEDSM; 2014.
86. Reshadatjoo H, Pormahmod N, Moltagh SY. The effect of cross-winds on an indirect dry cooling tower with or without windbreaks. Proceedings of the Institution of Mechanical Engineers, Part A: Journal of Power and Energy. 2011;225(5):635-46.
87. Du Preez AF, Kroger DG. Effect of the shape of the tower supports and walls on the performance of a dry-cooling tower subjected to cross winds. Heat Transfer Engineering. 1995;16(2):42-9.
88. Uzair M. Wind Induced Heat Losses from Solar Dish-receiver Systems: Auckland University of Technology; 2018.

Appendix A: Literature summary

The dynamic similarity should be performed for the listed parameters listed in Table A.1.

Table A.1. Dynamic similarity in scaled model.

Parameter	Relation	Meaning
Aspect ratio	$\tau = \frac{H}{D}$	Ratio of the tower height to the base diameter
Crosswind Reynolds	$Re_{cw} = \rho D v_{cw}/\mu$	Crosswind flow patterns
Reynolds number inside the tower	$Re_i = \rho D v_i/\mu$	Flow patterns inside the tower
Densimetric Froude number	$Fr = \frac{\rho v_i^2}{(\rho_o - \rho)gH}$	Ratio of the flow inertia to the external field
Euler number	$Eu = \frac{\Delta P}{\rho v_i^2}$	Represents the air pressure drop of the cooling tower
Velocity ratio	$r = \frac{v_{cw}}{v_i}$	Crosswind velocity to the vertical air inside the tower

The summary of previous studies on NDDCTV can be found in Table A.2

Table A.2. Summary of NDDCTV studies.

Authors	Tower dimension (Height* Base diameter* Outlet Diameter) (m)	Type of study	Remarks
Ma et al. (39)	(173* 155*91)	CFD (Realizable k-ε) (Steady state)	The angle of windbreak walls around the tower affects the flow distribution inside the tower.
Zhao et al. (83)	(172*152*96)	CFD (Standard k-ε) (Steady state)	During windy condition, an air circulation zone formed which deteriorates the cooling performance of that region.
Zhao et al. (17)	(172*152*96)	CFD (Standard k-ε) (Steady state)	Crosswinds increased the exit water temperature.
Yang et al. (40)	(195*177.6*120)	CFD (Realizable k-ε) (Steady state)	The cooling performance of the upwind deltas are superior to other deltas.
Al-Waked and Behnia (19)	(129*95*52)	CFD (Standard k-ε) (Steady state)	An improvement of 15% was predicted at crosswind velocity of 10 m/s by using windbreakers.
Wang et al. (43)	(170*85*146)	CFD (steady state)	As crosswind increases, the main vortices become stronger and larger. The high crosswind speeds can be favourable factor in the outlet.
Su et al. (31)	(125*108*60)	CFD (Standard k-ε) (Steady state)	Determined the unfavourable effect of crosswinds on NDDCTV.
Goodarzi (16)	(120*100*60)	CFD (Standard k-ε) (Steady state)	Changing the geometry can affect the performance of the NDDCTV.

Goodarzi and Keimanesh (45)	(120*100*60)	CFD (Standard k-ε) (Steady state)	Higher initial cost, improves the cooling efficiency both with and without wind compared to solid windbreakers.
Goodarzi and Keimanesh (84)	(120*100*60)	CFD (Standard k-ε) (Steady state)	Producing power from wind and also increases the cooling efficiency of the cooling tower by using wind turbines as windbreakers.
Darbandi et al. (85)	(150*118*64)	CFD (Standard k-ε) (Steady state)	Under windy conditions the efficiency of the windward sectors increases while the side and leeward decreases.
Reshadatjoo et. al (86)	(150*118*64)	CFD (k-ω) (Steady state)	The windbreakers are more effective at higher wind speeds compared to lower ones.

Table A.3 lists the previous studies on NDDCTH.

Table A.3. Summary of NDDCTH studies.

Authors	Tower dimension (Height* Base diameter* Outlet Diameter) (m)	Type of study	Remarks
Al-Waked and Behnia (19)	(129*95*52)	CFD (Standard k-ε) (Steady state)	Increasing the crosswind speed decreases the performance of tower for all wind seed range.

			An improvement of 15% was predicted at crosswind velocity of 10 m/s by using windbreakers.
Du Preez and Kröger (21)	(165*144)	CFD- Steady state	Horizontal heat exchanger demonstrated better thermal performance under windy conditions compared to vertical ones.
Du Preez and Kröger (87)	165*144)	CFD- Steady state	Tower supports have positive impact on the performance of the system.
Wu et al. (49)	(207*192*130)	CFD (Realizable k-ε) (Steady state)	The outlet water temperature of the heat exchanger increases with increasing wind speed.

Table A.4 summarizes the findings of the previous short NDDCT studies.

Table A.4. Summary of previous studies on short NDDCT.

Author	Type of study	Findings/ Remarks
Lu et al. (23)	CFD- Steady state- Realizable k-ε	• The heat rejection of a short NDDCT reaches to a minimum value by increasing the crosswind speed and then increases.
Lu et al. (53)	CFD- unsteady state- standard k-ω	• The difference between steady state results and the time-averaged transient results was sufficiently small. • Vorticity magnitude was used to identify the flow circulations. • The windbreak walls improved the performance of the NDDCT. • The heat rejection rate of short and large NDDCTs are different

Lu et al. (54)	Wind tunnel test (scale ratio 1:12.5	• By decreasing of the dimensions of the short NDDCT, the minimum heat transfer rate occurs at lower crosswind speeds.
Li et al. (55)	CFD- Steady state- Realizable k-ε	• The heat transfer rate of the windward section decreases with the presence of the crosswind and then improves gradually at high crosswind speed.
Li et al. (56)	CFD- Steady state- Realizable k-ε	• The water mass flow rate to each heat exchanger bundle can be controlled by proportional control valve with respect to the air mass flow rate.
Li et al. (57)	Full scale experiment	• The NDDCT was tested at constant heat flux and was proposed for a 1MW CST sCO_2 power plant.
Li et al. (58)	Full scale experiment	• Crosswinds affected the temperature distribution inside the cooling tower significantly.
Dong et al. (60, 61)	1D analytical modelling/ CFD- Steady state- Realizable k-ε/ Full scale experiment	• The start-up time is shorter when the flow is uniform.
Liu et al. (62)	CFD- Steady state- Realizable k-ε	• The inlet cover improved the performance of the Gatton NDDCT during windy condition.
Lu et al. (63)	CFD- Steady state- Realizable k-ε	• The swirling ratio plume vortex which was created by introducing a number of blower-powered air jets within the tower increased the cooling performance of the tower.

A summary of previous studies regarding the effect of wind on multiple NDDCTs is listed Table A.5.

Table A.5. Summary of previous studies on multiple NDDCTs.

Authors	Type of study	Dimensions	Number of towers	Remarks
Zhai and Fu (65)	CFD (Steady state- Realizable k-ε) Experimental (wind tunnel test scale 1:100)	(125m *108m *60 m)	2 tower in-tandem arranged	The windward tower protects the leeward tower from the direct incidence of the crosswind.
Irtaza et al. (66)	Numerical (CFD standard k-ε, RNG k-ε, realizable k-ε) Experimental (wind tunnel test 1:283)	(172.5m*134.60m*78.82m)	5 and 3 cooling towers interact with each other	Both shielding and interfering effects were observed, which led to either reduction or enhancement.
WU and Koh (67)	Numerical	----------	4	The model predicts only the specification of plumes
Liao et al. (68)	Numerical (CFD- steady state- realizable k-ε)	(125m*96m*66m)	2	The windward tower protects the leeward tower during windy conditions.
Yang et al. (69)	Numerical (CFD- steady state- standard k-ω	(173m*129.6m*88m)	2	Effect of the neighbouring buildings has been discussed on the performance of the towers.

Appendix B: Mesh and boundary domain sensitivity analysis

The mesh sensitivity for a single NDDCT during no-wind condition was performed and heat rejection was selected to monitor the effect of number of elements on the simulation. Figure B.1 shows the mesh sensitivity analysis and it shows the heat rejection deviation is less than 1% when the number of cells is over 2,000,000.

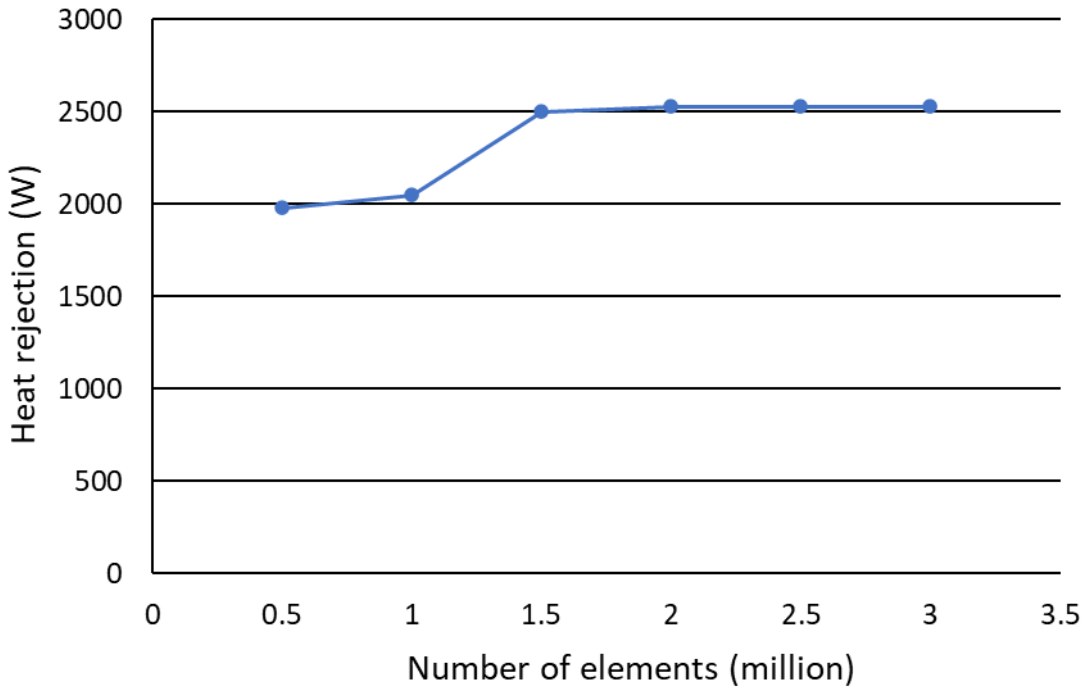

Figure B.1. Mesh sensitivity analysis for a single NDDCT at no-wind condition.

The mesh sensitivity for a single NDDCT during windy condition was performed at wind speed of 4 m/s. The normalized heat rejection of the radiator was selected to monitor the effect of increasing the mesh elements on the thermal performance of the NDDCT. The mesh sensitivity analysis is shown in Figure B.2. The normalized heat rejection deviation is less than 1% when the number of cells is over 3,000,000. With further refinement the number of cells reached to 3,200,000 for single NDDCT simulation during windy condition.

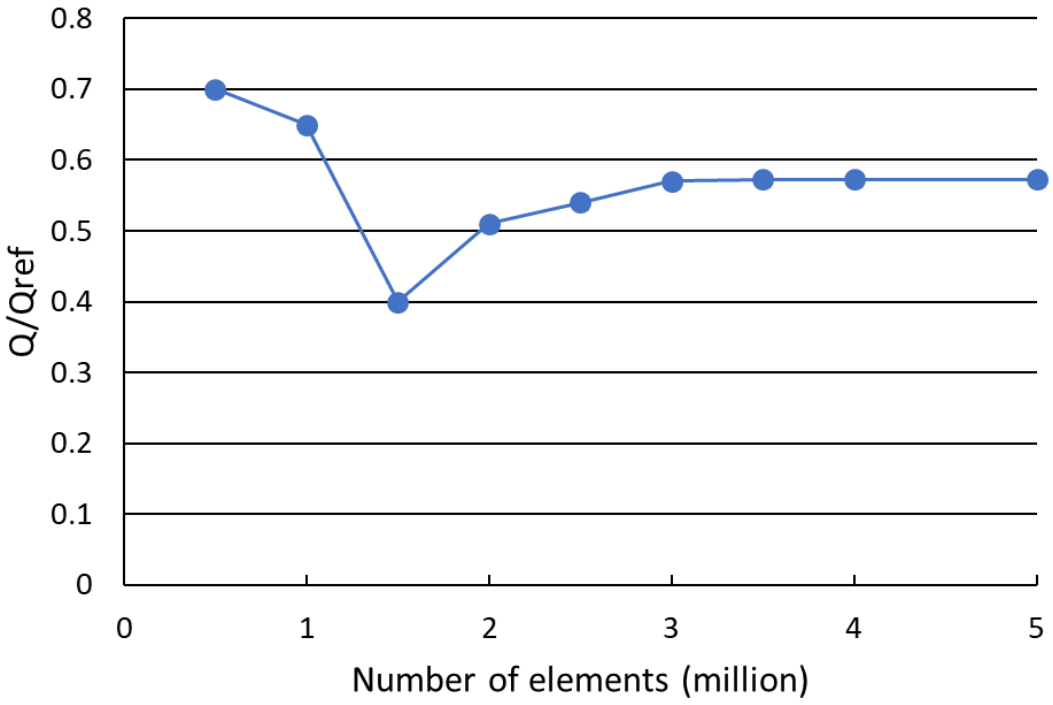

Figure B.2. Mesh sensitivity analysis for a single NDDCT at wind speed of 4 m/s.

The mesh sensitivity analysis for two NDDCTs were performed at wind speed of 4 m/s at tower different tower spacings and wind incidence angles. Figure B.3Figure B.4Figure B.5 show the mesh sensitivity analysis of two NDDCTs at wind incidence angle of 0° at tower spacings of 1.8D, 2.6D, and 4.2D respectively.

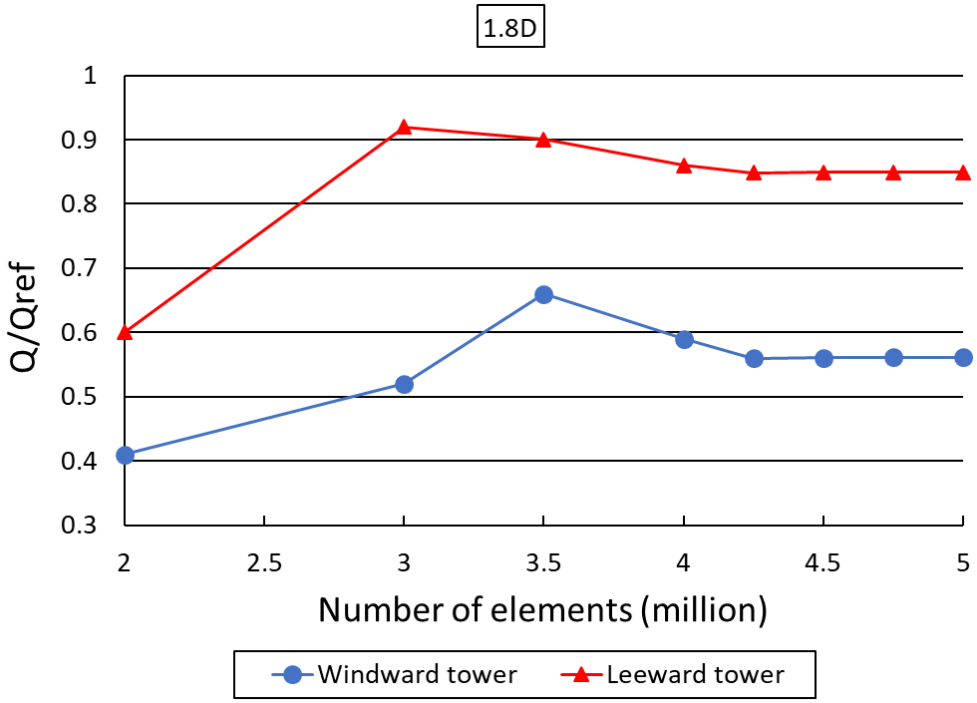

Figure B.3. Mesh sensitivity analysis for two NDDCTs at wind speed of 4 m/s, tower spacing of 1.8D, and wind incidence angle of 0°.

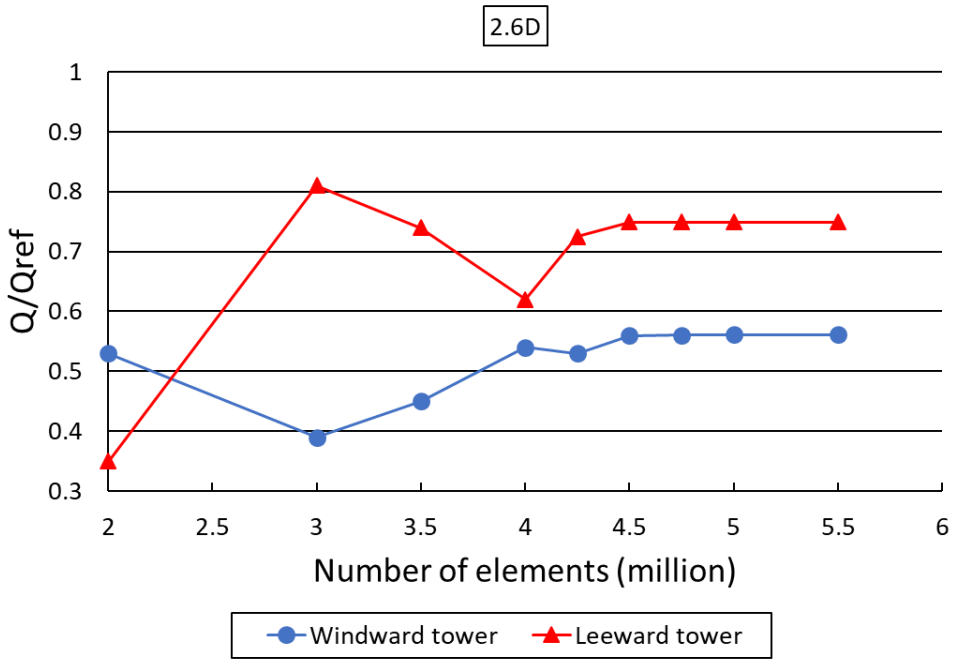

Figure B.4. Mesh sensitivity analysis for two NDDCTs at wind speed of 4 m/s, tower spacing of 2.6D, and wind incidence angle of 0°.

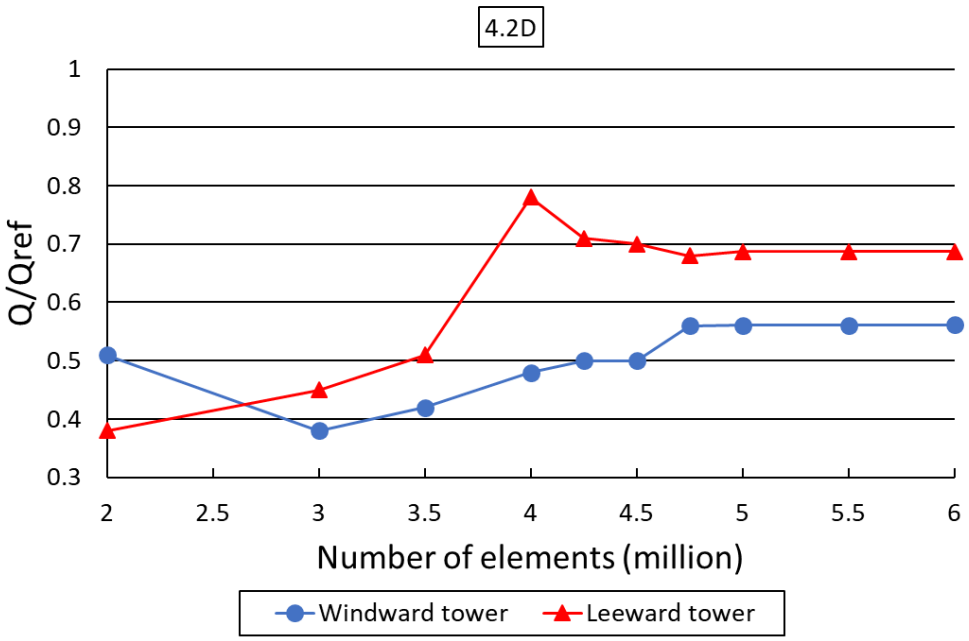

Figure B.5. Mesh sensitivity analysis for two NDDCTs at wind speed of 4 m/s, tower spacing of 4.2D, and wind incidence angle of 0°.

Figure B.6Figure B.7Figure B.8 show the mesh sensitivity analysis for two NDDCTs at wind incidence angle of 45° at tower spacings of 1.8D, 2.6D, and 4.2D. The normalized heat rejection of the towers was monitored to ensure that increasing the number of elements do not affect the simulation results.

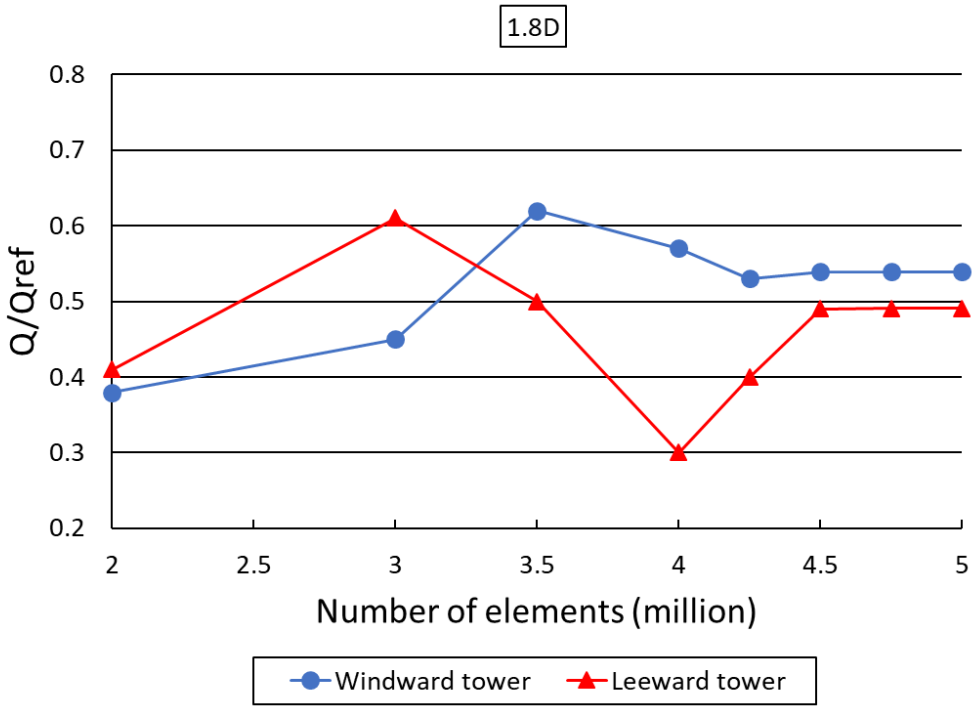

Figure B.6. Mesh sensitivity analysis for two NDDCTs at wind speed of 4 m/s, tower spacing of 1.8D, and wind incidence angle of 45°.

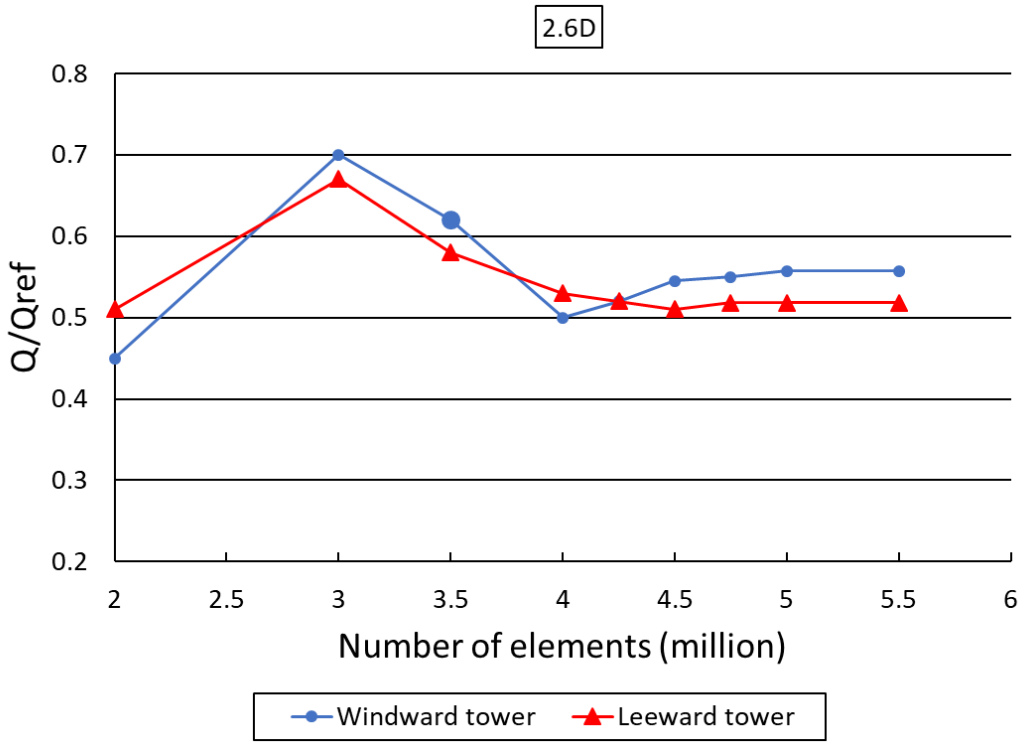

Figure B.7. Mesh sensitivity analysis for two NDDCTs at wind speed of 4 m/s, tower spacing of 2.6D, and wind incidence angle of 45°.

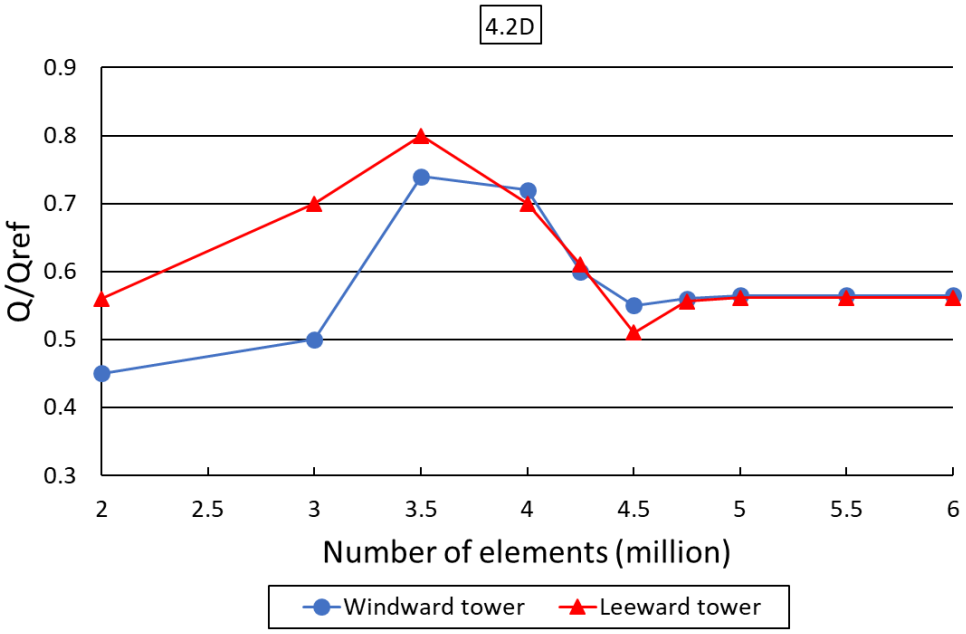

Figure B.8. Mesh sensitivity analysis for two NDDCTs at wind speed of 4 m/s, tower spacing of 4.2D, and wind incidence angle of 45°.

The mesh sensitivity for wind incidence angle of 90° was performed with the same criteria as 0° and 45° for tower spacings of 1.8D, 2.6D, and 4.2D (Figure B.9Figure B.10Figure B.11).

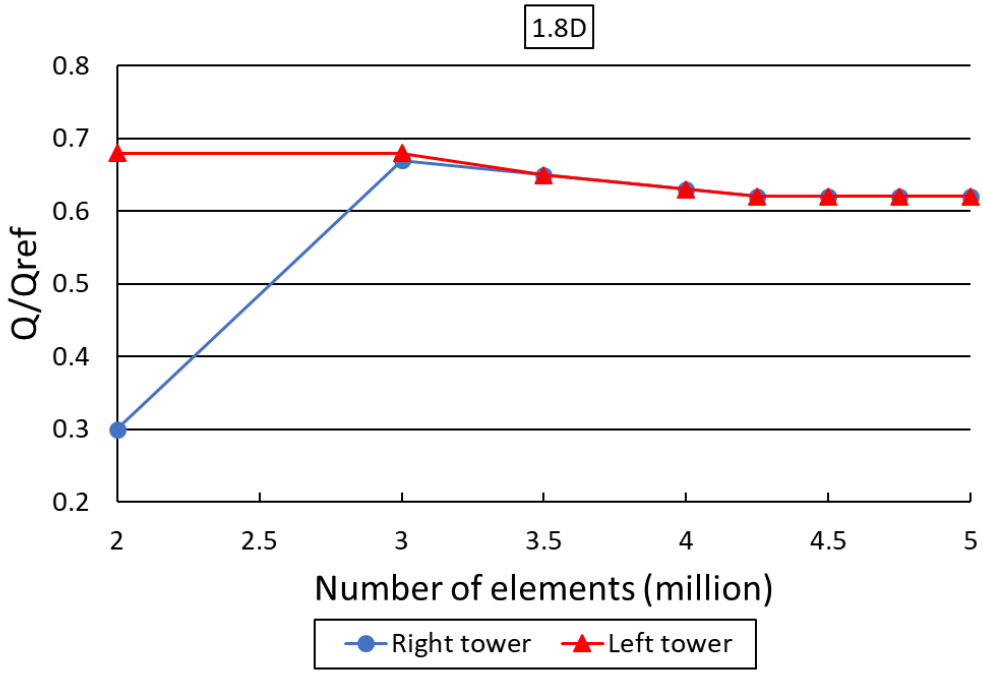

Figure B.9. Mesh sensitivity analysis for two NDDCTs at wind speed of 4 m/s, tower spacing of 1.8D, and wind incidence angle of 90°.

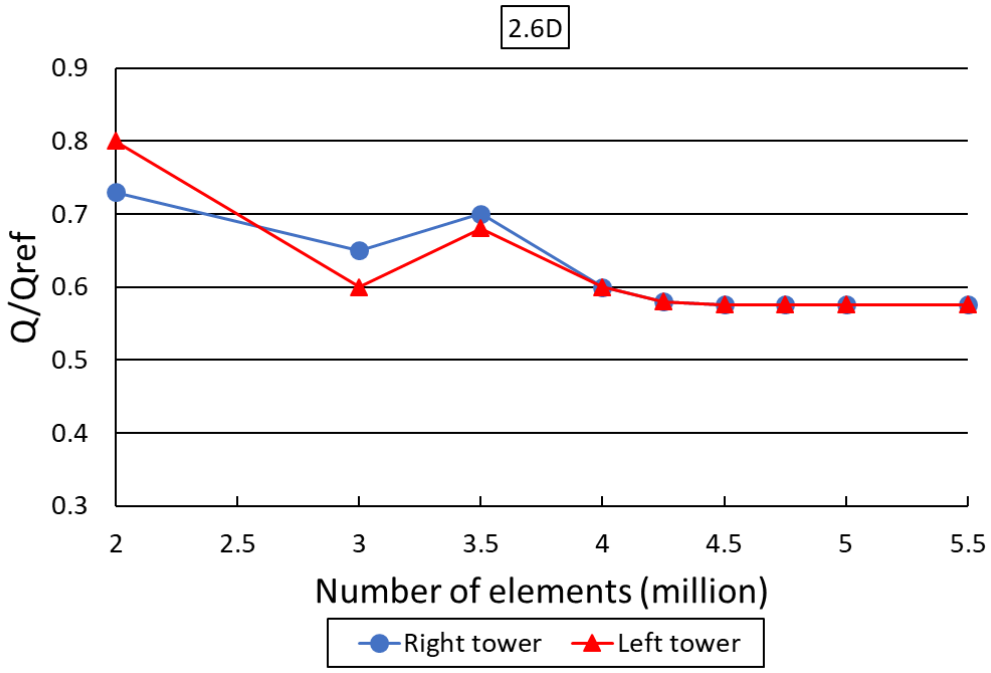

Figure B.10. Mesh sensitivity analysis for two NDDCTs at wind speed of 4 m/s, tower spacing of 2.6D, and wind incidence angle of 90°.

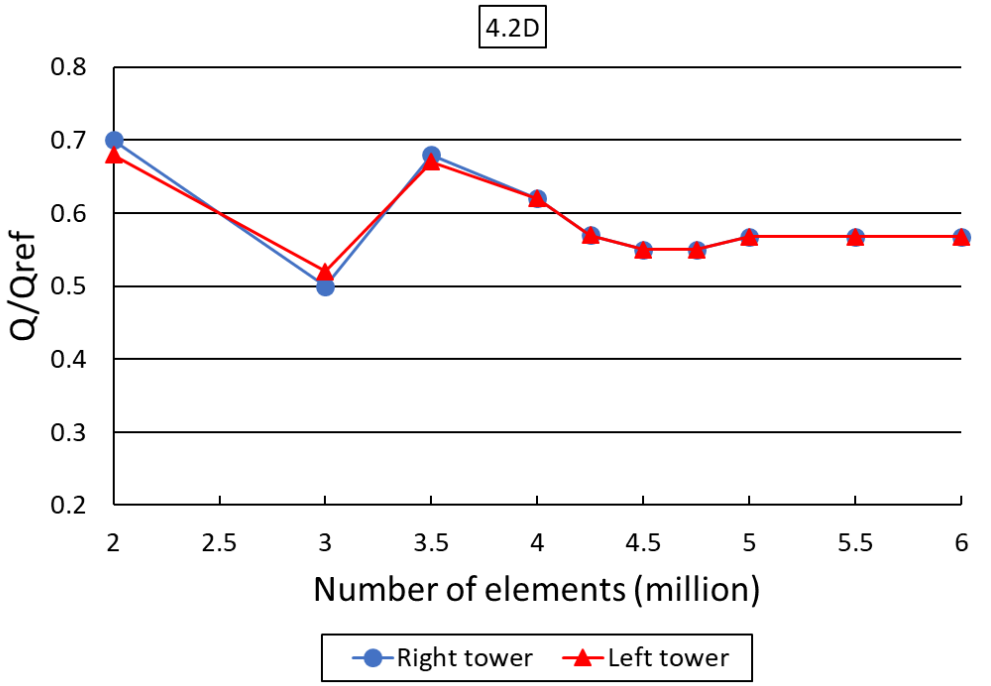

Figure B.11. Mesh sensitivity analysis for two NDDCTs at wind speed of 4 m/s, tower spacing of 4.2D, and wind incidence angle of 90°.

The boundary domain size for simulation of two NDDCTs during windy conditions are listed in Table B. **1.**

Table B. 1. Boundary domain size of two NDDCTs at different tower spacings and wind incidence angles.

Wind incidence angle/tower spacing	Height (m)	Breadth (m)	Length (m)
0°/1.8D	90	144	150
0°/2.6D	90	144	165
0°/4.2D	90	144	190
45°/1.8D	90	160	150
45°/2.6D	90	170	165
45°/4.2D	90	180	190
90°/1.8D	90	170	150
90°/2.6D	90	190	150
90°/4.2D	90	220	150

Figure B.12Figure B.13Figure B.14 show the mesh sensitivity analysis of three NDDCTs at wind incidence of 0° at tower spacings of 1.8D, 2.6D, and 4.2D respectively.

Table B.2 indicates the final number of mesh cells after performing the grid independence test at different tower spacings and wind incidence angles, at which the heat rejection of the towers remains constant after this number of mesh cells.

Table B.2. Final numbers of mesh cells at different wind incidence angles and tower spacings.

Wind incidence angle	Tower spacing	Final numbers of mesh cells (million)
0°	1.8D	4.3
0°	2.6D	4.5
0°	4.2D	4.9
45°	1.8D	4.5
45°	2.6D	4.7
45°	4.2D	5
90°	1.8D	4.5
90°	2.6D	4.6
90°	4.2D	4.8

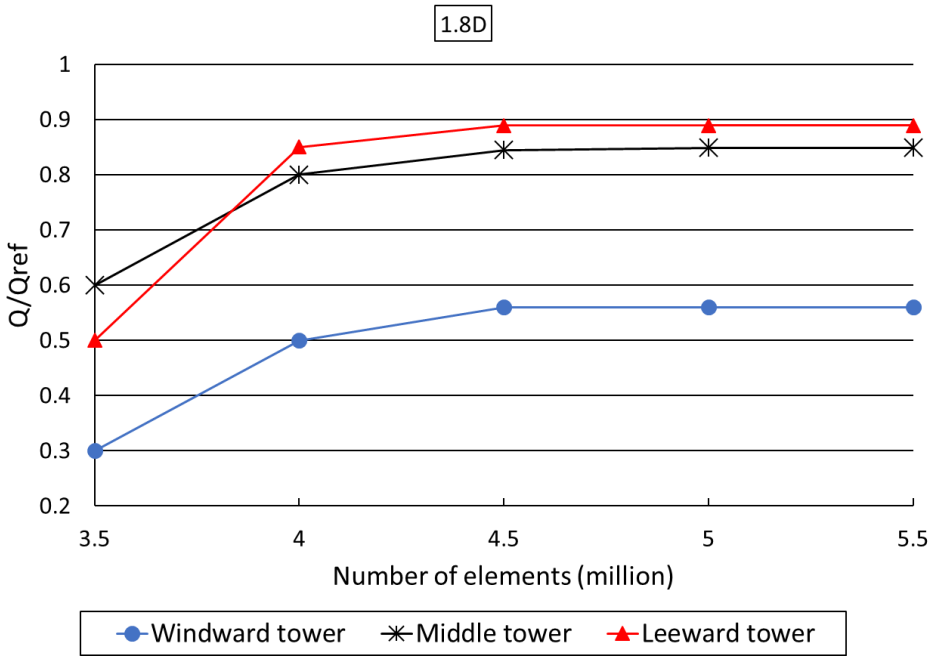

Figure B.12. Mesh sensitivity analysis for three NDDCTs at wind speed of 4 m/s and tower spacing of 1.8D.

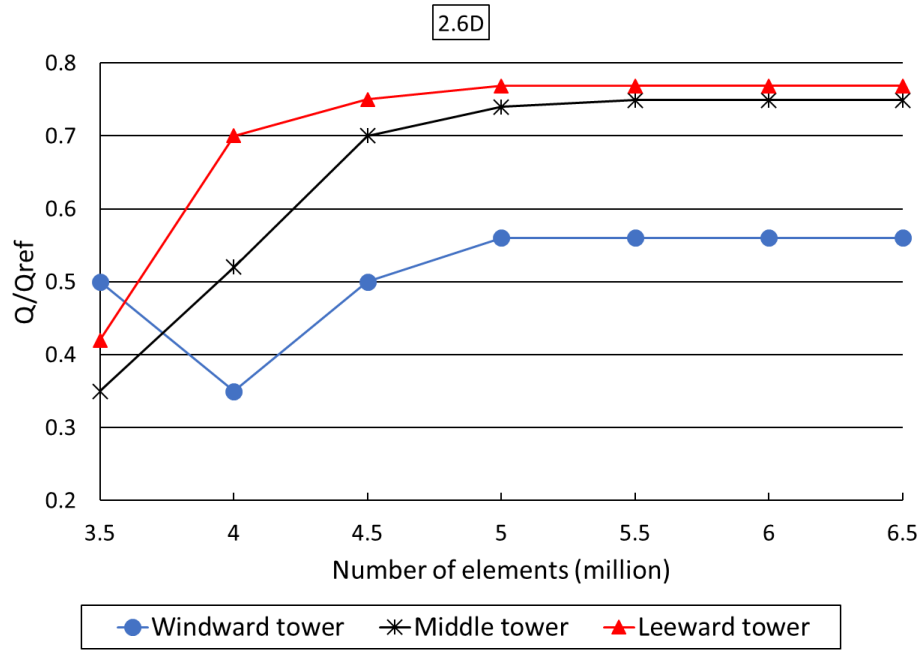

Figure B.13. Mesh sensitivity analysis for three NDDCTs at wind speed of 4 m/s and tower spacing of 2.6D.

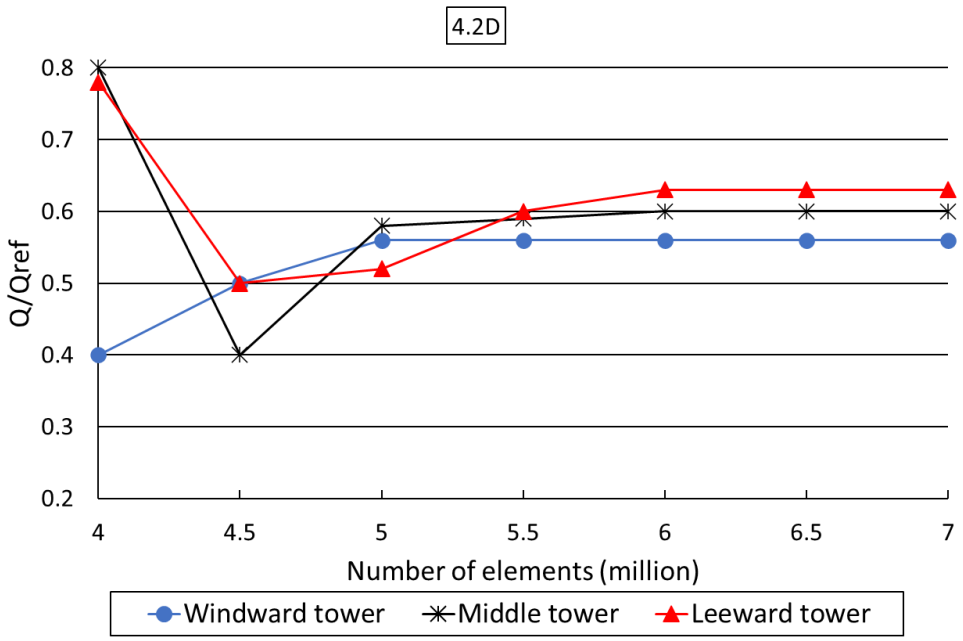

Figure B.14. Mesh sensitivity analysis for three NDDCTs at wind speed of 4 m/s and tower spacing of 4.2D.

A mesh sensitivity analysis for a single NDDCT with different sizes was carried out for Chapter 5 and is shown in Figure B.15.

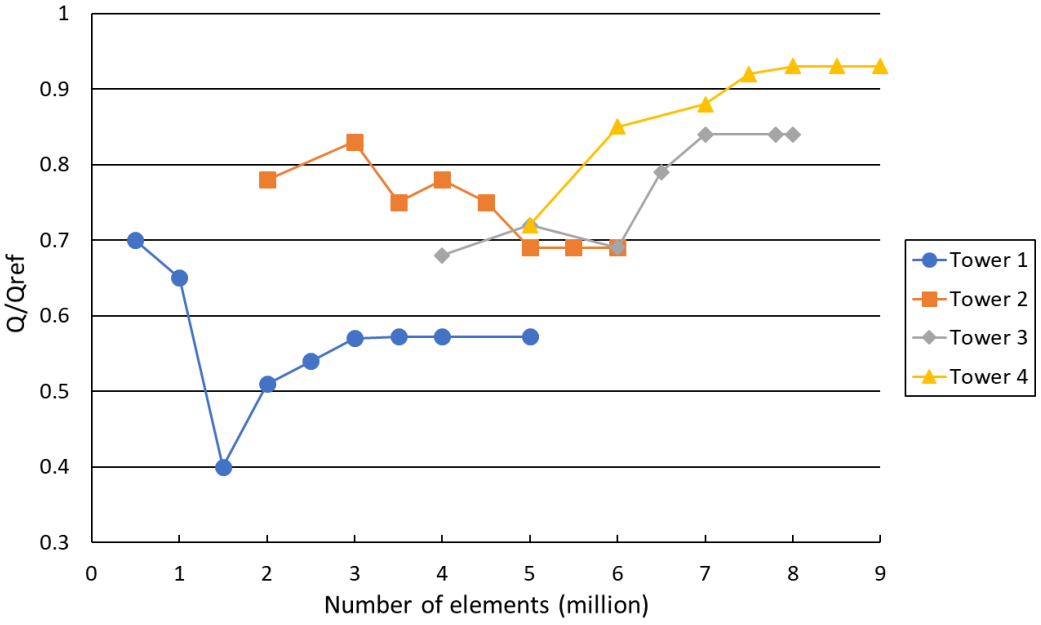

Figure B.15. Mesh sensitivity analysis for a single NDDCT at wind speed of 4 m/s and different sizes.

Appendix C: Two-tower velocity profile at wind incidence of 0°

In Chapter 3, it was shown that by increasing the tower spacing the flow circulation at the bottom of the leeward tower expands. This has been addressed by showing the velocity contour and velocity streamlines at the bottom of the cooling towers. Here, to further illustrate the flow behaviour at the bottom of the leeward tower, the velocity profile for the leeward tower at tower spacings of 1.8D, 2.6D, and 4.2D where r/R is the normalized radial distance from the centreline on top of the radiator surface is shown Figure C.1. From these, it can be seen that with an increase in the crosswind velocity, the velocity magnitude at the windward side of the tower decreases. The fluid velocity in the flow circulation is lowest in the core region and increases as moves away from it to its sides. The velocity profile at high wind velocities reaches a minimum value which shows the centre of the circulation. By increasing the wind velocity, the minimum value moves toward the centre of the tower. Further, the low velocity region at the bottom of the leeward tower moves toward the leeward face of the tower with an increasing the tower spacing. This shows that the flow recirculation becomes larger at the bottom of the leeward tower at larger tower spacings

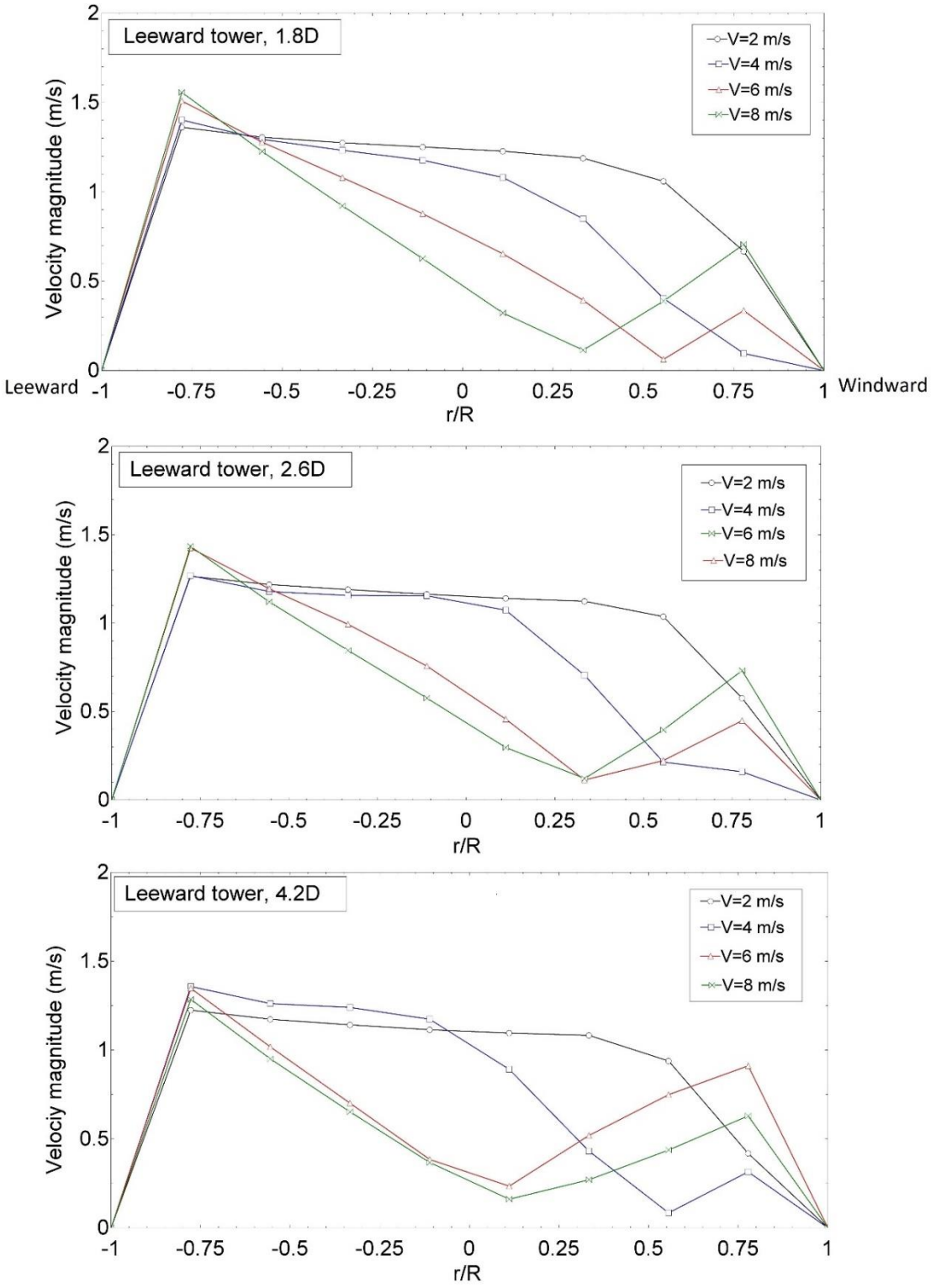

Figure C.1. Velocity magnitude at bottom centreline of the leeward tower at different tower spacings.

Appendix D: Wind tunnel visualization

D.1. Experimental setup

In order to compare some of the findings of the CFD simulations in Chapter 2, a wind tunnel test using tuft flow visualization was carried out. Experiments were performed in a 500mm x 500m test section which was extended 500mm upstream and 1000 mm downstream on a 1:150 scale models of the simulated tower in this study. A thread rake was mounted at the inlet of test section to show the streamlines around the towers. The sewing threads were further enhanced with UV lighting. The sides of the wind tunnel were blackened, and the lights of the room were turned off. The images of the flow were captured using a digital SLR camera. The scale model of the cooling tower was manufactured using a hollow pipe and four 1mm diameter were used as the support of the tower. A honeycomb structure was mounted at the inlet of the wind tunnel to provide a uniform flow velocity. The wind tunnel has been tested for a homogenous flow in the experiments (88). Figure D.1 shows the schematic drawing of the experimental setup. The towers were placed in the wind tunnel at different tower spacings of 1.8D, 2.6D, and 4.2D (D is the diameter of the tower).

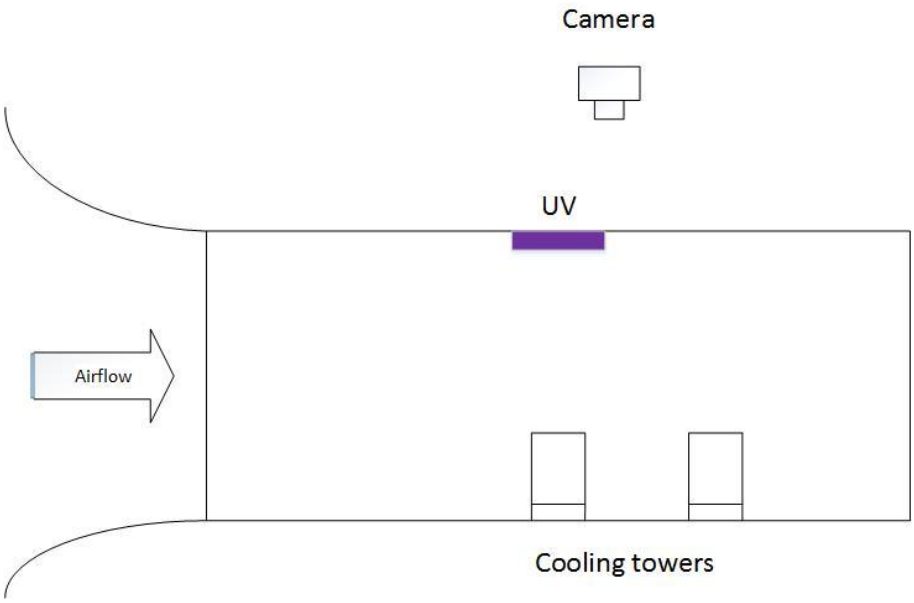

Figure D.1. Schematic view of the wind tunnel experiment.

D.2. Numerical method

In doing this, the same domain size and cylinder dimensions used in the wind tunnel tests were simulated using CFD simulations. The heat exchangers were not modelled in this section and same tower spacing used in the wind tunnel test were applied to the CFD simulations. The computational domain and cooling towers were discretised using 2.8 million structured elements. A free stream velocity of 3.2m/s was used at a temperature of 20°C. This results to a free stream Reynolds number of 1.77×10^{4}, considering the diameter of the cooling tower (0.0835m) and the kinematic viscosity of 1.51×10^{-5}. This free stream velocity was used in both CFD and wind tunnel experiment.

D.3. Comparison between CFD and wind tunnel tests

The threads are at the height of 0.033m from the ground and same streamlines from the similar points in CFD simulations were extracted and displayed in Figure D.2, Figure D.**3**, and Figure D.**4** . **Figure D.2**shows the comparison between the similar streamlines of the wind tunnel test and CFD simulations at tower spacing of 1.8D. The similarity between streamlines show that there is an agreement between the CFD and wind tunnel results.

The streamlines after the windward tower redirects and converges after the leeward tower. By increasing the tower spacing to 2.6D (Figure D.3) and then 4.2D (Figure D.4), the streamlines converge after the windward tower and move towards the leeward tower. This offers that wind windward tower protects the leeward tower and by increasing the tower spacing, this protection decreases as suggested by the streamlines. This is in agreement with the findings of the Chapter 3 for wind incidence of 0°.

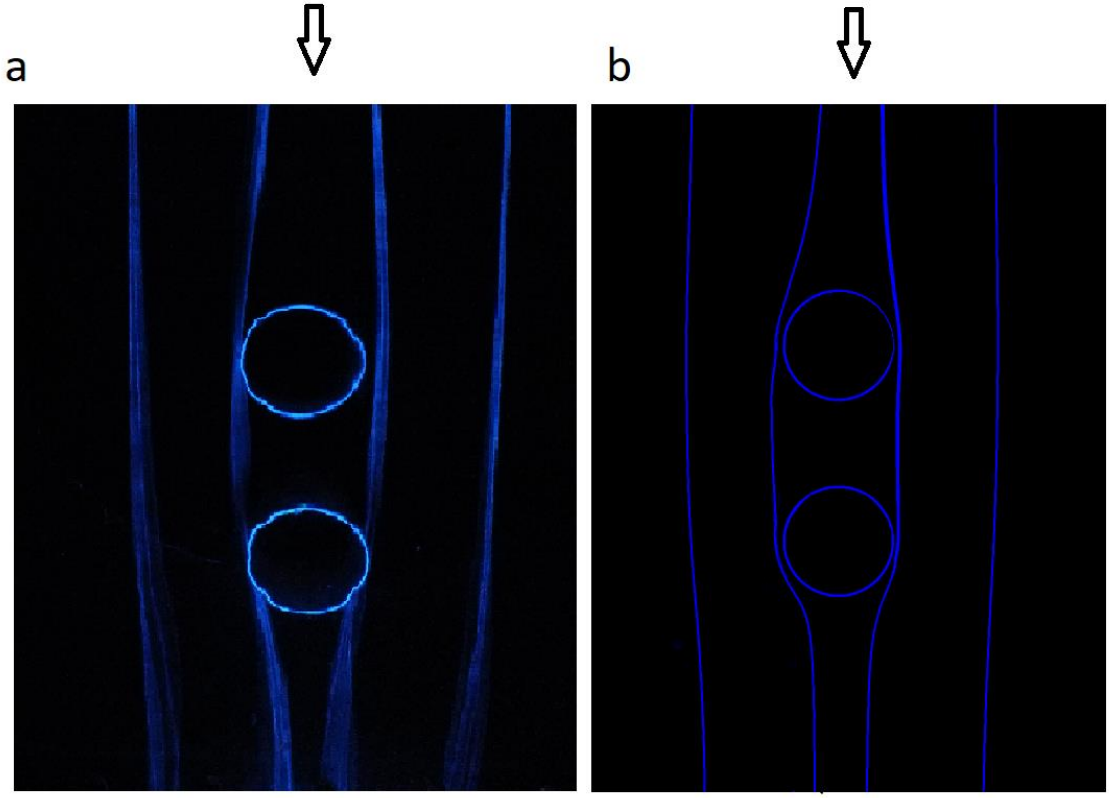

Figure D.2. Streamline Comparison between a) wind tunnel test and b) CFD simulation at tower spacing of 1.8D.

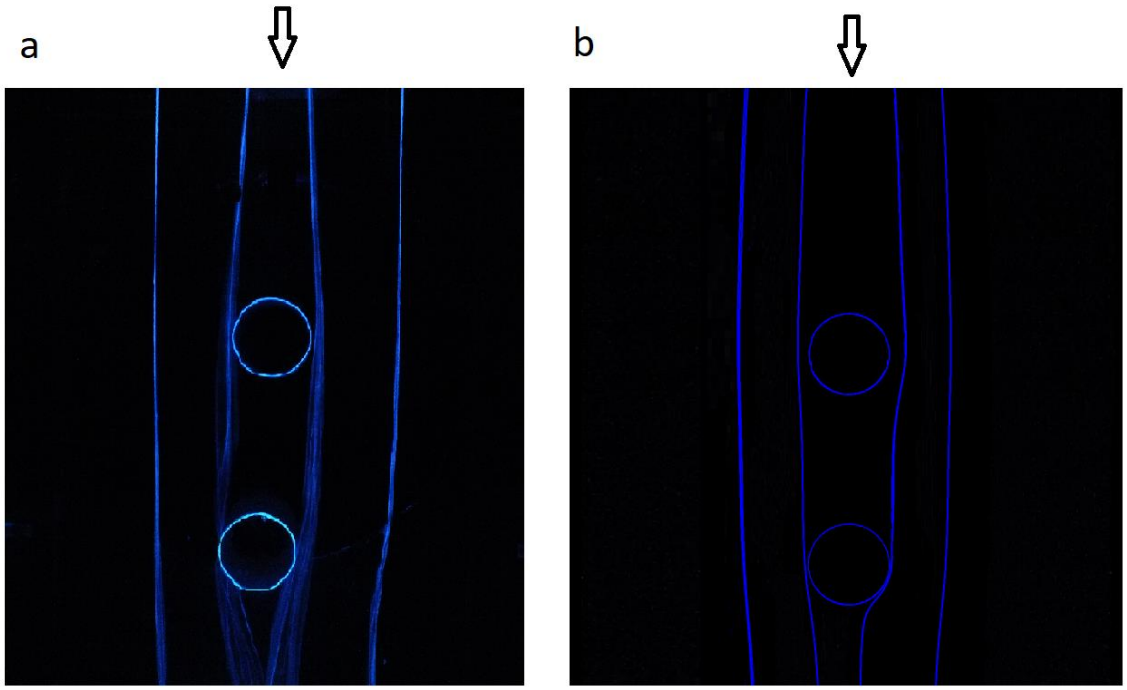

Figure D.3. Streamline Comparison between a) wind tunnel test and b) CFD simulation at tower spacing of 2.6D.

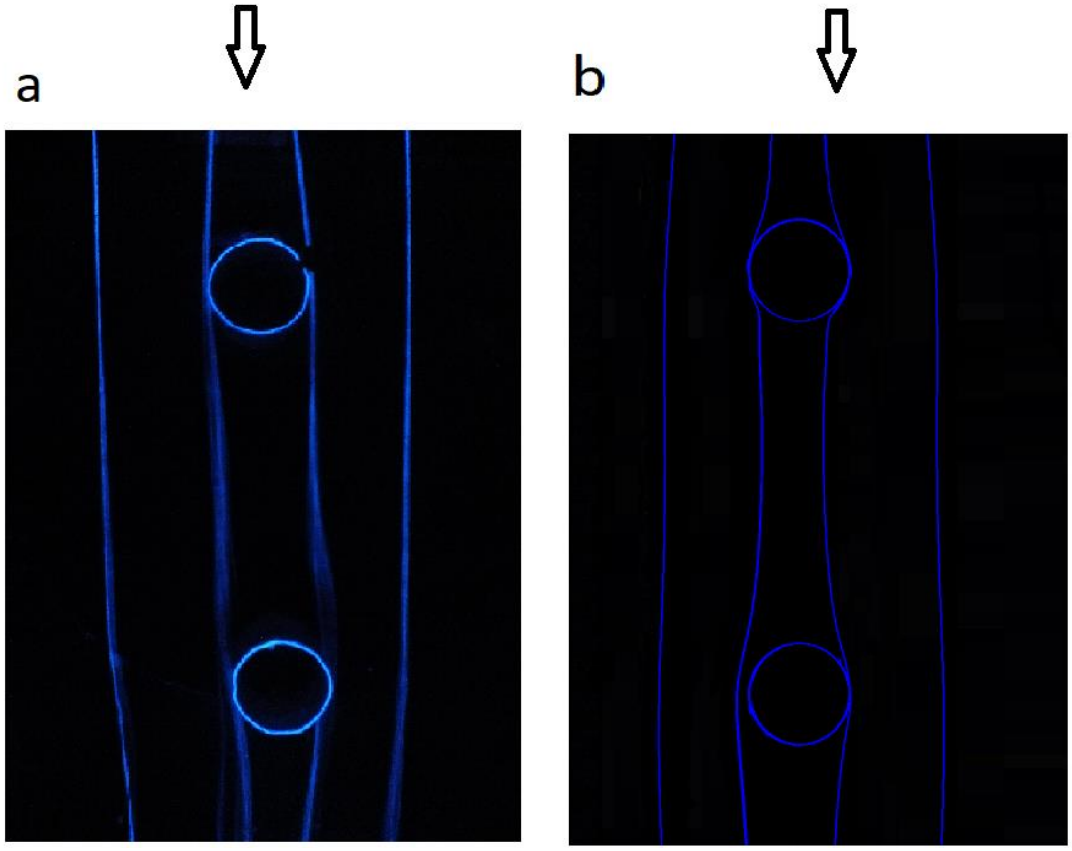

Figure D.4. Streamline Comparison between a) wind tunnel test and b) CFD simulation at tower spacing of 4.2D.